Titre: Title:	Numerical analysis of cylindrical waveguide for microwave and acoustic applications by method of lines
Auteur: Author:	Minying Yang
Date:	2001
Type:	Mémoire ou thèse / Dissertation or Thesis
Référence: Citation:	Yang, M. (2001). Numerical analysis of cylindrical waveguide for microwave and acoustic applications by method of lines [Master's thesis, École Polytechnique de Montréal]. PolyPublie. https://publications.polymtl.ca/26934/

UNIVERITÉ DE MONTREAL

NUMERICAL ANALYSIS OF CYLINDRICAL WAVEGUIDE FOR MICROWAVE AND ACOUSTIC APPLICATIONS BY METHOD OF LINES

MINYING YANG
DÉPARTEMENT DE GÉNIE ÉLECTRIQUE
ÉCOLE POLYTECHNIQUE DE MONTRÉAL

MÉMOIRE PRÉSENTÉ EN VUE DE L'OBTENTION
DU DIPLÔME DE MAÎTRISE ÈS SCIENCES APPLIQUÉES
(GÉNIE ÉLECTRIQUE)

NOVEMBRE 2001

UNIVERSITÉ DE MONTREAL

ÉCOLE POLYTECHNIQUE DE MONTRÉAL

Ce mémoire intitulé :

NUMERICAL ANALYSIS OF CYLINDRICAL WAVEGUIDE FOR MICROWAVE AND ACOUTIC APPLICATIONS BY METHOD OF LINES

présenté par : YANG Minying

En vue de l'obtention du diplôme de : Maîtrise ès sciences appliquées

A été dûment accepté par le jury d'examen constitué de :

M. LAURIN Jean-Jacques, Ph.D., président

M. WU Ke, Ph.D., membre et directeur de recherche

M. AMRAM Maurice, Ph.D., membre et codirecteur de recherche

M. LAVILLE Frédéric, Ph.D., membre

To my family

ACKNOWLEDGEMENT

This thesis is a summary of my research work from January 1999 to December 2001 at the Department of Electrical and Computer Engineering, École Polytechnique de Montréal, towards the completion of my Master's Degree of Applied Science. I am grateful to many people who have directly or indirectly helped me to complete this research work.

First of all, I would like to express my deep gratitude to my directors, Prof. Ke Wu and co-director, Prof. Maurice Amram, for their continuous guidance, invaluable advice and warm encouragement throughout the whole work, and for the financial support that made it possible for me to finish this research work and this theses in time.

Secondly, I am very grateful to the members of my committee, Prof. Jean-Jacques Laurin and Prof. Frédéric Laville for their comprehensive review of this thesis.

Specially, I would like to acknowledge Dr. Zhongfang Jin for his helpful discussions in this work.

Also, I would like to thank Mr. René Archambault for his help in the use of computer software.

Finally, my thanks go to all professors and my colleagues in the Poly-Grames Research Center for their kindness, helpful discussions and friendship.

RÉSUMÉ

L'objectif du projet de maîtrise est d'étudier l'utilisation de la Méthode des Lignes en coordonnées cylindriques pour la modélisation numérique des cavités cylindriques et des guides d'onde cylindriques remplis de disques dans les applications micro-ondes et acoustiques.

Les structures périodiques ont une caractéristique importante : l'existence des bandes passantes discrètes séparées par des bandes interdites. Les structures périodiques sont utilisées dans plusieurs applications. Dans le domaine des micro-ondes, par exemple on peut citer les accélérateurs linéaires de particules, les tubes d'onde et les réseaux de filtres micro-ondes. Les diélectriques artificiels et les grilles de diffraction sont des exemples de structures périodiques. Ces structures, ainsi que les plaques ondulées sont aussi utilisées comme outils pour guider les ondes de surface dans les antennes. Dans l'ingénierie acoustique, les structures périodiques sont utilisées comme filtres acoustiques en guide d'onde ou silencieux afin de réduire le niveau du bruit se propageant dans un tuyau ou rayonnant à partir du sommet de la barrière d'autoroute.

La Méthode des Lignes, une méthode de différence finie semi-analytique, est une des techniques les plus efficaces pour les applications dans le domaine des fréquences. L'idée de base de cette technique est de réduire un système d'équations aux dérivées partielles à des équations différentielles en discrétisant toutes sauf une des variables indépendantes. L'analyse de la structure de guide d'onde cylindrique remplie de disques se fait en utilisant la technique d'adaptation des modes pour les applications micro-ondes qui est détaillée dans la littérature. On a choisi la " Méthode des Lignes" dans ce

projet car la procédure semi-analytique est plus rapide. Cette méthode, appliquée aux coordonnées cylindriques, a été présentée dans ce mémoire. Les solutions des équations de Helmholtz à deux dimensions ont été obtenues en utilisant la Méthode des Lignes après la discrétisation des variables θ ou z en appliquant la procédure de découplage. Cette méthode a été appliquée de la même façon aux coordonnées cylindriques tri-dimensionnelles afin de discrétiser les directions angulaires et longitudinales. Les conditions aux frontières Dirichlet-Dirichlet, Neumann-Neumann, ainsi que les conditions aux frontières périodiques sont détaillées.

La validation initiale de la méthode a été réalisée en modélisant les résonateurs cylindriques inclus. Les Méthodes des Lignes bi- et tri-dimensionnelles sont utilisées afin d'obtenir des fréquences de résonance pour les modes TM et TE. Les résultats des simulations justifient les résultats obtenus par voie analytique. On a analysé deux structures de guides d'ondes cylindriques remples de disques présentées dans des articles publiés. On a utilisé la Méthode des Lignes bidimensionnelle cylindrique en appliquant les conditions aux frontières. Les résultats numériques obtenus ont été validés par les spécifications trouvées dans les articles mentionnés. Des analyses de paramètres du guide d'onde cylindrique périodique sont aussi étudiées. Les résultats simulés illustrent la dépendance des caractéristiques de dispersion à l'égard des paramètres géométriques tels que le diamètre du disque inséré et la longueur une période.

Au début, la Méthode des Lignes a été utilisée afin d'analyser des structures acoustiques à cause de la ressemblance entre les champs électromagnétiques et les champs acoustiques. Après l'étude d'un guide d'onde circulaire de longueur infinie en utilisant la méthode

bidimensionnelle cylindrique appliquée à un problème de propagation, un guide d'onde de longueur finie a été aussi étudié afin d'obtenir les fréquences de résonance par les Méthodes des Lignes bi- et tridimensionnelles. Les résultats obtenus sont en concordance avec les solutions analytiques. On a obtenu des résultats numériques pour un guide d'onde circulaire rempli de disques ayant une symétrie axiale en utilisant la Méthode des Lignes circulaire bidimensionnelle, résultats que sont en accord avec les valeurs expérimentales. Des études paramétriques pour le guide d'onde cylindrique acoustique périodique ont aussi été réalisées. Les résultats simulés montrent le rapport entre les caractéristiques de dispersion et les paramètres géométriques.

La technique de la Décomposition des Matrices en Valeurs Singulières a été utilisée dans ce projet afin de résoudre les problèmes numériques reliés aux pôles dans la fonction déterminant. On a réussi à augmenter la précision et la crédibilité des résultats calculés en utilisant une seule décomposition de valeur, on a aussi remarqué une diminution de la durée du temps de calcul.

ABSTRACT

The objective of the present Master's project is to investigate the use of the *Method of Lines* in cylindrical coordinates for the numerical modeling of cylindrical cavities and periodic disk-loaded cylindrical waveguide for both microwave and acoustic applications.

Periodic structures have one important characteristic in common. That is the existence of discrete passbands separated by stopbands. In microwave domain, the periodic structures find application in a variety of devices such as linear particle accelerators, traveling-wave tubes, and microwave filter networks. Artificial dielectric media and diffraction gratings are examples of periodic structures. Structures such as corrugated planes have also been used as surface wave-guiding devices for antenna applications. In acoustical engineering, periodic structures are designed for waveguide filters to lessen the low-frequency noise diffracting from the top of highway barriers, or silencers to reduce the level of noise propagating down a duct.

The *Method of Lines*, a semi-analytical finite difference method, is one of the most efficient methods for frequency domain applications. The basic idea of this method is to reduce a system of partial differential equations into ordinary differential equations by discretizing all but one of the independent variables. The analysis of the periodic disk-loaded cylindrical waveguide structure using the mode-matching technique for microwave applications is documented in the literature. The reason to select the *Method of Lines* in this work is that the semi-analytical procedure saves considerable computing memory and time. The *Method of Lines* procedure for cylindrical coordinates has been presented in this thesis. Solutions for two-dimensional

Helmholtz equations have been obtained by a two- dimensional cylindrical *Method of Lines* after discretizing the θ-variable or z-variable with the decoupling procedure applied. Similarly, a three-dimensional cylindrical *Method of Lines* was utilized to discretize both the angular and longitudinal space directions. Useful boundary conditions in this work such as Dirichlet-Dirichlet, Neumann-Neumann, and periodic boundary conditions are also illustrated in detail.

Initial validation of the method has been realized with the modeling of electromagnetic enclosed cylindrical resonators. Both the two- and three-dimensional cylindrical *Method of Lines* were used to obtain resonant frequencies for TM and TE modes. Simulation results show good agreements with results obtained by analytical solutions. Examples of periodic disk-loaded cylindrical waveguide structures from two papers were analyzed by using the two-dimensional cylindrical Method of Lines with the periodic boundary conditions performed. Numerical results were obtained, and found to converge to the published results. Parameter analyses of the periodic cylindrical waveguide were also studied. Simulated results illustrate the dependence of dispersion characteristics on geometrical parameters, such as the diameter of an inserted disk and the length of one period.

Due to the similarities between electromagnetic and acoustic fields, the *Method of Lines* (MoL) is introduced to analyze acoustic structures for the first time. After investigating an infinite long circular waveguide by two-dimensional cylindrical method for a propagation problem, an enclosed circular waveguide has also been studied to obtain the resonant frequencies by using both the two and three-dimensional CMoL. Computed results show good agreement with the analytic solutions. Numerical results for the

periodic disk-loaded circular waveguide with axial symmetry were also obtained by a two-dimensional CMoL, which give good agreement with the experimental results. Parameter studies for the periodic acoustic cylindrical waveguide were also performed. Simulated results show the relationship between the dispersion characteristics and the geometrical parameters.

The matrix Singular Value Decomposition (SVD) technique was adopted in this work in order to solve numerical problems related to the poles in the determinant function. By using this technique, the accuracy and reliability of computed results were improved, while the CPU time was significantly reduced comparing with directly evaluating determinant of the matrix.

CONDENSÉ EN FRANÇAIS
ANALYSE NUMÉRIQUE DES GUIDES D'ONDE CYLINDRIQUES POUR APPLICATIONS AUX MICRO-ONDES ET À L'ACOUSTIQUE EN UTILISANT LA MÉTHODE DES LIGNES

L'objectif de ce mémoire est l'investigation de l'utilisation de la Méthode des Lignes en coordonnées cylindriques pour la modélisation numérique de cavités cylindriques et de guide d'onde cylindrique chargé de disques périodiques pour des applications tant aux micro-ondes qu'à l'acoustique.

0.1 Introduction

Des cavités à micro-ondes sont des composantes importantes dans des systèmes de télécommunications. Ces cavités, complétées par certains éléments de couplage, forment les éléments essentiels des composants micro-ondes comme des filtres et des multiplexeurs. Une structure périodique chargée de disques contenant des cavités multiples peut donc être considérée comme une ligne de transmission infinie ou un guide d'onde périodiquement chargé d'éléments réactifs (des éléments de couplage). Ce type de structure périodique soutient la propagation d'ondes lentes (se propageant plus lentement qu'à la vitesse de phase de la ligne déchargée) et possède des bandes passantes et des bandes interdites semblables à celles des filtres. Il y a de nombreuses applications dans l'ingénierie micro-ondes comme les accélérateurs linéaires, les tubes d'ondes progressives de haute puissance (TWTs) et les réseaux de filtres micro-ondes. Les guides d'onde cylindriques sont aussi utilisés dans l'ingénierie d'acoustique. Beaucoup de conduits dans lesquels le son se propage ont des sections circulaires. Ainsi, il est désirable d'analyser des modes transversaux dans ces guides d'onde

cylindriques. De plus, des structures périodiques sont conçues pour des filtres de guides d'onde acoustiques ou des silencieux pour réduire le niveau de bruit se propageant à travers un conduit ou rayonnant à partir du sommet de barrières d'autoroute.

La Méthode de Lignes (MoL), une méthode de différences finies semi-analytique, est choisie afin d'analyser des structures périodiques, car elle est l'une des méthodes efficaces dans le domaine de fréquences pour résoudre les équations de Helmholtz. Comparée à d'autres méthodes dans ce domaine, comme la méthode des différences finies (FD) ou la méthode des éléments finis (FEM), elle exige moins de ressources informatiques. L'idée de base de la MoL est de réduire un système d'équations différentielles partielles à des équations différentielles ordinaires par la discrétisation de toutes, sauf une des variables indépendantes. En raison de la similitude entre les équations régissantes les champs électromagnétiques et acoustiques, la MoL est aussi appliquée aux structures périodiques acoustiques.

Ce mémoire est organisé en deux parties. Pour valider notre méthode, la Partie A contient l'analyse des champs électromagnétiques se propageant dans des guides d'onde cylindriques périodiques comme indiqué dans la Figure 1.1. La partie B est l'analyse des champs acoustiques dans des guides d'onde cylindriques périodiques semblables à ceux des micro-ondes. Chaque partie est divisée en deux sujets comme illustré dans la Figure 1.2. Les sujets A1 et B1 sont des problèmes de résonateurs. Il faut trouver les fréquences de résonance pour la cavité cylindrique fermée. Les sujets A2 et B2 sont des problèmes de propagation d'ondes - il faut trouver la constante de propagation dans la bande passante. Ce mémoire comporte sept chapitres. Le premier chapitre est l'introduction. Le deuxième chapitre

présente la méthode cylindrique bi- et tridimensionnelle des lignes (CMoL) appliquée aux équations d'Helmholtz on y montre les conditions aux frontières pour les ondes électromagnétiques et les ondes acoustiques, respectivement. Les troisième et quatrième chapitres sont reliés aux ondes électromagnétiques. Dans le troisième chapitre, nous avons résolu un problème aux « valeurs propres » pour un guide d'onde circulaire électromagnétique tel que montré ci-joint. Le méthode CMoL tant 2-D que 3-D a été utilisée afin d'obtenir les fréquences résonantes. Dans le quatrième chapitre, nous avons résolu un problème de propagation pour un guide d'onde circulaire chargé de disques périodiques avec la symétrie axiale par la 2-D CMoL. Les cinquième et sixième chapitres sont consacrés à l'étude de l'onde acoustique. Dans le cinquième chapitre, nous avons examiné un guide d'onde circulaire infiniment long par la 2-D CMoL pour un problème de propagation. Nous avons aussi étudié un guide d'onde circulaire acoustique fermé pour un problème aux «valeurs propres » en utilisant la méthode CMoL 2-D et 3-D afin d'obtenir des fréquences de résonance. Dans le sixième chapitre, nous avons examiné un guide d'onde circulaire chargé de disques périodiques avec la symétrie axiale par la méthode CMoL 2-D pour un problème de propagation. Les résultats obtenus sont en concordance avec les résultats expérimentaux. Les conclusions de ce mémoire et des recommandations pour le travail futur seront présentées dans le chapitre final.

0.2 Méthode de Lignes Cylindrique (CMoL)

On a proposé la méthode de lignes pour résoudre des équations différentielles partielles déjà dans les années 60. L'application de cette méthode a été proposée pour l'utilisation dans le domaine micro-ondes dans

les années 80. La plupart des applications sont pour des structures rectangulaires. Il y a seulement quelques publications directement liées à l'application de la MoL aux problèmes électromagnétiques en coordonnées cylindriques. De plus, autant que nous savons, la MoL n'a pas été appliquée pour analyser les structures acoustiques.

La Méthode de Lignes en coordonnées cylindriques a été présentée dans le chapitre 2. Les solutions pour les équations d'Helmholtz bidimensionnelles ont été obtenues par la Méthode cylindrique bidimensionnelle de Lignes après la discrétisation de la variable θ ou de la variable z en utilisant la procédure de décomposition. On montre la solution semi-analytique de l'équation 2-D d'Helmholtz, discrétisée dans la direction θ, dans l'équation (2.24) et on montre la solution pour la discrétisation dans la direction z dans l'équation (2.42). De même, la méthode cylindrique tridimensionnelle de lignes a été utilisée pour discrétiser tant les directions spatiales angulaires que longitudinales. Pour résoudre l'équation d'Helmholtz discrétisée (2.49), le produit de Kronecker a été présenté. En appliquant la procédure de décomposition, le système d'équations d'Helmholtz dans l'équation (2.54) peut être décomposé dans un système d'équations différentielles ordinaires indépendantes de type Bessel, la solution a été écrite dans l'équation (2.59). Si la région de la solution contient l'origine $r = 0$, B_k dans des équations (2.24) et (2.42), et B_{ki} dans l'équation (2.59) doivent être nulles puisque les fonctions de Bessel de 2^e espèce Y_{mk} sont singuliers.

On présente dans le deuxième chapitre l'expression des opérateurs de différence finie $[P]_\theta$, $[P]_z$, les matrices de la transformation orthogonales $[T]_\theta$, $[T]_z$ et les valeurs propres $[\lambda]$, $[\delta]$. La condition latérale de frontière $[P]_\theta$ est une condition naturelle de frontière, tandis que, pour $[P]_z$, les conditions

latérales de frontière peuvent être Dirichlet-Dirichlet, Neumann-Neumann et des conditions périodiques de frontière.

En conclusion, les méthodes cylindriques 2D et 3D de lignes sont présentées et des conditions utiles de frontière sont aussi détaillées.

0.3 Caractérisation du résonateur à micro-ondes en utilisant CMoL

Un résonateur cylindrique est analysé dans le troisième chapitre. Il peut être considéré comme un segment de la structure de guide d'onde cylindrique périodique chargée de disques quand le diamètre intérieur des disques est nul. Tant la méthode CMoL 2D- que 3D sont utilisées pour obtenir les fréquences de résonance pour les modes TM et TE. Les conditions latérales aux frontières pour $[P]_z$ sont obtenues en analysant les composants des champs montrés dans des équations (3.1a) à (3.1f). Il devrait être mentionné, que pour les modes TM dans un résonateur cylindrique, l'opérateur $[P]_z$ est dérivé de la condition de frontière latérale N-N. En même temps, pour les modes TE, le $[P]_z$ est satisfait par la condition de frontière D-D.

Les fréquences de résonances, présentées dans les Tableaux 3-3a et 3-4b, ont été obtenues à partir de l'équation (3.1). On montre les résultats des simulations en exécutant la méthode CMoL 2-D et la 3D aux Figures 3.2a, 3.2b, 3.3a, 3.3b, 3.4, et 3.5, en remarquant une bonne concordance avec les résultats attendus.

0.4 Analyse d'un guide d'onde circulaire périodique micro-ondes chargé de disques

Au quatrième chapitre, nous avons résolu un problème de propagation dans des guides d'onde cylindriques périodique chargé de disques avec la symétrie axiale en utilisant la méthode CMoL 2-D. Les paramètres géométriques des structures sont trouvés dans les articles de Pruiksma et al. [6] et [7]. Ces deux articles ont décrit l'investigation des guides d'onde cylindriques périodiques chargés de disques pour les modes TM. Des analyses de paramètres sont aussi effectuées afin d'investiguer la dépendance des caractéristiques de dispersion des structures périodiques à l'égard des paramètres géométriques.

Pour résoudre notre problème, la structure montrée à la Figure 4.1 est divisée en deux régions uniformes (régions I et II). Des lignes de discrétisation pour une période sont aussi montrées. On donne la matrice différence $[P]_z$ la région correspondante I et la région II dans l'équation (4.3a) et (4.3b). Après l'application des procédures de décomposition, les solutions sont écrites dans les équations (4.7a), (4.7b) respectivement. En combinant les conditions de frontières, nous avons obtenu les équations aux valeurs propres (4.11). La solution non "nulle" existe seulement si le déterminant de la matrice [JYM] dans l'équation (4.12) est égal à 0. Ainsi nous pouvons rechercher les racines satisfaisant notre cas. On s'approche d'habitude du problème de résoudre des équations aux valeurs propres en évaluant directement le déterminant de la matrice. Cependant, en raison de la présence de pôles, il est difficile de détecter les zéros qui peuvent être près de ceux-ci. On propose la technique de décomposition de valeur singulière (SVD) pour éliminer des pôles. De plus, nous rencontrons aussi un problème

de débordement numérique en évaluant directement le déterminant de la matrice [JYM] d'une grande taille. Dans ce travail, nous utilisons d'abord la méthode SVD pour diagonaliser la matrice [JYM] à l'aide de deux matrices unitaires, [U] et [V] ([U] h [U] = [I] et [V] h [V] = [I]) et [U] h [JYM] [V] =diag [s_1, s_2, ..., s_n], où $s_1 > s_2 \ldots > s_n$. Alors, le déterminant de la matrice [JYM] est égal à $\prod_{k=1}^{n} s_k$. Dans notre situation, nous choisissons la valeur du dernier élément s_n comme suggéré par Xiao et d'autres en [13]. Dans le sous-programme Matlab, s_n a déjà la valeur la plus petite parmi tous les éléments diagonaux dans la matrice diag [s_1, s_2, ..., s_n]. Ainsi, la découverte des zéros du déterminant de la matrice [JYM], est équivalente à la découverte des points minimaux locaux de s_n.

Une structure périodique peut être considérée comme une ligne de transmission chargée de réactances connectées en série ou parallèle et espacées à des intervalles réguliers. Selon la théorie de la petite ouverture de Colin, une petite ouverture circulaire de rayon **a** dans le centre du mur transversal dans un guide circulaire de rayon **b**, pour un mode TM_{01} est équivalente à la susceptance capacitive shunt $B = \frac{0.92b^4}{|\alpha_e|\lambda_g}$, où $|\alpha_e| = \frac{2}{3}a^3$, λ_g est la longueur d'onde guidée. Nous pouvons évaluer la bande passante et la bande interdite en utilisant l'équation de propagation de la structure périodique infinie.

Des recherches numériques ont été exécutées pour les structures dans les deux articles mentionnés ci-dessus. La Figure 4.2 montre les caractéristiques de dispersion de la structure chargée de disques pour le Cas A, qui est mentionné en [7]. Un bon accord a été obtenu entre les résultats de

simulation de la méthode CMoL 2-D et ceux des équations analytiques. La déviation apparaît pour le retard de phase βd plus grand que π/2. Pour le même retard de phase βd, les différences relatives entre les fréquences de la méthode CMoL 2-D et ceux d'équations analytiques sont petites et autour de 1 %. La Figure 4.3 montre les caractéristiques de dispersion de la structure chargée de disques pour le Cas B. Un bonne coïncidence existe entre les résultats de la simulation méthode CMoL 2-D et ceux des équations analytiques. Il y a une différence entre les résultats de la méthode CMoL 2-D et ceux de la mesure expérimentale. Notez que nous négligeons l'épaisseur des disques insérés. Pour plus d'exactitude on prend en considération l'épaisseur de ces disques. De plus, le modèle expérimental présente des imperfections.

Les Figures 4.4 et 4.5 montrent les caractéristiques de dispersion avec la variation des paramètres géométriques. Le retard de phase βd diminue avec l'augmentation du diamètre intérieur des disques insérés et augmente avec l'augmentation de la longueur d'une période pour le cas A.

Pour conclure, nous avons examiné un guide d'onde circulaire périodique chargé de disques en symétrie axiale en utilisant la méthode CMoL 2-D. Des résultats numériques sont comparés avec ceux obtenus des équations analytiques trouvées dans le livre de Collin. Une bonne coïncidence a été obtenue entre les deux méthodes. La déviation existe toujours entre les résultats de la méthode CMoL 2-D et les données des mesures. Le besoin d'une analyse plus rigoureuse inclut l'impact de l'épaisseur de disques insérés. On doit aussi considérer les imperfections du modèle de lexan construit à l'échelle 1/8. On a effectué par la suite une étude paramétrique

pour évaluer les paramètres importants dans l'obtention d'un grand déphasage.

0.5 CMoL appliqué aux guides d'onde circulaires acoustiques

La CMoL est utilisée pour analyser en coordonnées cylindriques des structures guides d'onde acoustiques ayant la section transversale circulaire.

Les équations d'Helmholtz (tant la 2-D que la 3D) sont tirées des équations d'onde acoustiques. Pour un guide d'onde cylindrique de longueur infinie, la méthode de lignes cylindrique 2D CMoL (la 2-D CMoL) est utilisée afin d'analyser les caractéristiques de propagation. En discrétisant la direction spatiale angulaire seulement, l'équation d'Helmholtz bidimensionnelle en coordonnées cylindriques devient un système d'équations différentielles ordinaires qui peuvent être résolues analytiquement dans la direction radiale après une transformation orthogonale. Pour un résonateur acoustique, la CMoL 3D est utilisée pour discrétiser les directions spatiales angulaires et longitudinales simultanément. L'équation d'Helmholtz résultante est un système d'équations différentielles unidimensionnelles couplées. En appliquant la procédure de décomposition, chaque équation différentielle peut alors être résolue analytiquement dans la direction radiale après une transformation orthogonale.

L'application de CMoL aux structures acoustiques est évaluée pour le guide d'onde circulaire infiniment long et la cavité cylindrique. On montre les résultats numériques pour ce guide d'onde dans des Figures 5.1 à 5.7 et le Tableau 5-1. On montre les solutions analytiques de la cavité cylindrique dans le Tableau 5-2. On montre des résultats des simulations en exécutant

les programmes CMoL 2-D et 3D dans les Figures 5.9 et 5.10. En les comparant avec la solution analytique, on peut noter une bonne concordance entre les résultats obtenus.

0.6 Les caractéristiques de dispersion d'une structure de guide d'onde acoustique périodique chargée de disques

Dans le chapitre 6, en utilisant la CMoL 2-D, les caractéristiques de dispersion ont été obtenues pour un guide d'onde acoustique périodique. Nous supposons que seulement des modes (0, n) se propagent dans la structure. Le mode fondamental, noté (0,0), génère des modes supérieurs (0,n) au niveau des discontinuités. Les procédures sont semblables à celles décrites dans le chapitre 4 sauf que les conditions aux frontières sont différentes. La structure est aussi divisée en deux régions. Les équations aux « valeurs propres » sont obtenues comme dans l'équation (6.19).

Les instruments utilisés sont décrits dans la Figure 6.2. Comme montré, le son se propage dans un guide d'onde cylindrique périodique pour atteindre un microphone ou il atteint directement un autre microphone. L'onde acoustique se propageant dans la structure périodique avec une vitesse inférieure à celle qu'elle a en espace libre. Ainsi, il y a un retard de phase entre les deux microphones. De plus, on retrouve des bandes passantes et bandes interdites caractéristiques des structures périodiques. Dans la Figure 6.2, le diamètre du guide d'onde cylindrique périodique est 254 mm, tandis que le diamètre des disques insérés est 25.4 mm. La longueur d'une période est 12,7 mm. En utilisant la CMoL 2-D les retards de phases dans les bandes passantes pour la structure périodique sont obtenus et montrés à la Figure 6.3. Comme inscrit dans le Tableau 6.1, on trouve un total de six

bandes passantes séparées par des bandes interdites au-dessous 8kHz. On montre le retard de phase des cinq bandes passantes PB-I, PB-II, PB-III, PB-IV et PB-V dans les Figures 6.4a, 6.4b, 6.4c, 6.4d et 6.4e. Le retard de phase de la bande passante PB-VI n'est pas analysé ici car le rapport du signal/bruit est trop petit pour les données expérimentales. Les résultats théoriques et expérimentaux dans les bandes passantes PB-II, PB-III et PB-V sont en concordance.

Afin d'illustrer la variation du retard de phase avec le changement des paramètres géométriques de la structure périodique, une analyse paramétrique est aussi développée et montrée sur les Figures 6.5 et 6.6.

0.7 Conclusion

Dans ce mémoire, une étude numérique détaillée des cavités cylindriques et des guides d'onde cylindriques périodique chargés de disques pour des applications tant aux micro-ondes qu'acoustiques a été présentée en utilisant la Méthode de Lignes (MoL) 2D et 3D. Les procédures de la Méthode de Lignes en coordonnées cylindriques ont été décrites en détail. Des résonateurs cylindriques à micro-ondes et acoustiques ont été analysés en utilisant tant la CMoL 2-D que la 3D. Des accords excellents ont été obtenus entre des résultats théoriques CMoL et ceux des expressions analytiques. Quant aux structures cylindriques périodiques, en raison de la symétrie axiale de la structure périodique et en raison de la symétrie axiale du départ de l'onde, seulement la CMoL 2-D a été utilisée pour analyser les caractéristiques de dispersion des guides d'onde périodiques chargés de disques. Ici, la source acoustique est une onde plane venant d'un haut-parleur et la source électromagnétique est l'évaluation de l'onde TEM d'un

connecteur coaxial. Les bandes passantes pour les applications tant micro-ondes qu'acoustiques se retrouvent comme attendu. Il y a une légère différence entre les retards de phase théoriques et expérimentaux. Une telle déviation résulte en partie de l'erreur numérique comme l'exécution de la CMoL 2-D pour analyser la structure périodique. Une autre vient de l'impact de la discontinuité de l'entrée et la sortie. Finalement, des modes non axiaux peuvent exister si les structures ne possèdent pas la symétrie axiale stricte ou le démarrage de la source cause une dépendance de la variable angulaire.

Pour continuer le travail dans ce mémoire, premièrement, l'analyse des structures de guide d'onde cylindrique chargées de disque périodique dans l'ingénierie micro-ondes peut être étendue à l'analyse des modes hybrides en utilisant la CMoL 3D. Deuxièmement, dans l'ingénierie acoustique, la section transversale circulaire peut ne pas avoir de symétrie axiale. Dans cette circonstance, les modes se propageant dans la structure ne sont plus les M_{0n}, c'est-à-dire que la discrétisation de la variable θ est exigée. On a besoin d'implanter CMoL 3D afin d'analyser de telles structures périodiques. La MoL semi-analytique peut être utilisée pour analyser les modes acoustiques existant dans quelques substrats piézoélectriques ayant un grillage périodique. Ces trois sujets sont les recommandations pour des travaux à venir.

TABLE OF CONTENTS

LIST OF TABLES

LIST OF FIGURES

LIST OF SYMBOLS AND NOTATIONS

CMoL	cylindrical method of lines
FD	finite difference
FEM	finite element method
MoL	method of lines
SVD	singular value decomposition
TE	transverse electric
TM	transverse magnetic

CHAPTER 1

INTRODUCTION

The purpose of this thesis is to investigate the use of Method of Lines [1] (MoL) in the numerical modeling of cylindrical cavities and periodic disk-loaded cylindrical waveguides for microwave and acoustic applications.

Microwave cavities are important components in telecommunication systems. These cavities, together with certain coupling elements, form the fundamental building blocks of microwave components such as microwave filters and multiplexers. A disk-loaded periodic structure consisting of multiple cavities can be regarded as an infinite transmission line or waveguide periodically loaded with reactive elements (coupling elements). This kind of periodic structure supports slow-wave propagation (slower than the phase velocity of the unloaded line), and has passband and stopband characteristics similar to those of filters. It has a lot of applications in microwave engineering such as linear accelerators, high power traveling wave tubes (TWTs), and microwave filter networks [2,3,4].

The cylindrical waveguides are also used in acoustics engineering. Many ducts in which sound propagates have circular cross-sections. Thus, it is desirable to analyze cross modes in these cylindrical waveguides. Moreover, the investigation of acoustic periodic disk-loaded waveguide is helpful for the design of a new type of silencer which will be used to control the low-frequency noise level over the top of highway barriers.

The Method of Lines (MoL), a semi-analytical finite difference method, is chosen to analyze periodic structures, since it is one of the efficient methods in frequency domain to solve Maxwell and Helmholtz equations. Compared with other methods for computational electromagnetic such as finite difference (FD) method or finite element method (FEM), it requires less computational resources. The basic idea of the MoL is to reduce a system of partial differential equations into ordinary differential equations by discretizing all but one of the independent variables. Due to the similarity between electromagnetic and acoustic fields, MoL is also applicable to acoustic periodic structures.

There are two parts in this thesis. In order to validate our method, Part A deals with electromagnetic field analysis of periodic cylindrical waveguides as shown in Figure 1.1. Part B is related to the acoustic field analysis of similar periodic cylindrical waveguides as microwave ones.

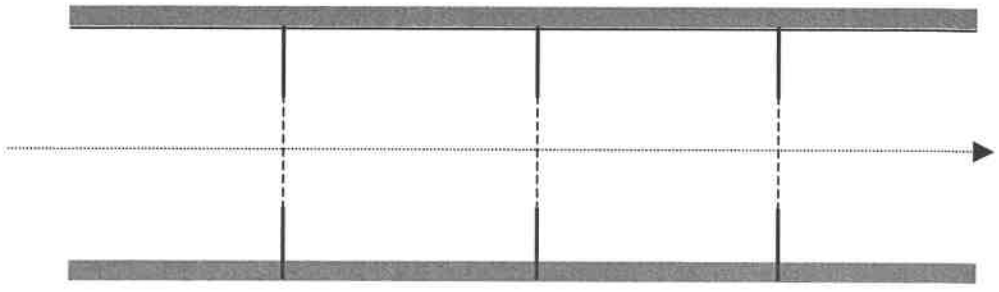

Figure 1.1 Periodic cylindrical waveguide

Each part is divided into two topics as illustrated in Figure 1.2. Topics A1 and B1 are resonator problems. This is to calculate the resonant frequencies for an enclosed cylindrical cavity. Topics A2 and B2 are wave propagation problems. We find out the propagation constants over the passband.

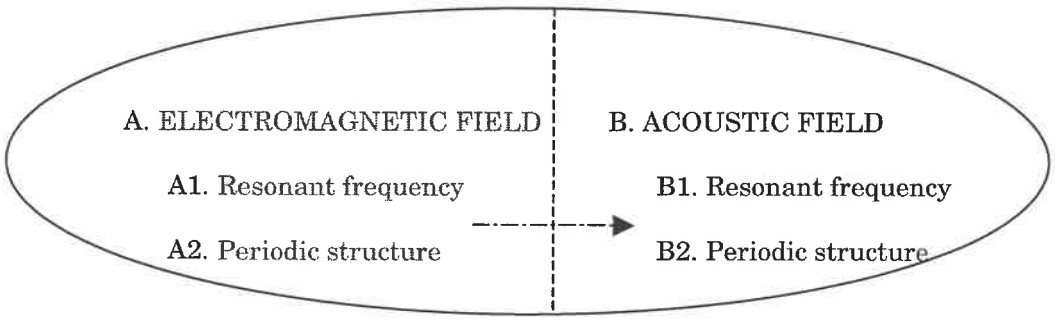

Figure 1.2 Construction of this thesis

1.1 Review of the literature

For a periodic disk-loaded cylindrical waveguide, the electromagnetic field analysis was first qualitatively and quantitatively discussed in Chu and Hansen's paper [5]. Based on the equations described in that paper [5], Qureshi [6] studied the characteristics of a cylindrical disk-loaded slow-wave structure by theoretical, experimental, and computational techniques. More recently, Pruiksma *et al.* [7] presented an analytical description of electromagnetic field in a periodically disk-loaded circular waveguide by using the mode-matching technique. In this thesis, the method of lines (MoL) is chosen to analyze such periodic cylindrical waveguides. Its semi-analytical procedure saves a lot of computing time compared to other numerical methods such as finite element method, finite difference method, and mode matching technique.

The MoL was firstly proposed by Schulz and Pregla [8] to analyze planar waveguides. The extension to planar periodic structures was investigated by Worm and Pregla [9], while Diestel and Worm have developed a nonuniform procedure [10]. Pascher and Pregla [11] introduced the use of the Kronecker product of matrices for two-dimensional discretization and a fast algorithm for the solution of the characteristic equation for the periodic structures. K.Wu *et al.*[12,13] presented a novel technique based on the Method of Lines algorithm for various complicated planar structures.

For the disk-loaded cylindrical waveguides, the method of lines should be developed in cylindrical coordinates. Thorbun, Agostron, and Tripathi [14] discretized the r-variables in Helmholtz equations with circular lines and successfully solved the remaining equations along the θ-direction. However, they did not elaborate on how to solve the problem at r= 0 (center of the coordinate system), which represents a singular point. Xiao *et al.* [15] suggested discretizing the θ-variable by radial straight lines. The transformation matrices [T], the finite difference operator [P], and the eigenvalues [λ], are different from those in a rectangular coordinates system. Matrix singular value decomposition (SVD) [16] was suggested to solve the numerical convergence problems. In this thesis, we extend Xiao *et al.*[15]'s method to analyze periodic microwave and acoustic waveguides.

1.2 Organization of thesis

Based on the above discussion, this work is centred on numerical analysis of cylindrical waveguide for acoustic and microwave problems by method of lines. The thesis consists of seven chapters. The first chapter is the

introduction. The second chapter presents two- and three- dimensional cylindrical method of lines (CMoL) applied to Helmholtz equations and illustrates the boundary conditions for electromagnetic wave and acoustic wave, respectively.

The third and fourth chapters are related to electromagnetic waves. In third chapter, we solve an eigenvalue problem for an enclosed electromagnetic circular waveguide. Both 2D- and 3D- CMoL are used to obtain resonant frequencies. In the fourth chapter, we solve a propagation problem for a periodic disk-loaded circular waveguide with axial symmetry by 2D CMoL.

The fifth and sixth chapters are related to acoustic waves. In the fifth chapter, we investigate an infinite long circular waveguide by 2D CMoL for a propagation problem, and then we study an enclosed acoustic circular waveguide for an eigenvalue problem by both 2D- and 3D- CMoL to obtain resonant frequencies. In the sixth chapter, we investigate a periodic disk-loaded circular waveguide with axial symmetry by 2D CMoL for a propagation problem. A good agreement is observed by comparing the numerical results with the experimental results.

The conclusions of this thesis and recommendation for future work are presented in the final chapter.

CHAPTER 2

CYLIDRICAL METHOD OF LINES (CMoL)

This chapter generally presents the cylindrical method of lines (CMoL) applied to solve Helmholtz equation in a circular coordinates system. The lateral boundary conditions are also illustrated for the applications of CMoL in the following chapters.

2.1 Introduction

The method of lines was used to solve partial differential equations back in the 60's. The application of this method to the microwave was first proposed in the 80's. Most of the applications were related to structures in rectangular coordinates. There are only several papers [14,15,17] in connection with the application of MoL to electromagnetic problems in cylindrical coordinates. As far as we know, the MoL has not been applied to analyze the acoustic structures yet.

In this work, the CMoL is selected to analyze a periodic cylindrical waveguide as shown in Figure 1.1 for both electromagnetic and acoustic problems. The basic idea of our method is to reduce a system of partial differential equations to ordinary differential equations by discretizing all but one of the independent variables in Helmholtz equation. Besides analyses of the periodic cylindrical waveguides in this thesis, the CMoL is also used to investigate two geometries related to periodic structures. One is an infinite long cylindrical waveguide as the inner diameter of disks in a

periodic structure is equal to the outer diameter of disks. The other is an enclosed cylindrical resonator as the inner diameter of disks equals to zero.

2.2 2D and 3D Helmholtz equations in the cylindrical coordinates

For a general problem, a 3D Helmholtz equation in the cylindrical coordinates is required which can be described by the scalar potential $\psi(r,\theta,z)$ as follows,

$$\frac{1}{r}\frac{\partial}{\partial r}\left(r\frac{\partial\psi(r,\theta,z)}{\partial r}\right)+\frac{1}{r^2}\frac{\partial^2\psi(r,\theta,z)}{\partial\theta^2}+\frac{\partial^2\psi(r,\theta,z)}{\partial z^2}+k_0^2\psi(r,\theta,z)=0 \tag{2.1}$$

where the dependence $e^{j\omega t}$ has been assumed and $k_0=\omega/c=2\pi f/c$.

For some special cases such as an infinite long cylindrical waveguide and a circular waveguide with axis symmetry, the above 3D Helmholtz equation degenerates into a 2D Helmholtz equation. The scalar potential $\psi(r,\theta,z)$ evolves into $\psi(r,\theta)e^{-j\beta z}$ or $\psi(r,z)$.

For an infinite long circular cylindrical waveguide, by assuming the dependence as $e^{j(\omega t-\beta z)}$, the scalar potential $\psi(r,\theta,z)$ can be written as $\psi(r,\theta)e^{-j\beta z}$, and $\psi(r,\theta)$ satisfies the Helmhotz equation in polar coordinates with r and θ

$$\frac{1}{r}\frac{\partial}{\partial r}\left(r\frac{\partial\psi(r,\theta)}{\partial r}\right)+\frac{1}{r^2}\frac{\partial^2\psi(r,\theta)}{\partial\theta^2}+\left(k_0^2-\beta^2\right)\psi(r,\theta)=0 \tag{2.2}$$

For a circular waveguide with axis of symmetry, by assuming the dependence as $e^{j\omega t}$, the scalar potential $\psi(r,\theta,z)$ can be revised as $\psi(r,z)$ with modes independent on θ. The potential $\psi(r,z)$ satisfies the Helmhotz equation in variables r and z as follows,

$$\frac{1}{r}\frac{\partial}{\partial r}\left(r\frac{\partial\psi(r,z)}{\partial r}\right)+\frac{\partial^2\psi(r,z)}{\partial z^2}+k_0^2\psi(r,z)=0 \tag{2.3}$$

Here, in the case of considering a microwave problem, the scalar potential ψ is referred to electric potential ψ^e or magnetic potential ψ^h. The electromagnetic field can be calculated by

$$\vec{E}=\nabla\times\nabla\times(\psi^e\vec{u}_z)/j\omega\varepsilon-\nabla\times(\psi^h\vec{u}_z) \tag{2.4}$$

and

$$\vec{H}=\nabla\times(\psi^e\vec{u}_z)+\nabla\times\nabla\times(\psi^h\vec{u}_z)/j\omega\mu_0 \tag{2.5}$$

In acoustics, the scalar potential ψ is referred to the velocity potential and is related to all the acoustic parameters. From the velocity potential, acoustic pressure P and particle velocity **u** can be derived by the following equations

$$P=-j\rho\omega\psi \tag{2.6}$$

and

$$\vec{u}=\nabla\psi \tag{2.7}$$

where ρ is the density of the medium.

2.3 Semi-analytical solution of 2D Helmholtz equation ——Discretizing in the θ-direction

As mentioned in section 2.2, by assuming the dependence as $e^{j(\omega t-\beta z)}$, the scalar potential $\psi(r,\theta)$ satisfies the Helmhotz equation in polar coordinates r and θ

$$\frac{1}{r}\frac{\partial}{\partial r}\left(r\frac{\partial\psi(r,\theta)}{\partial r}\right)+\frac{1}{r^2}\frac{\partial^2\psi(r,\theta)}{\partial\theta^2}+\left(k_0^2-\beta^2\right)\psi(r,\theta)=0 \qquad (2.2)$$

The domain of calculation is discretized along the angular direction by an ensemble of straight lines along the r-direction, which is shown in Figure 2.1.

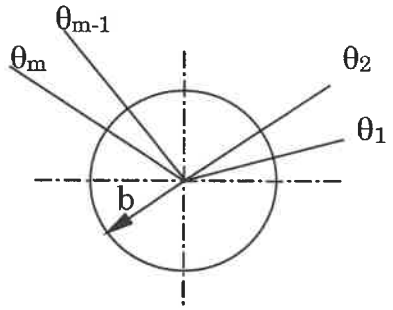

Figure 2.1 Discretion along angular direction

The uniformly discretized θ-variable reads then

$$\psi_k=\psi_1+(k-1)h_\theta=2\pi k/N_\theta \qquad \text{and} \quad k=1,2,\ldots,N_\theta \qquad (2.8)$$

where $h_\theta=2\pi/N_\theta$ (2.9)

with N_θ being the number of discretization lines, and h_θ being the angular spacing between the lines.

Using the central finite differences

$$\left.\frac{\partial \psi}{\partial \theta}\right|_{k+0.5} = \frac{\psi_{k+1} - \psi_k}{h_\theta} + o(h^2) \tag{2.10}$$

($h_\theta = 2\pi/N_\theta$), the above equation can be written in matrix form

$$h_\theta \left.\frac{\partial \overline{\psi}}{\partial \theta}\right|_{k+0.5} = [D]_\theta \overline{\psi} \tag{2.11}$$

where
$$\overline{\psi} = \begin{bmatrix} \psi(r,\theta_1) \\ \psi(r,\theta_2) \\ \dots \\ \psi(r,\theta_{N\theta-1}) \\ \psi(r,\theta_{N\theta}) \end{bmatrix} \tag{2.12}$$

and
$$[D]_\theta = \begin{bmatrix} -1 & 1 & 0 & \dots & 0 & 0 \\ 0 & -1 & 1 & \dots & 0 & 0 \\ 0 & 0 & -1 & \dots & 0 & 0 \\ \dots & \dots & \dots & \dots & \dots & \dots \\ 0 & 0 & 0 & \dots & -1 & 1 \\ 1 & 0 & 0 & \dots & 0 & -1 \end{bmatrix} \tag{2.13}$$

Here $\overline{\psi}$ is a vector with N_θ elements, and $[D]_\theta$ is a $N_\theta \times N_\theta$ bi-diagonal matrix. It should be noted that in cylindrical coordinates, the field components satisfy the periodic condition without any phase delay because any physical characteristic repeats itself after rotating 360°. This periodic condition is usually called a natural boundary condition. The operator $[D]_\theta$ used here is applied to this condition, namely

$$\psi(r,\theta_k) = \psi(r, 2\pi + \theta_k) \qquad or \qquad \psi_k = \psi_{N_\theta + k} \tag{2.14}$$

The central finite difference scheme is used again to calculate the second order partial differential operator from the first order one as

$$
\begin{aligned}
h_\theta^2 \frac{\partial^2 \overline{\psi}}{\partial \theta^2}\bigg|_i &= h \frac{\partial}{\partial \theta}\left(h_\theta \frac{\partial \overline{\psi}}{\partial \theta} \right)\bigg|_i \\
&= h_\theta \frac{h_\theta \dfrac{\partial \psi}{\partial \theta}\bigg|_{i+0.5} - h_\theta \dfrac{\partial \psi}{\partial \theta}\bigg|_{i-0.5}}{h_\theta} \\
&= \left(-[D]_\theta^t \right)[D]_\theta \overline{\psi} \\
&= -[P]_\theta \overline{\psi}
\end{aligned}
\tag{2.15}
$$

where $[P]_\theta = [D]_\theta\,[D]_\theta^t = [D]_\theta^t\,[D]_\theta$ (2.16)

and

$$
[P]_\theta = \begin{bmatrix}
2 & -1 & 0 & \dots & 0 & 0 & -1 \\
-1 & 2 & -1 & \dots & 0 & 0 & 0 \\
\dots & \dots & \dots & \dots & \dots & \dots & \dots \\
\dots & \dots & \dots & \dots & \dots & \dots & \dots \\
0 & 0 & 0 & \dots & -1 & 2 & -1 \\
-1 & 0 & 0 & \dots & 0 & -1 & 2
\end{bmatrix}
\tag{2.17}
$$

Here $[D]_\theta^t$ is the transpose matrix of $[D]_\theta$. By introducing equation (2.17) into equation (2.2), a set of ordinary differential equations is obtained,

$$
r \frac{d}{dr}\left(r \frac{d\overline{\psi}}{dr} \right) + k_c^2 r^2 \overline{\psi} - \frac{[P]_\theta \overline{\psi}}{h_\theta^2} = \overline{\gamma}
\tag{2.18}
$$

and

$$
\overline{\gamma} = \frac{h_\theta^2 \partial^4 \overline{\psi}}{12 \partial \theta^4} + \frac{h_\theta^4}{360} \frac{\partial^2 \overline{\psi}}{\partial \theta^6} + o\left(h^6\right)
\tag{2.19}
$$

where γ is the error terms introduced by the finite difference operation, and $k_c^2 = k_0^2 - \beta^2$. The next task is to find an orthogonal matrix [T] to transform the variables in order to decouple the above equation and find an analytical

solution for it in radial direction. The matrix $[P]_\theta$ can be factorized by an orthogonal matrix [T] as

$$[T]^t[P]_\theta[T]=\text{diag}\{\lambda_1,\lambda_2,\ldots,\lambda_k,\ldots,\lambda_{N\theta}\}=[\lambda]_\theta \tag{2.20}$$

where

$$T_{ij}=\{\cos\alpha_{ij}+\sin\alpha_{ij}\}/(N_\theta)^{1/2},\ \lambda_k=2-2\cos\Delta_k \tag{2.21}$$

and $$\alpha_{ij}=ijh_\theta,\ \Delta_k=kh_\theta,\ h_\theta=2\pi/N_\theta,\quad \text{and}\quad i,j,k=1,2,\ldots,N_\theta \tag{2.22}$$

Assuming that $\overline{\psi}=[T]\overline{\varphi}$, the set of coupled Helmholtz equations in equation (2.18) can be decoupled into a set of independent ordinary differential equations of Bessel forms:

$$\frac{d}{rdr}\left(r\frac{d\varphi_k}{dr}\right)+\left(k_c^2-\frac{\mu_k^2}{r^2}\right)=0 \tag{2.23}$$

where $\mu_k=2\sin(\Delta_k/2)/h_\theta$, $\overline{\varphi}=[\varphi_1,\varphi_2,\ldots,\varphi_k,\ldots,\varphi_{N\theta}]$, and $k=1,2,\ldots,N_\theta$. φ_k is the transformed potential function, and can be written as a superposition of Bessel and Neumann function of u_k-order

$$\varphi_k=A_kJ_{\mu_k}(k_cr)+B_kY_{\mu_k}(k_cr) \tag{2.24}$$

where A_k and B_k are constants. $J_{\mu k}(k_cr)$ is the first kind of Bessel function of order μ_k and $Y_{\mu k}(k_cr)$ is the second kind of Bessel function (Neumann function) of order μ_k.

2.4 Semi-analytical solution of 2D Helmholtz equation ——Discretizing in the z-direction

As mentioned in section 2.2, by assuming the dependence as $e^{j\omega t}$ and no θ dependence, the scalar potential $\psi(r,z)$ satisfies the Helmhotz equation in polar coordinates r and z

$$\frac{1}{r}\frac{\partial}{\partial r}\left(r\frac{\partial\psi(r,z)}{\partial r}\right)+\frac{\partial^2\psi(r,z)}{\partial z^2}+k_0^2\psi(r,z)=0 \tag{2.3}$$

The domain of calculation is discretized along the longitudinal direction by an ensemble of parallel lines along the z-direction, which is shown in Figure 2.2.

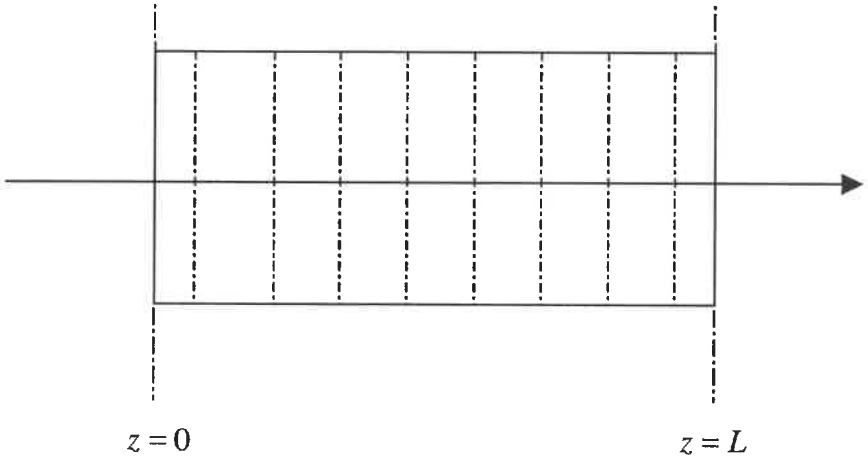

Figure 2.2 Discretion along z-direction

The uniformly discretized z-variable reads then

$$\psi_k=\psi_1+(k-1)h_z \qquad \text{and} \qquad \text{k= 1,2,..., } N_z \tag{2.25}$$

with N_z the number of discretization lines, and h_z being the longitudinal spacing between the lines.

Using the central finite differences

$$\left.\frac{\partial \psi}{\partial z}\right|_{k+0.5} = \frac{\psi_{k+1} - \psi_k}{h_z} + o(h^2) \tag{2.26}$$

the above equation can be written in matrix form

$$h_z \left.\frac{\partial \overline{\psi}}{\partial z}\right|_{k+0.5} = [D]_z \overline{\psi} \tag{2.27}$$

where $$\overline{\psi} = \begin{bmatrix} \psi(r, z_1) \\ \psi(r, z_2) \\ \dots \\ \psi(r, z_{Nz-1}) \\ \psi(r, z_{Nz}) \end{bmatrix} \tag{2.28}$$

Here $\overline{\psi}$ is a vector with N_z elements, and $[D]_z$ is a $N_z \times N_z$ matrix. The first order difference operator $[D]_z$ and h_z depend on the lateral boundary conditions. In this thesis, there are three kinds of boundary conditions of interest in the z-direction: Dirichlet-Dirichlet (D-D), Neumann-Neumann (N-N), and periodic boundary conditions.

For D-D boundary condition, we have

$$h_z = \frac{L}{N_z + 1} \tag{2.29a}$$

$$\psi(r, z)\big|_{z=0} = \psi(r, z)\big|_{z=L} = 0 \tag{2.29b}$$

For N-N boundary condition, we have

$$h_z = \frac{L}{N_z} \tag{2.30a}$$

$$\left.\frac{\partial \psi(r,z)}{\partial z}\right|_{z=0} = \left.\frac{\partial \psi(r,z)}{\partial z}\right|_{z=L} = 0 \tag{2.30b}$$

and for periodic boundary condition, we have

$$h_z = \frac{L}{N_z} \tag{2.31a}$$

$$\psi(r,z) = e^{j\beta L}\psi(r,z+L) \tag{2.31b}$$

The central finite difference scheme is again used to calculate the second order partial differential operator from the first order one as

$$\begin{aligned} h_z^2 \left.\frac{\partial^2 \overline{\psi}}{\partial z^2}\right|_i &= h \frac{\partial}{\partial z}\left(h_z \left.\frac{\partial \overline{\psi}}{\partial z}\right)\right|_i \\ &= h_z \frac{h_z \left.\frac{\partial \psi}{\partial z}\right|_{i+0.5} - h_z \left.\frac{\partial \psi}{\partial z}\right|_{i-0.5}}{h_z} \\ &= \left(-[D]_z^t\right)[D]_z \overline{\psi} \\ &= [P]_z \overline{\psi} \end{aligned} \tag{2.32}$$

where $[P]_z = -[D]_z [D]_z^t = -[D]_z^t [D]_z$ (2.33)

$$\text{and} \quad [P]_z = \begin{bmatrix} -2 & 1 & \dots & \dots & \dots & \dots \\ 1 & -2 & 1 & \dots & \dots & \dots \\ \dots & \dots & \dots & \dots & \dots & \dots \\ \dots & \dots & \dots & \dots & \dots & \dots \\ \dots & \dots & \dots & 1 & -2 & 1 \\ \dots & \dots & \dots & \dots & 1 & -2 \end{bmatrix} \quad \text{for D-D} \tag{2.34a}$$

$$= \begin{bmatrix} -1 & 1 & \dots & \dots & \dots & \dots \\ 1 & -2 & 1 & \dots & \dots & \dots \\ \dots & \dots & \dots & \dots & \dots & \dots \\ \dots & \dots & \dots & \dots & \dots & \dots \\ \dots & \dots & \dots & 1 & -2 & 1 \\ \dots & \dots & \dots & \dots & 1 & -1 \end{bmatrix} \quad \text{for N-N} \tag{2.34b}$$

$$= \begin{bmatrix} -2 & 1 & \dots & \dots & \dots & e^{j\beta L} \\ 1 & -2 & 1 & \dots & \dots & \dots \\ \dots & \dots & \dots & \dots & \dots & \dots \\ \dots & \dots & \dots & \dots & \dots & \dots \\ \dots & \dots & \dots & 1 & -2 & 1 \\ e^{-j\beta L} & \dots & \dots & \dots & 1 & -2 \end{bmatrix} \quad \text{for periodic boundary condition}$$

(2.34c)

Here $[D]_z^t$ is the transpose matrix of $[D]_z$. By introducing equation (2.34) into equation (2.3), a set of ordinary differential equations are obtained,

$$\frac{d}{rdr}\left(r\frac{d\overline{\psi}}{dr}\right)+\frac{[P]_z\overline{\psi}}{h_z^2}+k_0^2\overline{\psi} = 0 \tag{2.35}$$

The next task is to find an orthogonal matrix [T] to transform the variables in order to decouple the above equation and also to find its analytical solution in radial direction. The matrix $[P]_z$ can be factorized by an orthogonal matrix [T] as

$$[T]^t[P]_z[T]=\mathrm{diag}\{\delta_1,\delta_2,\ldots,\delta_k,\ldots,\delta_{Nz}\} \tag{2.36}$$

The orthogonal matrix [T] and the eigenvalues $[\delta]$ are written as in the following forms according to different lateral boundary conditions.

For D-D boundary condition,

$$[T]_{mn}=\sqrt{\frac{2}{N_z+1}}\sin\frac{mn\pi}{N_z+1} \tag{2.37a}$$

$$\delta_k=-4\sin^2\frac{k\pi}{2(N_z+1)} \tag{2.37b}$$

and $m,n,k=1,2,\cdots,N_z$.

For N-N boundary condition,

$$[T]_{mn}=\begin{cases}\sqrt{\frac{2}{N_z}}\cos\frac{(m-0.5)(n-1)}{N_z} & ;\ n>1\\ \sqrt{\frac{1}{N_z}} & ;\ n=1\end{cases} \tag{2.38a}$$

$$\delta_k=-4\sin^2\left(\frac{(k-1)\pi}{2N_z}\right) \tag{2.38b}$$

and $m,n,k=1,2,\cdots,N_z$.

For periodic boundary condition,

$$[T]_{mk}=\sqrt{\frac{1}{N_z}}\,e^{jm\zeta_k} \tag{2.39a}$$

$$\delta_k = -4\sin^2\left(\frac{\zeta_k}{2}\right) \tag{2.39b}$$

with $$\zeta_k = \frac{2\pi(k-1)-\beta L}{N_z} \tag{2.39c}$$

where $m,n,k = 1,2,\cdots,N_z$, β is the propagation constant in z-direction and L is the length of one period.

Assuming that $\overline{\psi} = [T]\overline{\varphi}$, the set of coupled Helmholtz equations in equation (2.35) can be decoupled into a set of independent ordinary differential equations of Bessel forms:

$$\frac{d}{rdr}\left(r\frac{d\varphi_k}{dr}\right) + \chi_k^2\varphi_k = 0 \tag{2.40}$$

where $$\chi_k^2 = k_0^2 + \frac{\delta_k}{h_z^2} \tag{2.41}$$

Here k=1,2,...,N_z. φ_k is the transformed potential function, and can be written as a superposition of Bessel and Neumann function of 0-order

$$\varphi_k = A_k J_0(\chi_k r) + B_k Y_0(\chi_k r) \tag{2.42}$$

where A_k and B_k are constants. $J_0(\chi_k r)$ is the first kind of Bessel function of zero order and $Y_0(\chi_k r)$ is the second kind of Bessel function (Neumann function) of zero order.

2.5 Semi-analytical solution of 3D Helmholtz equation ——Discretizing in the θ- and z- directions

As mentioned in section 2.2, by assuming the dependence as $e^{j\omega t}$, the scalar potential $\psi(r,\theta,z)$ satisfies the Helmhotz equation in coordinates r, θ and z

$$\frac{1}{r}\frac{\partial}{\partial r}\left(r\frac{\partial\psi(r,\theta,z)}{\partial r}\right)+\frac{\partial^2\psi(r,\theta,z)}{\partial z^2}+\frac{\partial^2\psi(r,\theta,z)}{\partial z^2}+k_0^2\psi(r,\theta,z)=0 \qquad (2.1)$$

The domain of calculation is now discretized in θ- and z-directions by a number of straight lines along the r-directions. The θ-variables are discretized uniformly by using radial lines at $\psi_{ki}=\psi_{1i}+(k-1)h_\theta$, $k=1,2,\cdots,N_\theta$, with h_θ being the angular spacing between the lines. The z-variable is discretized uniformly by using radial lines at

$$\psi_{ki}=\psi_{k1}+(i-1)h_z, \qquad i=1,2,\ldots,N_z \qquad (2.43)$$

with h_z being the spacing between the lines in z-direction.

The first order finite difference operator is approximated by the central finite differences as

$$\left.\frac{\partial\psi}{\partial\theta}\right|_{k+0.5}=\frac{\psi_{k+1}-\psi_k}{h_\theta} \quad \text{and} \quad \left.\frac{\partial\psi}{\partial\theta}\right|_{i+0.5}=\frac{\psi_{i+1}-\psi_i}{h_z} \qquad (2.44)$$

where the vector ψ is in matrix form as

$$\overline{\psi}=[\psi]=\begin{bmatrix}\psi_{11} & \psi_{12} & \cdots & \psi_{1i} & \cdots & \psi_{1N_z}\\ \psi_{21} & \psi_{22} & \cdots & \psi_{2i} & \cdots & \psi_{2N_z}\\ \cdots & \cdots & \cdots & \cdots & \cdots & \cdots\\ \psi_{ki} & \psi_{k2} & \cdots & \psi_{ki} & \cdots & \psi_{kN_z}\\ \cdots & \cdots & \cdots & \cdots & \cdots & \cdots\\ \psi_{N_\theta 1} & \psi_{N_\theta 2} & \cdots & \psi_{N_\theta i} & \cdots & \psi_{N_\theta N_z}\end{bmatrix} \qquad (2.45)$$

or its derivatives

$$h_\theta \frac{\partial \overline{\psi}}{\partial \theta}\bigg|_{k+0.5} = [D]_\theta \overline{\psi} \quad , \quad h_z \frac{\partial \overline{\psi}}{\partial \theta}\bigg|_{i+0.5} = \overline{\psi}[D]_z^t \tag{2.46}$$

Using the central finite difference scheme again to calculate the second order partial differential operator from the first order one yields

$$h_\theta^2 \frac{\partial^2 \overline{\psi}}{\partial \theta^2}\bigg|_k = \left(-[D]_\theta^t\right)[D]_\theta \overline{\psi} = -[P]_\theta \overline{\psi} \tag{2.47}$$

$$h_z^2 \frac{\partial^2 \overline{\psi}}{\partial z^2}\bigg|_i = \overline{\psi}\left(-[D]_z^t\right)[D]_z = \overline{\psi}\left([P]_z^t\right) \tag{2.48}$$

where $[P]_\theta = [D]_\theta [D]_\theta^t = [D]_\theta^t [D]_\theta$, and an orthogonal matrix $[T]_\theta$ can be found in section 2.3. $[P]_z = -[D]_z [D]_z^t$, and an orthogonal matrix $[T]_z$ can be found in section 2.4. Substituting equations (2.47) and (2.48) into equation (2.1), the 3D Helmholtz equation will be as follows:

$$\frac{d}{rdr}\left(r\frac{d\overline{\psi}}{dr}\right) - \frac{[P]_\theta \overline{\psi}}{r^2 h_\theta^2} + \frac{\overline{\psi}[P]_z^t}{h_z^2} + k_0^2 \overline{\psi} = 0 \tag{2.49}$$

In order to solve equation (2.49), the Kronecker product [4] is introduced here. If **A** and **B** are $m \times n$ and $p \times q$ matrices, respectively, the Kronecker product is an $mp \times nq$ matrix defined by

$$A \otimes B = \begin{bmatrix} a_{11}B & \cdots & a_{1n}B \\ \vdots & \vdots & \vdots \\ a_{m1}B & \cdots & a_{mn}B \end{bmatrix} \tag{2.50}$$

At first, matrix $\overline{\psi}$ in equation (2.49) is replaced by a vector $\overline{\psi}$

$$\overline{\psi} = [\psi]_{(N_\theta \times N_z)\times 1}$$
$$= [\psi_{11} \quad \psi_{21} \quad \cdots \quad \psi_{N_\theta 1} \quad \psi_{12} \quad \psi_{22} \quad \cdots \quad \psi_{N_\theta 2} \quad \cdots \quad \cdots \quad \psi_{1N_z} \quad \psi_{2N_z} \quad \cdots \quad \psi_{N_\theta N_z}]^t \tag{2.51}$$

Secondly, matrices $[P]_\theta$ and $[P]_z$ in equation(2.49) are replaced by matrices $[\hat{P}]_\theta$ and $[\hat{P}]_z$, respectively.

$$[P]_\theta \rightarrow [\hat{P}]_\theta = I_z \otimes [P]_\theta \tag{2.52a}$$

$$[P]_z \rightarrow [\hat{P}]_z = [P]_z \otimes I_\theta \tag{2.52b}$$

where I_z and I_θ are identity matrices of a dimension of N_z and N_θ, respectively. The second order partial differential operators then become as follows,

$$h_\theta^2 \frac{\partial^2 \overline{\psi}}{\partial \theta^2} = -[\hat{P}]_\theta \overline{\psi} \tag{2.53a}$$

and

$$h_z^2 \frac{\partial^2 \overline{\psi}}{\partial z^2} = [\hat{P}]_z \overline{\psi} \tag{2.53b}$$

Thus, the equation (2.49) is evolved into

$$\frac{1}{r}\frac{\partial}{\partial r}\left(r\frac{\partial \overline{\psi}}{\partial r}\right) - \frac{[\hat{P}]_\theta}{r^2 h_\theta^2}\overline{\psi} + \frac{[\hat{P}]_z}{h_z^2}\overline{\psi} + k_0^2 \overline{\psi} = 0 \tag{2.54}$$

By defining the transformed quantities as $\overline{\psi} = \hat{T}\overline{\varphi}$, where an orthogonal matrix $\hat{T} = T_z \otimes T_\theta$, the above equation (2.54) becomes

$$\frac{1}{r}\frac{\partial}{\partial r}\left(r\frac{\partial}{\partial r}\left(\hat{T}\overline{\varphi}\right)\right) - \frac{[\hat{P}]_\theta}{r^2 h_\theta^2}\left(\hat{T}\overline{\varphi}\right) + \frac{[\hat{P}]_z}{h_z^2}\left(\hat{T}\overline{\varphi}\right) + k_0^2\left(\hat{T}\overline{\varphi}\right) = 0 \tag{2.55}$$

Multiplying $\hat{T}^t$ from the left side of equation (2.55) and the set of Helmholtz equations in equation (2.54) can be decoupled into a set of independent ordinary differential equations of Bessel form

$$\frac{d}{rdr}\left(r\frac{d\overline{\varphi}}{dr}\right)+\left[\left(k_0^2\hat{I}+\frac{\hat{\delta}_z}{h_z^2}\right)-\frac{\hat{\lambda}_\theta}{r^2h_\theta^2}\right]\overline{\varphi}=0 \tag{2.56}$$

or

$$\frac{d}{rdr}\left(r\frac{d\varphi_{ki}}{dr}\right)+\left(\chi_{ii}^2-\frac{\hat{\mu}_k^2}{r^2}\right)\varphi_{ki}=0, \tag{2.57}$$

where $$\chi_{ii}^2=\left(k_o^2+\frac{\hat{\delta}_{zii}}{h_z^2}\right),\qquad \hat{\mu}_k^2=\frac{\hat{\lambda}_{\theta kk}}{h_\theta^2} \tag{2.58}$$

where φ_{ki} (k=1,2,3,...,N_θ; i=1,2,3,...N_z) is called the transformed potential function. In every uniform region, a solution of equation (2.56) or (2.57) may be written as a superposition of Bessel functions of u_k-order,

$$\varphi_{ki}=A_{ki}J_{\mu_k}(\chi_{ii}r)+B_{ki}Y_{\mu_k}(\chi_{ii}r) \tag{2.59}$$

It should be noticed that when the region of the solution contains the origin $r=0$, B_k in equations (2.24) and (2.42), as well as B_{ki} in equation (2.59) must be zero since Y_{μ_k} is singular. Once equations (2.23), (2.40) and (2.57) are solved in every uniform region, the potentials ψ can be obtained by $\overline{\psi}=[T]\overline{\varphi}$ or $\overline{\psi}=\hat{T}\overline{\varphi}$.

2.6 Conclusion

In this chapter, semi-analytical solutions of 2D and 3D Helmholtz equations have been presented by implementing cylindrical Method of Lines. The solution of 3D Helmholtz equation was derived by discretizing the potential $\psi(r,\theta,z)$ in the θ and z directions, in the meantime the Kronecker product was introduced. For the infinite long cylindrical waveguide or the circular waveguide with axis symmetry, the 3D Helmholtz equation was evolved into the 2D Helmholtz equations. The solutions of 2D Helmholtz equations have been obtained by discretizing the θ-variable or z-variable with the decoupling procedure applied. From the third chapter to the sixth chapter, these solutions will be used to solve electromagnetic and acoustic wave problems.

CHAPTER 3

CHARATERIZATION OF MICROWAVE RESONATORS USING CMoL

In this chapter, we present an eigenvalue problem for an enclosed electromagnetic circular waveguide. Based on the method illustrated in Chapter Two, both 2D- and 3D- CMoL are used to obtain the resonant frequencies.

3.1 Introduction

A cylindrical resonator as shown in Figure.3.1 is analyzed in this chapter. Such a cylindrical resonator can be regarded as one segment of a periodic structure as shown in Figure 1.1. The periodic structure is composed of multiple segments with coupling between neighbor ones.

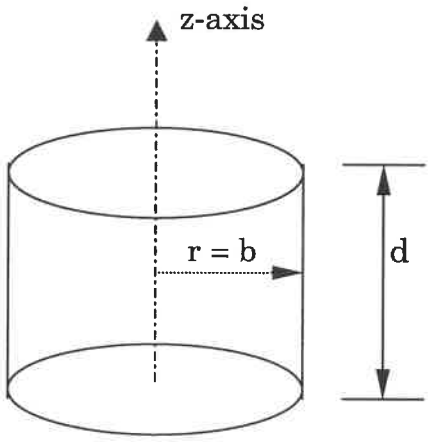

Figure 3.1 A cylindrical resonator

Two cases are analyzed in the following. Case A is from Pruiksma et al. [7]'s paper, and Case B is from Wallett et al.[6]'s paper. Both of these two papers describe the investigation of periodic disk-loaded cylindrical waveguids for TM modes. The geometrical parameters are listed in Table 3-1, and are used to validate our 2D and 3D CMoL programs for both TE and TM modes.

Table 3-1 Main parameters for microwave cylindrical resonators

	Case A		Case B	
Outer radius b	39	mm	0.15	inch
Length d	33.33	mm	0.17	inch
Mode of interest	TM_{0n} mode		TM_{01} mode	
Frequency of interest	2.944-3.040 GHz		14.50-16.00 GHz	

3.2 Solution of 3D Helmholtz equation by 3D CMoL

Based on the method in Chapter Two, a program of 3D CMoL for microwave cylindrical resonators is developed for both TE and TM modes. Here, both the angular and longitudinal variables θ and z have been discretized.

The finite difference operator $[P]_\theta$, the orthogonal transformation matrix $[T]_\theta$, and the eigenvalues $[\lambda]$ are the same for both TE and TM modes, which can be found in Chapter Two, section 2.3.

The lateral boundary conditions in the z-direction can be obtained by analyzing the field components. From equations (2.4), (2.5) in Chapter Two, we can write the six field components in cylindrical coordinates as follows,

$$E_\theta = \frac{1}{j\omega\varepsilon}\left(\frac{1}{r}\frac{\partial^2\psi^e}{\partial\theta\partial z}\right)+\frac{\partial\psi^h}{\partial r} \tag{3.1a}$$

$$E_r = \frac{1}{j\omega\varepsilon}\left(\frac{\partial^2\psi^e}{\partial r\partial z}\right)-\frac{1}{r}\frac{\partial\psi^h}{\partial\theta} \tag{3.1b}$$

$$E_z = -\frac{1}{j\omega\varepsilon}\left(\frac{1}{r}\frac{\partial}{\partial r}\left(r\frac{\partial\psi^e}{\partial r}\right)+\frac{1}{r^2}\frac{\partial^2\psi^e}{\partial\theta^2}\right) \tag{3.1c}$$

$$H_\theta = \frac{1}{j\omega\mu_0}\left(\frac{1}{r}\frac{\partial^2\psi^h}{\partial\theta\partial z}\right)-\frac{\partial\psi^e}{\partial r} \tag{3.1d}$$

$$H_r = \frac{1}{j\omega\mu_0}\left(\frac{\partial^2\psi^h}{\partial r\partial z}\right)+\frac{1}{r}\frac{\partial\psi^e}{\partial r} \tag{3.1e}$$

$$H_z = -\frac{1}{j\omega\mu_0}\left(\frac{1}{r}\frac{\partial}{\partial r}\left(r\frac{\partial\psi^h}{\partial r}\right)+\frac{1}{r^2}\frac{\partial^2\psi^h}{\partial\theta^2}\right) \tag{3.1f}$$

We know that on an electric wall the tangential component of electric field **E** and the normal component of magnetic field **H** are zeros, that is, $\vec{n}\times\vec{E}=0$ and $\vec{n}\bullet\vec{H}=0$. In Figure 3.1, for the electric walls located at the top and bottom planes z=0 and d, we have the tangential components of electric field $E_\theta=E_r=0$, and the normal component of magnetic field $H_z=0$. Since the TM modes may be derived from electric potential ψ^e, from equations (3.1a) and (3.1b), we obtain the boundary conditions for electric potential ψ^e as follows,

$$\left.\frac{\partial \psi^e}{\partial z}\right|_{z=0,d} = 0 \tag{3.2}$$

Similarly, the TE modes may be derived from magnetic potential ψ^h. Thus, from equations (3.1a) and (3.1b), we obtain the boundary conditions for magnetic potential ψ^h as follows

$$\left.\psi^h\right|_{z=0,d} = 0 \tag{3.3}$$

That is to say, for TM modes, the finite difference operator $[P]_z$ along the z-direction may be derived from N-N lateral boundary condition. While, for the TE modes, the matrix $[P]_z$ is satisfied with the D-D boundary condition. The expressions of $[P]_z$, the transformation matrix $[T]_z$, and the eigenvalues $[\delta]$ can be found according to these two boundary conditions.

By means of the Kronecker product, the final solution of 3D Helmholtz equation for the cylindrical resonator is now written as,

$$\overline{\psi} = \hat{T}\overline{\varphi} \tag{3.4a}$$

or

$$[\psi_{ki}] = \hat{T}\left[J_{\hat{\mu}_k}(\chi_{ii} r)\right][A_{ki}] \tag{3.4b}$$

where

$$\hat{T} = T_z \otimes T_\theta \tag{3.5}$$

$$\hat{\mu}_k = \left(\frac{\hat{\lambda}_{\theta_{kk}}}{h_\theta^2}\right)^{\frac{1}{2}} \quad \text{with} \quad \left|\hat{\lambda}\right|_\theta = I_z \otimes [\lambda]_\theta \tag{3.6}$$

$$\chi_{ii} = \left(k_0^2 + \frac{\hat{\delta}_{z_{ii}}}{h_z^2}\right)^{\frac{1}{2}} \quad \text{with} \quad \left|\hat{\delta}\right|_z = [\delta]_z \otimes I_\theta \tag{3.7}$$

For TM modes, since $[P]_z$ belong to N-N case, the expressions of the transformation matrix T_z and the eigenvalues $[\delta]_z$ can be found in equations (2.38a) and (2.38b) in Chapter Two. For TE modes, since $[P]_z$ belongs to D-D case, the expressions of the transformation matrix T_z and the eigenvalues $[\delta]_z$ can be found in equations (2.37a) and (2.37b).

In Figure 3.1, for the electric walls located at the circumference of $r = b$, the boundary conditions are $E_z = E_\theta = 0$ and $H_r = 0$. Thus, for TM modes, we have

$$\psi^e\big|_{r=b} = 0 \tag{3.8}$$

Combining the above equation with equation (3.4b), we obtain

$$\hat{T}\left[J_{\hat{\mu}_k}(\chi_{ii}b)\right][A_{ki}] = 0 \tag{3.9}$$

The nontrivial solution requires the zero determinant of the matrix $\left[J_{\hat{\mu}_k}(\chi_{ii}b)\right]$:

$$\det\left\{\left[J_{\hat{\mu}_k}(\chi_{ii}b)\right]\right\} = 0 \tag{3.10}$$

Similarly, for TE modes, at the circumference of $r = b$, we have

$$\left.\frac{\partial \psi^h}{\partial r}\right|_{r=b} = 0 \tag{3.11}$$

From equation (3.4b), we get

$$\hat{T}\left.\frac{d\left[J_{\hat{\mu}_k}(\chi_{ii}r)\right]}{dr}\right|_{r=b}[A_{ki}] = 0 \tag{3.12}$$

Since $xJ_n'(x) = nJ_n(x) - xJ_{n+1}(x)$ [4], we can obtain

$$[Z]=\left.\frac{d\left[J_{\hat{\mu}_k}(\chi_{ii}r)\right]}{dr}\right|_{r=b}=\left[\frac{\hat{\mu}_k}{b}J_{\hat{\mu}_k}(\chi_{ii}b)-\chi_{ii}J_{\hat{\mu}_k+1}(\chi_{ii}b)\right] \tag{3.13}$$

The nonzero solution of equation (3.12) exists only if the determinant of the matrix [Z] equals to zero. That is,

$$\det\{\ [Z]\ \}=0 \tag{3.14}$$

The resonant frequencies for TM and TE modes can be obtained by solving the equations (3.10) and (3.14), which will be shown in the numerical verification.

3.3 Solution of 2D Helmholtz equation by 2D CMoL

The individual TE and TM modes [18] can be identified by means of the three integers m, n, and k, which are defined as follows:

m = number of full-period variations of E_r with respect to θ

n = number of half-period variations of E_θ with respect to r

k = number of half-period variations of E_r with respect to z

Therefore, if we are only interested in TE_{0nk} or TM_{onk} modes, 2D CMoL is used to obtain the resonant frequencies. In such situation, electromagnetic fields are independent of the variable θ.

Based on the method described in Chapter Two, a program of 2D CMoL for microwave cylindrical resonators is developed for both TE_{0nk} and TM_{onk} modes. Here, only the longitudinal variable has been discretized. The solution can be written as

$$\overline{\psi}=T_z\overline{\varphi} \tag{3.15a}$$

or $$[\psi_k] = T_z [J_0(\chi_k r)][A_k] \tag{3.15b}$$

where $$\chi_k = \left(k_0^2 + \frac{\delta_k}{h_z^2} \right)^{\frac{1}{2}} \tag{3.15c}$$

$k = 1,2,\cdots,N_z$, T_z and δ_k are the orthogonal matrix and the eigenvalues of $[P]_z$. The values of the matrix $[P]_z$ for TE and TM modes, respectively, are the same as those described in the above section. Applying the boundary conditions at $r = b$, for TM_{0nk} modes, we have

$$\det\{ [J_0(\chi_k b)] \} = 0 \tag{3.16}$$

and for TE_{onk} modes, we have

$$\det\{ [\chi_k J_1(\chi_k b)] \} = 0 \tag{3.17}$$

The resonant frequencies can be obtained by solving the above two equations.

3.4 SVD Technique

In equations (3.10), (3.14), (3.16) and (3.17), numerical solutions require the zero determinant of a matrix [Z]. We can search the roots by directly evaluating the determinant of the matrix [Z]. However, in some cases, the presence of poles makes it difficult to detect the zeros as the zeros near the poles as discussed by Labay *et al.*[16]. Thus, it was suggested to use the singular value decomposition technique (SVD) to eliminate poles. Moreover, there are lower and upper limits for the internal representation of a double real number in computer memory. The numerical overflow problem may occur when directly evaluating the determinant of a matrix [Z] with a large size.

In this thesis, SVD method is first used to diagonalize the matrix [Z] by two unitary matrices, [U] and [V] ($[U]^h[U]=[V]^h[V]=[I]$ and $[U]^h[Z][V]=\text{diag}[s_1,s_2,\ldots,s_n]$, where $s_1 > s_2 > \ldots > s_n$. The absolute value of the determinant of the matrix [Z] equals to $\prod_{k=1}^{n} s_k$. Here, instead of calculating $\prod_{k=1}^{n} s_k$, we just pick the last element s_n as suggested by Xiao *et al.* [15]. In Matlab subroutine, the diagonal element s_k is already in the decreasing order. Thus, the finding of the zero determinant of the matrix [Z], is equivalent to the finding of the local minimum points of s_n.

3.5 Numerical verification

In order to validate the MoL algorithm derived in this chapter, both 2D CMoL and 3D CMoL programs are performed to obtain the resonant frequencies. First, we calculate some resonant frequencies for both TE and TM modes from analytical solutions. Then, we investigate the convergences of resonant frequencies for both 2D and 3D CMoL.

3.5.1 Expected resonant frequencies from analytical solutions

The resonant frequencies of TE and TM modes are given by the expression [17]

$$f^2b^2 = 34.825\left\{\left(\frac{\chi_{mn}}{\pi}\right)^2 + \left(\frac{kb}{d}\right)^2\right\} \tag{3.18}$$

Here, f is in GHz, both b and d in inches. As illustrated in section 3.3, the integers m, n, and k are referred to the numbers of variations electric field components with respect to θ, r and z, respectively.

The values of χ_{mn} [18] are listed in Table 3-2. There are two columns of values in Table 3-2. The values of the second column are for TE modes and the fourth column values are for TM modes. It should be noted that the dominant TM mode is TM_{01k} and the electric field component E_r is independent of θ. However, the lower order TE mode is TE_{11k} and the electric field component E_r varies one period along θ-direction. Moreover, for the higher order TE modes such as TE_{01k}, the electric field component E_r is independent of θ.

Table 3-2 Values of χ_{mn}

TE-mode	χ_{mn}	TM-mode	χ_{mn}
11k	1.841	01k	2.405
21k	3.054	11k	3.832
01k	3.832	21k	5.136
31k	4.201	02k	5.520
41k	5.318	31k	6.380
12k	5.332	12k	7.016
51k	6.415	41k	7.588
22k	6.706	22k	8.417
02k	7.016	03k	8.654

3.5.1.1 Case A (b=39 mm=1.535 inch and d=33.33 mm=1.312 inch)

Part of resonant frequencies of case A for the first four TE and the first four TM modes (k=0 and 1) are listed in Table 3-3a and 3-3b. These values are derived from equation (3.18).

Table 3-3a Resonant frequencies of case A for TE mode

K	1
TE_{11k}	5.031
TE_{21k}	5.848
TE_{01k}	6.498
TE_{31k}	6.831

Table 3-3b Resonant frequencies of case A for TM mode

K	0	1
TM_{01k}	2.943	5.375
TM_{11k}	4.689	6.498
TM_{21k}	6.285	7.729
TM_{02k}	6.755	8.116

3.5.1.2 Case B (b=7.62 mm=0.3 inch and d=4.32 mm=0.17 inch)

Part of resonant frequencies of case B for the first four TE and the first four TM modes (k=0 and 1) are listed in Table 3-4a and 3-4b. These values are obtained from equation (3.18).

Table 3-4a Resonant frequencies of case B for TE mode

K	1
TE_{11k}	36.577
TE_{21k}	39.632
TE_{01k}	42.199
TE_{31k}	43.554

Table 3-4b Resonant frequencies of case B for TM mode

k	0	1
TM_{01k}	15.059	37.839
TM_{11k}	23.994	42.199
TM_{21k}	32.159	47.320
TM_{02k}	34.563	48.986

3.5.2 Resonant frequencies from 2D and 3D CMoL solutions

By performing 2D and 3D CMoL programs, resonant frequencies are obtained from numerical simulations. Root searching is first illustrated by four examples. Then, the convergences of both 2D and 3D CMoL are investigated.

3.5.2.1 Roots searching

In this section, four examples as shown in Figs.3.2a, 3.2b, 3.3a and 3.3b are used to illustrate roots searching for both 2D and 3D CMoL programs.

In both Figures.3.2a and 3.2b, the resonant frequency of TE_{011} mode is obtained for Case A by using 2D CMoL. In Figure 3.2a, the determinant of the matrix [Z] is used to find the numerical solution, while in Figure 3.2b, the SVD method is implemented and only the least singular value is used for roots searching. In both Figures.3.2a and 3.2b, Nz is set to be 40.

Figure 3.2a shows that the real and imaginary parts of determinant values with solid and dashdot curves, respectively. The imaginary part of the determinant values is multiplied by a factor of 10^{15} for visibility of variation. As illustrated in Figure 3.2a, there are two zero-crossing points near frequency of 6.426 GHz for the two curves. These two points merge together as expected. This zero-crossing point referring to 6.426 GHz is just the numerical solution of 2D CMoL by calculating the determinant of the coefficient matrix.

For comparison, Figure 3.2b shows the least singular values. As mentioned above, here SVD techniques are implemented to search the roots. There is one local minimum point near frequency of 6.426 GHz. This point is just the numerical solution of 2D CMoL by using SVD technique.

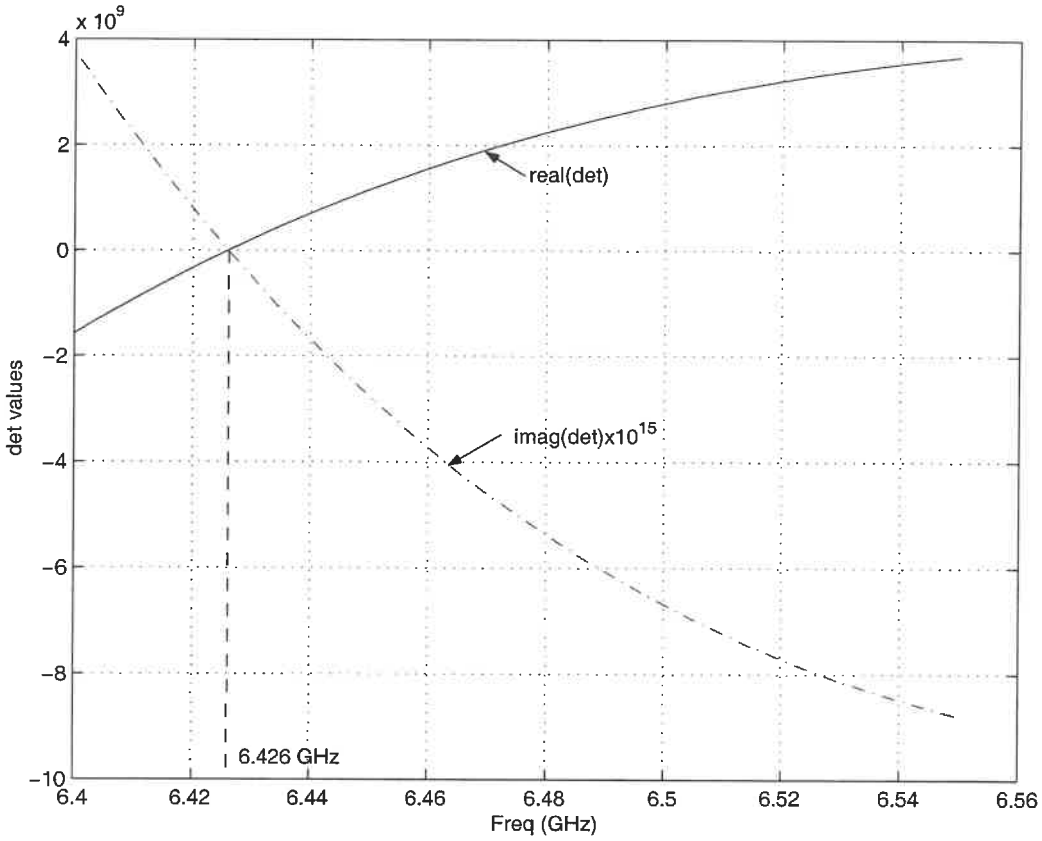

Figure 3.2a Resonant frequency of TE_{011} mode for Case A by using 2D CMoL and by calculating the determinant

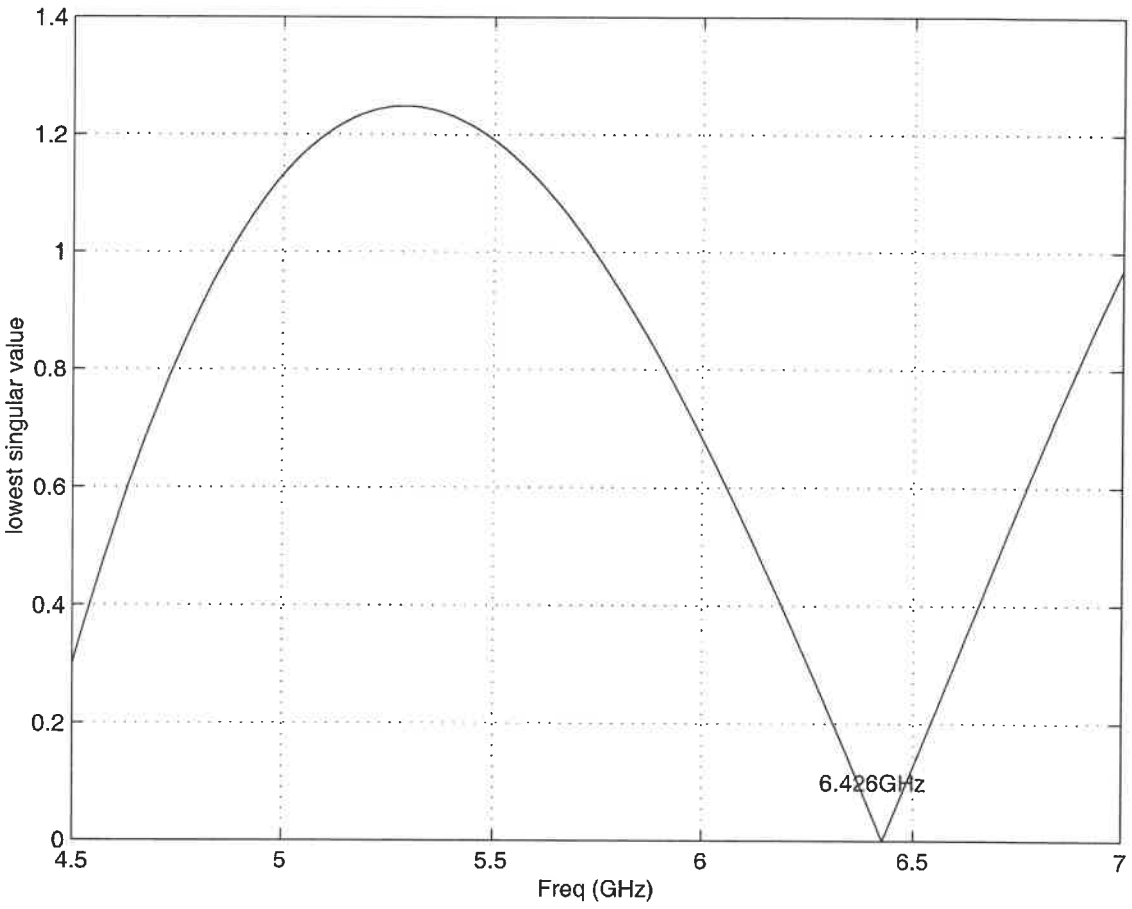

Figure 3.2b Resonant frequency of TE_{011} mode for Case A
by using 2D CMoL and by using the least singular element

In both Figures.3.3a and 3.3b, the resonant frequency of TM_{111} mode is obtained for Case A by using 3D CMoL. In Figure 3.3a, the determinant of the matrix [Z] is used to find the numerical solution, while in Figure 3.3b, the SVD method is implemented and only the least singular value is used for roots searching. In both Figures 3.3a and 3.3b, Nz is set to 7 and N_θ is set to 16.

Figure 3.3a shows that the real and imaginary parts of determinant values with solid and dashdot curves, respectively. As illustrated in Figure 3.3a, there are two zero-crossing points near frequency of 6.467 GHz for the two curves. These two points merge together as expected. This zero-crossing point referring to 6.467 GHz is just the numerical solution of 3D CMoL by calculating the determinant of the coefficient matrix.

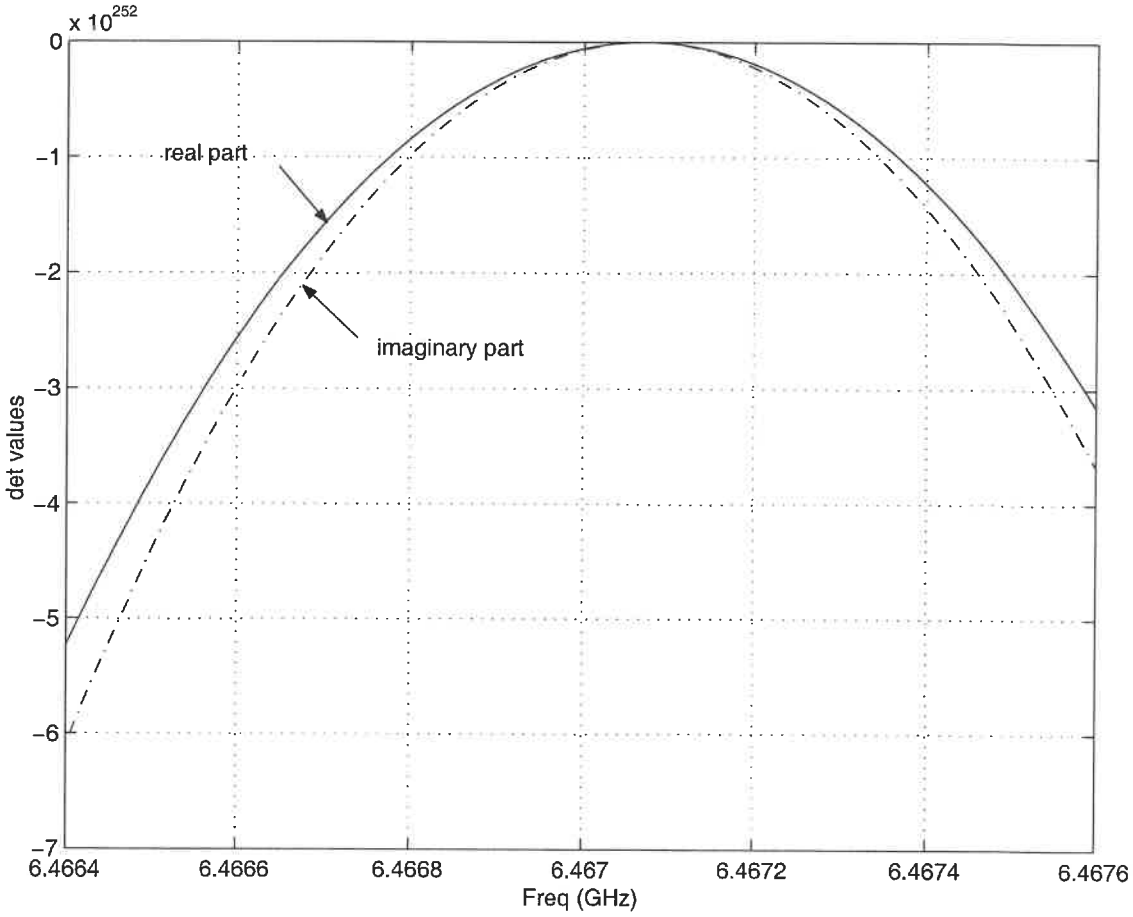

Figure 3.3a Resonant frequency of TM_{111} mode for Case A by using 3D CMoL and by calculating the determinant

For comparison, Figure 3.3b shows the least singular values. As mentioned above, here SVD technique are implemented to search the roots. There is one local minimum point near frequency of 6.467 GHz. This point is just the numerical solution of 3D CMoL by using SVD technique.

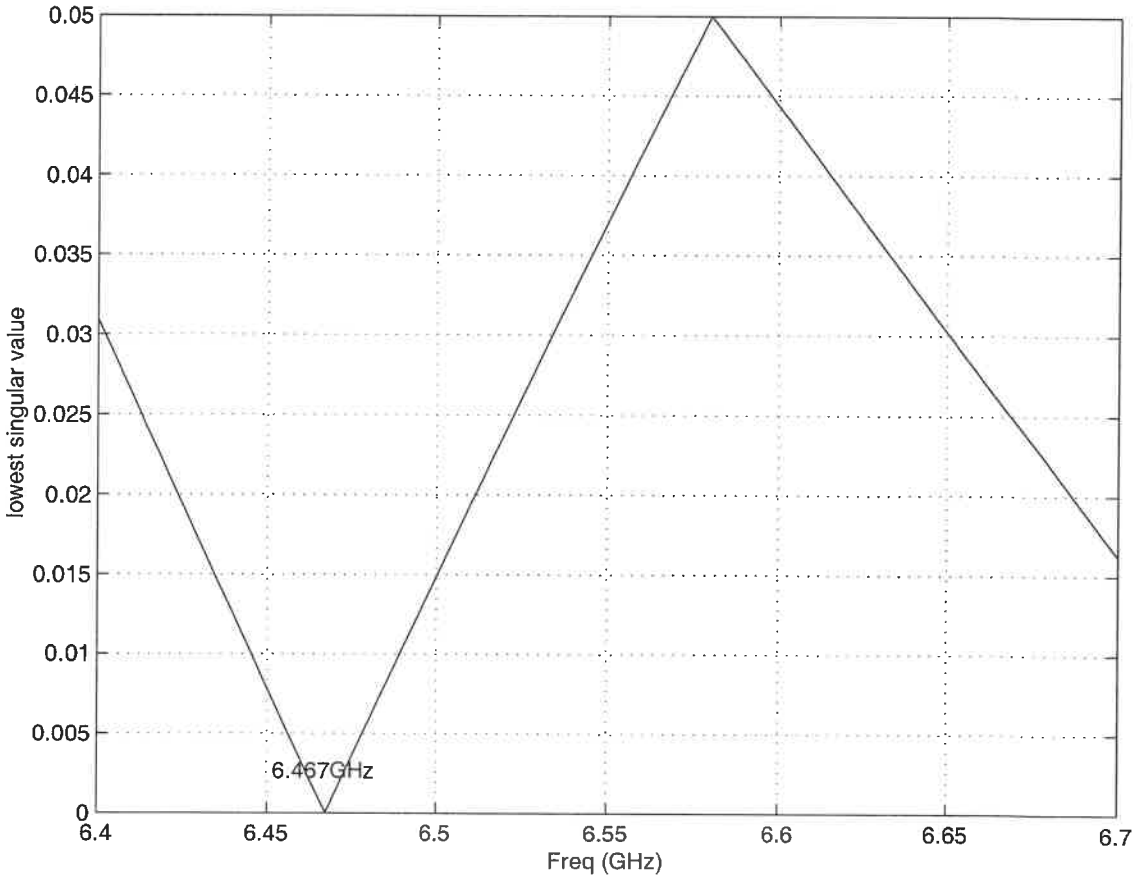

Figure 3.3b Resonant frequency of TM_{111} mode for Case A by using 3D CMoL and by using the least singular element

3.5.2.2 Convergence of 2D and 3D CMoL

After illustrating the root searching in the previous section, we investigate the convergence of 2D and 3D CMoL in this section. Two examples are used to demonstrate the convergence of our method.

In Figure 3.4, resonant frequencies of TM_{011} mode and TE_{011} mode for case A are obtained by using 2D CMoL. The resonant frequencies of TM and TE modes for case A are converged to the analytical values 5.374 and 6.498 GHz, respectively. For this special case, the resonant frequency converges more quickly for TM mode than for TE mode.

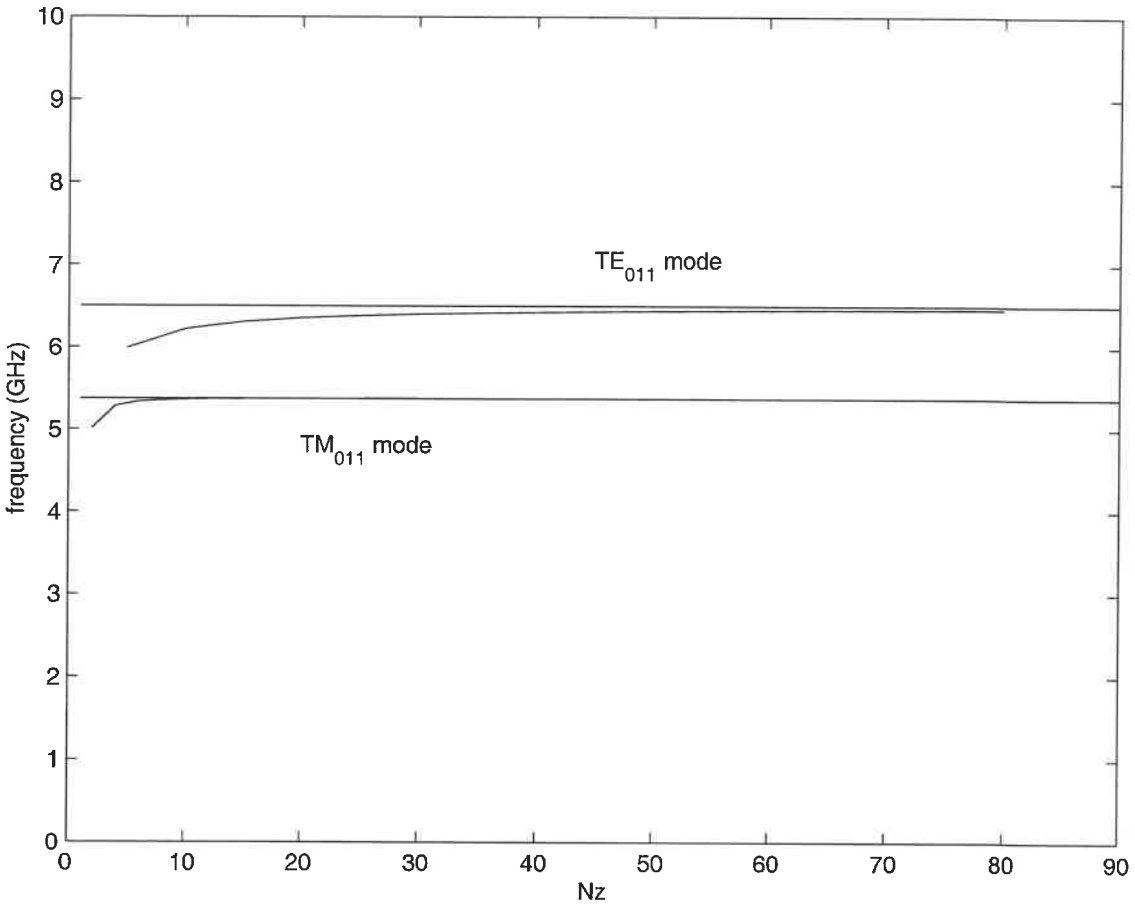

Figure 3.4 Convergence of 2D CMoL

In Figure 3.5, resonant frequencies of TM_{111} mode and TE_{111} mode for case B are obtained by using 3D CMoL. The resonant frequencies of TM and TE modes for case B are converged to the analytical values 42.20 and 36.58 GHz, respectively. For this special case, the resonant frequency converges more quickly for TM mode than for TE mode.

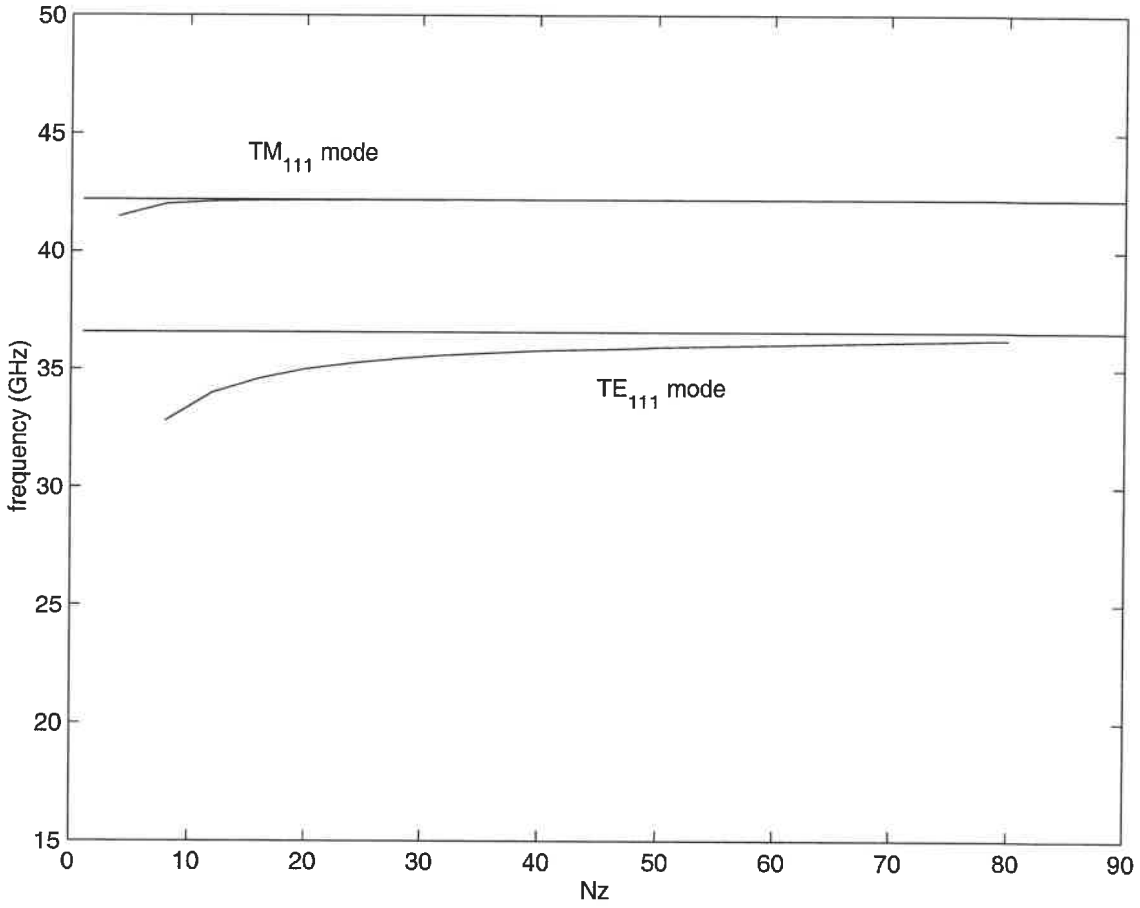

Figure 3.5 Convergence of 3D CMoL

3.6 Conclusion

In this chapter, we present an eigenvalue problem for an enclosed electromagnetic circular waveguide. Both 2D- and 3D- CMoL are used to obtain resonant frequencies. Numerical results converge for both 2D and 3D CMoL. Good agreement is obtained between simulated results and those from analytical equations. Convergence of 2D and 3D CMoL are also studied. The resonant frequency converges more quickly for TM mode than for TE mode.

CHAPTER 4

ANALYSIS OF MICROWAVE PERIODIC DISK-LOADED CICULAR WAVEGUIDE

In the previous chapter, we have solved an eigenvalue problem for an enclosed electromagnetic circular waveguide. Both 2D- and 3D- CMoL are used to obtain resonant frequencies. In this chapter, we will solve a propagation problem for a periodic disk-loaded circular waveguide with axial symmetry by using 2D CMoL.

4.1 Introduction

Two cases, which are used to analyze circular resonators in section 3.1, are analyzed in this chapter. As mentioned in the previous chapter, Case A is from Pruiksma *et al.* [7]'s paper, and Case B is from Wallett *et al.*[6]'s paper. Both of these two papers investigated periodic structures with TM modes. The geometrical parameters are listed in Table 3-1. For Case B, there are ten periods cascaded together. For Case A, a sufficiently good number of periods is assumed. Because both of the two structures are of axial symmetry, only the transverse magnetic field TM_{0n} modes are of interest. Thus, 2D CMoL is used to investigate the propagation characteristics of periodic disk-loaded cylindrical waveguides.

4.2 Method of analysis

The basic idea of MoL is to reduce a system of partial differential equations into ordinary differential equations by discretizing all but one of

the independent variables in Helmholtz equation. For TM_{0n} modes, electromagnetic fields are independent of variable θ. 3D Helmholtz equation has degenerated into 2D Helmholtz equation. Here, z variable is discretized while r variable leaves for analytical solutions. For proper selected outer diameter of cylindrical waveguides and for proper operating frequency range, only TM_{01} mode is the propagating mode. Other TM_{0n} modes represent attenuating modes.

For a periodic structure with axial symmetry, by assuming the dependence as $e^{j\omega t}$, the scalar potential $\psi(r,z)$ satisfies the 2D Helmhotz equation with variables r and z as below

$$\frac{1}{r}\frac{\partial}{\partial r}\left(r\frac{\partial\psi(r,z)}{\partial r}\right)+\frac{\partial^2\psi(r,z)}{\partial z^2}+k_0^2\psi(r,z)=0 \tag{4.1}$$

Here, for TM modes, the scalar potential $\psi(r,z)$ is referred to electric potential ψ^e. By discretizing along the z-direction, a set of ordinary differential equations is obtained,

$$\frac{d}{rdr}\left(r\frac{d\overline{\psi}}{dr}\right)+\frac{[P]_z\overline{\psi}}{h_z^2}+k_0^2\overline{\psi}=0 \tag{4.2}$$

where $\overline{\psi}=\begin{bmatrix}\psi(r,z_1)\\ \psi(r,z_2)\\ \dots\\ \psi(r,z_{N_z-1})\\ \psi(r,z_{N_z})\end{bmatrix}$ and $[P]_z$ is a N_z x N_z matrix.

In order to solve our problem, a periodic disk-loaded cylindrical waveguide as shown in Figure 4.1 is divided into two uniform regions (regions I and II). Discretization lines for one period are also illustrated in Figure 4.1. Here, β is the propagation constant in the z-direction and L is the period length. b and a are the radii of outer and inner circles, respectively.

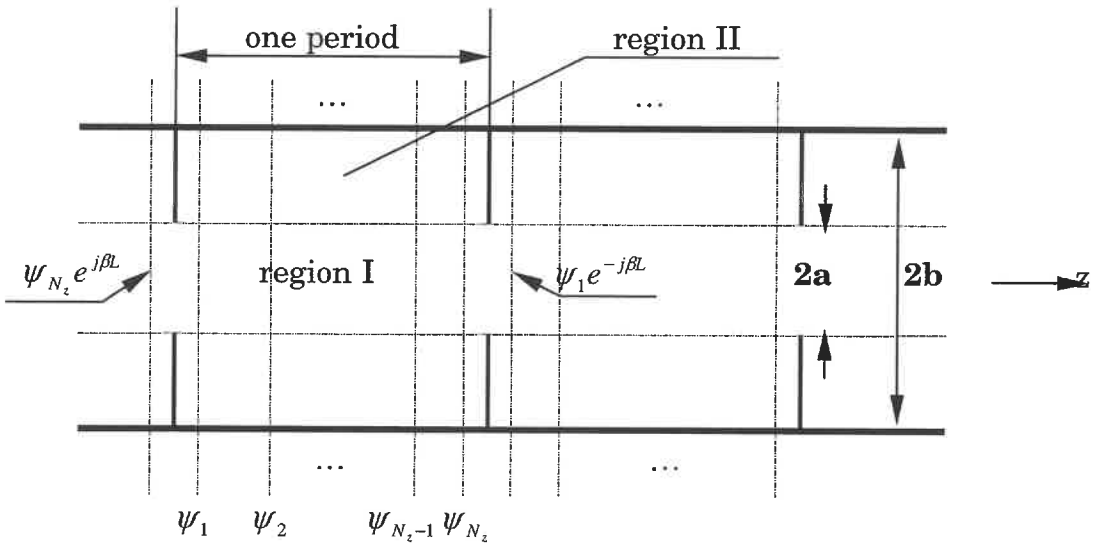

Figure 4.1 Discretization lines for a periodic cylindrical structure

The matrix $[P]_z$ has different expressions for region I and region II. From Chapter Three, the lateral boundary conditions for region II belong to N-N case. Thus, the matrix $[P]_z$ for region II is written as

$$[P]_z^{II} = \begin{bmatrix} -1 & 1 & \cdots & \cdots & \cdots & \cdots \\ 1 & -2 & 1 & \cdots & \cdots & \cdots \\ \cdots & \cdots & \cdots & \cdots & \cdots & \cdots \\ \cdots & \cdots & \cdots & \cdots & \cdots & \cdots \\ \cdots & \cdots & \cdots & 1 & -2 & 1 \\ \cdots & \cdots & \cdots & \cdots & 1 & -1 \end{bmatrix} \quad (4.3a)$$

Corresponding to the periodic boundary conditions for region I, the matrix $[P]_z$ can be derived from Floquet's theorem as follows,

$$[P]_z^I = \begin{bmatrix} -2 & 1 & \dots & \dots & \dots & e^{j\beta L} \\ 1 & -2 & 1 & \dots & \dots & \dots \\ \dots & \dots & \dots & \dots & \dots & \dots \\ \dots & \dots & \dots & \dots & \dots & \dots \\ \dots & \dots & \dots & 1 & -2 & 1 \\ e^{-j\beta L} & \dots & \dots & \dots & 1 & -2 \end{bmatrix} \quad (4.3b)$$

The next step is to find an orthogonal matrix $[T_z]$ to transform the variables so as to decouple the above equation and to find an analytical solution for it in the radial direction. The matrix $[P]_z$ can be factorized by an orthogonal matrix $[T_z]$ as

$$[T_z]^t[P]_z[T_z]=\text{diag}\{\delta_1,\delta_2,\dots,\delta_k,\dots,\delta_{Nz}\} = [\delta] \quad (4.4)$$

where the respective matrices $[T_z]$ and $[\delta]$ for regions I and II can be found in Chapter Two. These matrices correspond to different boundary conditions. Assumed that $\overline{\psi} = [T]\,\overline{\varphi}$, the set of coupled Helmholtz equations in equation (4.2) can be decoupled into a set of independent ordinary differential equations of Bessel forms:

$$\frac{d}{rdr}\left(r\frac{d\varphi_k}{dr}\right) + \chi_k^2\varphi_k = 0 \quad (4.5)$$

and

$$\chi_k^2 = k_0^2 + \frac{\delta_k}{h_z^2} \quad (4.6)$$

where $k=1,2,\dots,N_z$. φ_k is the transformed potential function, and can be written as a superposition of Bessel and Neumann function of 0-order

$$\varphi_k^{II} = A_k J_0\left(\chi_k^{II} r\right) + B_k Y_0\left(\chi_k^{II} r\right) \quad \text{(region II)} \quad (4.7a)$$

and

$$\varphi_k^{I} = C_k J_o\left(\chi_k^{I} r\right) \quad \text{(region I)} \quad (4.7b)$$

where A_k, B_k and C_k are constants. $J_0(\chi_k r)$ is the first kind of Bessel function of zero order and $Y_0(\chi_k r)$ is the second kind of Bessel function (Neumann function) of zero order. For region II, both the terms of Bessel and Neumann functions exist. For region I, only the term of Bessel function is kept, because the term of Neumann function becomes infinity at the center r = 0.

The electric potential in regions I and II can be expressed as below:

$$\overline{\psi}^{I} = \left[T_z^{I}\right]\overline{\varphi}^{I} \tag{4.8a}$$

and

$$\overline{\psi}^{II} = \left[T_z^{II}\right]\overline{\varphi}^{II} \tag{4.8b}$$

At the interface between region I and region II, from the continuity conditions for the electric and magnetic fields, we have

$$\overline{\psi}^{I}\Big|_{r=a} = \overline{\psi}^{II}\Big|_{r=a} \tag{4.9a}$$

and

$$\left.\frac{\partial \overline{\psi}^{I}}{\partial r}\right|_{r=a} = \left.\frac{\partial \psi^{II}}{\partial r}\right|_{r=a} \tag{4.9b}$$

where a is the radius of aperture.

At the cylindrical circumference, we have

$$\overline{\psi}^{II}\Big|_{r=b} = 0 \tag{4.10}$$

since the characteristic of electric wall. Here b is the radius of cylindrical waveguide.

Combining equation (4.10) with equations (4.9a) and (4.9b), we have

$$[JYM]\begin{bmatrix} A \\ B \\ C \end{bmatrix} = 0 \tag{4.11}$$

where

$$[JYM] = \begin{bmatrix} J_0(\chi_k^{II} a) & Y_0(\chi_k^{II} a) & [T_z^{II}]^{-1}[T_z^{I}]J_0(\chi_k^{I} a) \\ \left.\frac{\partial J_0(\chi_k^{II} r)}{\partial r}\right|_{r=a} & \left.\frac{\partial Y_0(\chi_k^{II} r)}{\partial r}\right|_{r=a} & [T_z^{II}]^{-1}[T_z^{I}]\left.\frac{\partial J_0(\chi_k^{I} r)}{\partial r}\right|_{r=a} \\ J_0(\chi_k^{II} b) & Y_0(\chi_k^{II} b) & 0 \end{bmatrix} \tag{4.12}$$

The problem of solving equation (4.11) can be approached by directly evaluating the determinant of the matrix [JYM]. Nonzero solution exists only if the determinant of the matrix [JYM] equals to 0. But because the presence of poles makes it difficult to detect the zeros as the zeros near the poles as discussed by Labay *et al.*[14], and because there are lower and upper limits for the value of a double real number, SVD technique is used to find the solution in the following.

Similarly as performed in Section 3.4, SVD technique is first used to diagonalize the matrix [JYM] by two unitary matrices, [U] and [V] ($[U]^h[U]=[V]^h[V]=[I]$) and $[U]^h[JYM][V]=\mathrm{diag}[s_1,s_2,\ldots,s_n]$, where $s_1 > s_2 > \ldots > s_n$. Then, we just pick the last element s_n and find the local minimum point.

4.3 Estimations of passband and stopband

A periodic structure can be regarded as a transmission line loaded with reactances connected in series or parallel, and spaced at regular intervals. Harvey [18] reviewed the properties of periodic and guiding structures. Various types of surface-wave structures including cylindrical dielectric rods and corrugated surfaces were described. Based on wave analysis of periodic structures [3][4], analytical expressions are possibly obtained if the equivalent series reactance X or shunt susceptance B for the waveguide discontinuity can be accurately modeled. For electromagnetic field analysis, there are many papers published in this topic. Clarricoats and Slinn [19] investigated the waveguide problems by mode-matching methods. Mcdonald [20][21] presented polynomial expressions for the electric polarizabilities of small apertures. Iskander and Hamid [22] improved the single and multiaperture waveguide coupling theory. Eastham and Chang [23] presented closed-form solutions of circular and rectangular apertures in the transverse plane of a circular waveguide. Based on these contributions, approximate passband and stopband are obtained.

For TM_{01} mode, small apertures inside a cylindrical waveguide are modeled as shunted capacitances. The normalized susceptance B [3] can be expressed as below:

$$B = \frac{0.92b^4}{|\alpha_e|\lambda_g} \tag{4.13}$$

where $$|\alpha_e| = \frac{2}{3}a^3 \tag{4.14}$$

As described in [4], the propagation equation of infinite periodic structures can be written as

$$\cosh(\gamma d)=\cosh(\alpha d)\cos(\beta d)+j\sinh(\alpha d)\sin(\beta d)=\cos(kd)-\frac{B}{2}\sin(kd) \qquad (4.15)$$

where $\gamma=\alpha+j\beta$, k is the propagation constant of unloaded structure, The above equation is used to estimate the passband and stopband, since the right-hand side of equation (4.13) is purely real, we must have either $\alpha=0$ or $\beta=0$. If $\alpha=0,\beta\neq 0$. This case corresponds to a nonattenuating, propagating wave on the periodic structure, and defines the passband of the structure. Then equation (4.15) reduces to

$$\cos(\beta d)=\cos(kd)-\frac{B}{2}\sin(kd) \qquad (4.16)$$

which can be solved for β if the magnitude of the right-hand side is less than or equal to unity. If $\alpha\neq 0,\beta d=0,\pi$. In this case the wave does not propagate, but is attenuated along the structure; this is the stopband of the structure. Because the structure is lossless, power is not dissipated, but is reflected back to the input of the structure. The magnitude of equation (4.15) reduces to

$$\cosh(\alpha d)=\left|\cos(kd)-\frac{B}{2}\sin(kd)\right|\geq 1 \qquad (4.17)$$

which has only one solution ($\alpha > 0$) for positively traveling waves: $\alpha < 0$ applies for negatively traveling wave. If $\cos(kd)-(B/2)\sin(kd)\leq -1$, equation (4.17) is obtained from equation (4.15) by letting $\beta d=\pi$.

4.4 Numerical results

Based on the analysis in Section 4.2, numerical root searching has been performed for both of the two cases A and B as mentioned in Section 4.1.

Here, analytical passband has been estimated for both cases A and B by using equation (4.16). These analytical results are compared with other ones from literature and with our simulation data, which are obtained by using 2D CMoL. Two special groups of numerical simulations for case A are also performed to investigate the dependence of phase delay βd on the geometrical parameters.

As mentioned in Chapter Three, Case A is from Pruiksma *et al.* [7]'s paper, and Case B is from Wallett and Qureshi [6]'s paper. Both of these two papers investigated periodic structures with TM modes. Here, due to the axial symmetry, 2D CMoL method has been chosen to investigate the dispersion characteristics of the disk-loaded structure. SVD technique has been performed in our analysis. Instead of detecting zeros of the determinant of the matrix [JYM] in equation (4.12), we just pick the value of the last element s_n as suggested by Xiao *et al.* [13]. In Matlab subroutine, the last element s_n is already the lowest value among all the diagonal elements in matrix diag$[s_1,s_2,\ldots,s_n]$. Thus, the algorithm now searches the minima of the last element in the diagonal matrix.

Figure 4.2 shows the dispersion characteristics of the disk-loaded structure for Case A. Here, the curves with symbols of "Δ", "o" and "*" represent the numerical results from Pruiksma *et al.*[7], those from 2D CMoL method, and those from analytical equations in Collin's books [3,4]. A good agreement has been achieved between the simulation results from 2D CMoL method and those from analytical equations. Deviation appears for phase delay βd above π/2. For the same phase delay βd, the relative differences between the frequencies from 2D CMoL and those from analytical equations are around 1%. $[(f_{MoL} - f_{Collin})/f_{Collin} \times 100\%]$.

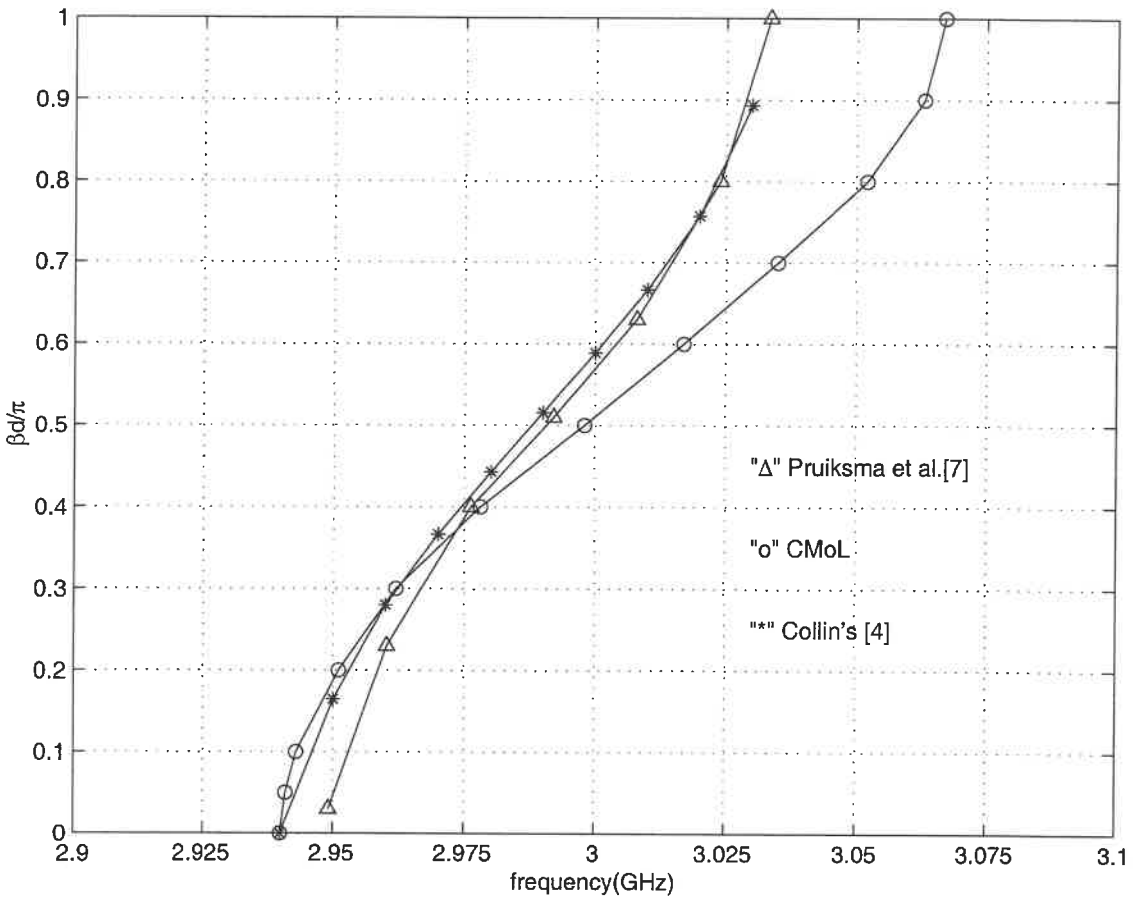

Figure 4.2 Dispersion characteristics of the disk-loaded structure for Case A (b≈39mm, a≈10mm and d≈33.33mm)

Figure 4.3 shows the dispersion characteristics of the disk-loaded structure for Case B. Here, the curves with symbols of "Δ", "+", "o" and "*" represent the theoretical and experimental results from Wallett and Qureshi[6], those from 2D CMoL method, and those from analytical equations in Collin's books [3,4]. A good agreement has been achieved between the simulation results from 2D CMoL method and those from analytical equations. There is difference between the results from 2D CMoL method and those from the experimental measurement. It should be noted that we neglect the thickness of the inserted disk. More accuracy needs considering the impact of the thickness of these disks.

In order to investigate the dependence of dispersion characteristics on the geometrical parameters, two special groups of numerical simulations for Case A have also been performed. Only one parameter varies in each group. In group one, the inner diameter of inserted disks changes from 2.5, 5 to 10 mm, while in group two, the length of one period varies from 16, 33 to 66 mm.

Figure 4.4 shows the dispersion characteristics of the frequency points with variation of the inner diameter of the inserted disks. The dash-dotted, dashed and solid curves represent the periodic structures with the values of inner diameter of inserted disks 2.5, 5 and 10 mm, respectively. As shown in Figure 4.4, the phase delay βd decreases with the increase of the inner diameter of the inserted disks.

The dispersion characteristics of the frequency points with the change of the length of one period for case A are shown in Figure 4.5. The dash-dotted,

solid and dashed curves represent the geometry size with the length of one period 16, 33 and 66 mm, respectively. As shown in Figure 4.5, the phase delay βd increases with the increase of the length of one period for Case A.

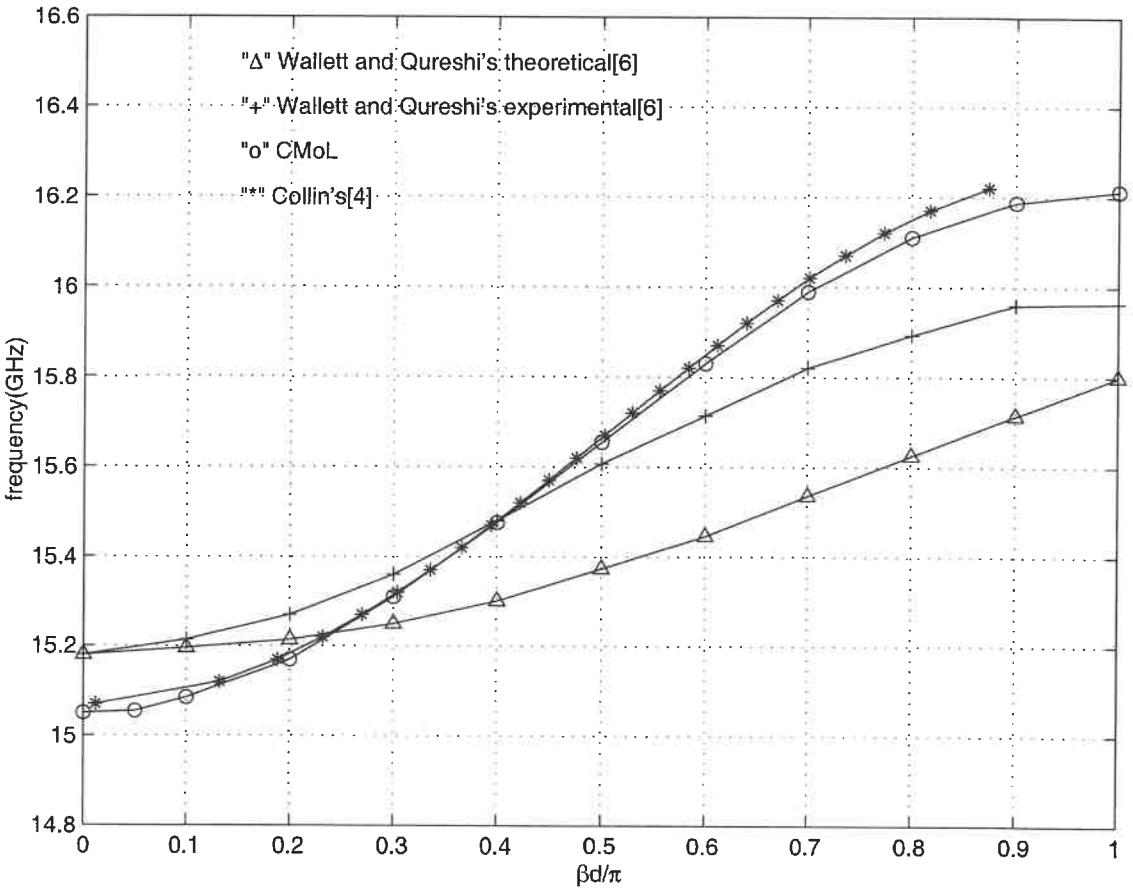

Figure 4.3 Dispersion characteristics of the disk-loaded structure for Case B (b=0.15", a=0.09375", t=0.01" and d=0.17")

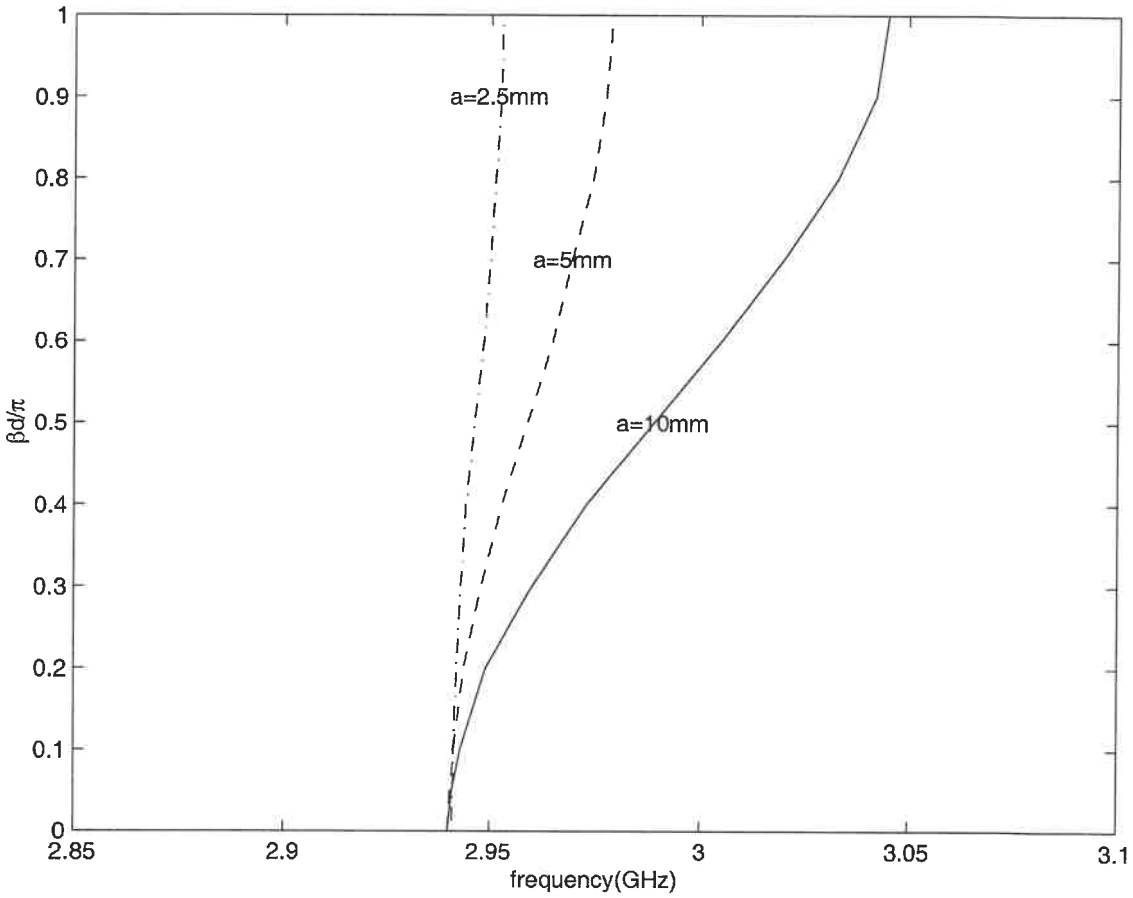

Figure 4.4 Variation of phase delay
with the change of the inner diameter of the inserted disks for Case A

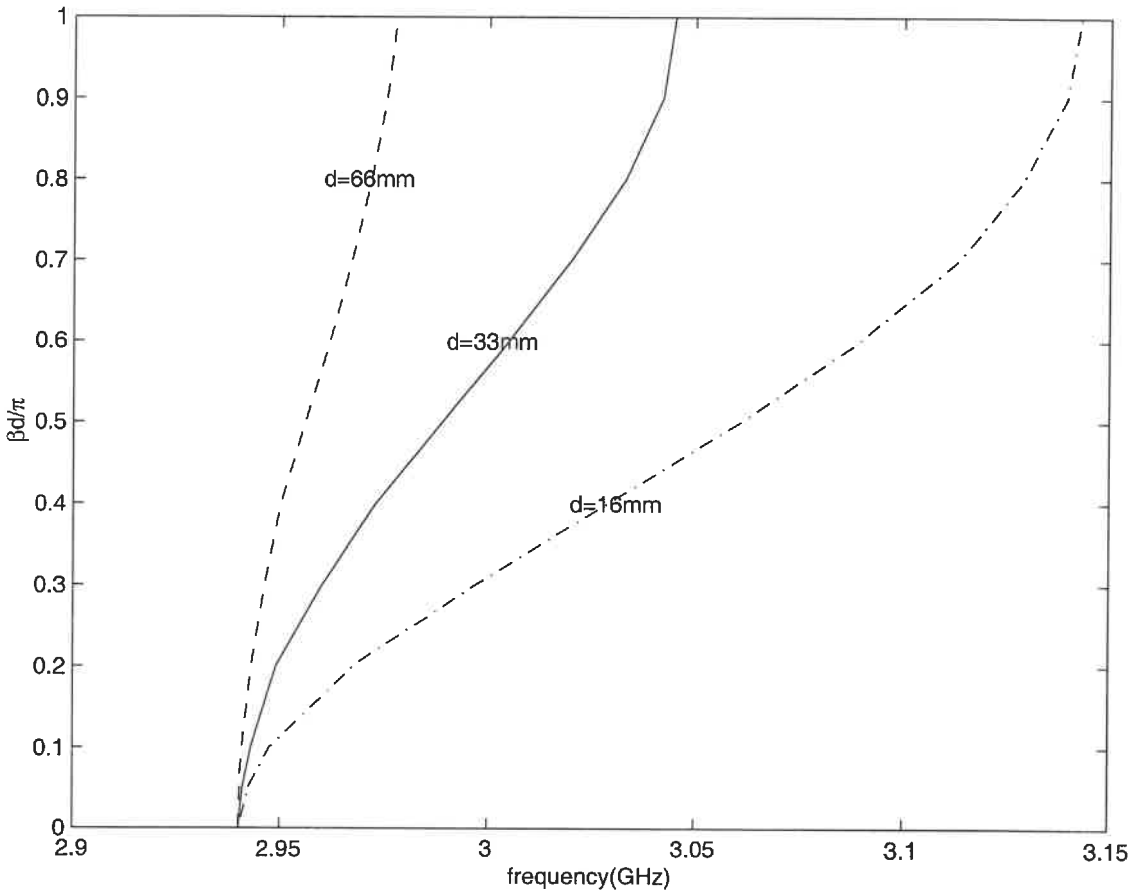

Figure 4.5 Variation of phase delay
with the change of the length of one period for Case A

4.5 Conclusion

In this chapter, we have investigated a periodic disk-loaded circular waveguide of axial symmetry by using 2D CMoL. Numerical results are compared with those obtained from analytical equations in Collin's books, and a good agreement has been achieved between these two methods. Deviation still exists between the results from 2D CMoL and the measurement data. More rigorous analysis need include the impact of the thickness of inserted disks. Parametric analysis has also been developed in order to investigate the dependence of dispersion characteristics on the geometrical parameters.

CHAPTER 5

CMoL APPLIED TO ACOUSTIC CIRCULAR WAVEGUIDE

The method of lines (MoL) can be used to analyze the acoustic waveguide structures with circular cross section in cylindrical coordinates. Both 2D and 3D cylindrical method of lines (CMoL) are extended to acoustic structures in this chapter. Some numerical results are obtained to demonstrate the usefulness of this approach.

5.1 Introduction

Many ducts in which sound propagates have circular cross-sections. Thus it is desirable to analyze cross-modes in cylindrical or circular ducts. The problem of wave propagation in a circular duct has received considerable theoretical and experimental attention over many years [26-30]. This chapter will present the application of CMoL to acoustic cylindrical waveguide and resonator. The Helmholtz equations (both 2D and 3D) are derived in details from acoustic wave equation. For an infinite long cylindrical waveguide, the cylindrical 2D method of lines (2D MoL) is used to analyze the propagation characteristics. By discretizing the angular space direction only, the two-dimensional Helmholtz equation in cylindrical coordinates becomes a set of ordinary differential equations, which can be solved analytically in the radial direction after an orthogonal transformation. For an acoustic resonator, the cylindrical 3D method of lines (MoL) is utilized to discretize the angular and longitudinal space directions simultaneously. The resulting Helmholtz equation is a set of coupled one-dimensional differential equations. Applying the decoupling procedure, each

differential equation can then be solved analytically in the radial direction after an orthogonal transformation.

5.2 Acoustic Wave Equation and Helmholtz Equation

The acoustic wave equation can be expressed in terms of the velocity potential Φ is

$$\frac{\partial^2\Phi}{\partial t^2} - c^2\nabla^2\Phi = 0 \tag{5.1}$$

Where c is the velocity of sound, which is the characteristic speed of propagation wave in medium. The velocity potential is related to all other acoustic parameters. For example, from the velocity potential Φ, acoustic pressure P and particle velocity u can be derived by the following equations

$$P = -\rho\frac{\partial\Phi}{\partial t} \tag{5.2}$$

and

$$\vec{u} = \nabla\Phi \tag{5.3}$$

where ρ is the density of the medium.

In cylindrical coordinates, the gradient of Φ can be written as

$$\nabla\Phi = \vec{a}_r\frac{\partial\Phi(r,\theta,z,t)}{\partial r} + \vec{a}_\theta\frac{\partial\Phi(r,\theta,z,t)}{r\partial\theta} + \vec{a}_z\frac{\partial\Phi(r,\theta,z,t)}{\partial z} \tag{5.4}$$

and the Laplacian operator can be written as

$$\nabla^2\Phi = \frac{1}{r}\frac{\partial}{\partial r}\left(r\frac{\partial\Phi(r,\theta,z,t)}{\partial r}\right)+\frac{1}{r^2}\frac{\partial^2(r,\theta,z,t)}{\partial\theta^2}+\frac{\partial^2\Phi(r,\theta,z,t)}{\partial z^2} \tag{5.5}$$

Substituting equation (5.5) into equation (5.1), the wave equation becomes

$$\frac{\partial^2\Phi(r,\theta,z,t)}{\partial t^2}-c^2\left[\frac{1}{r}\frac{\partial}{\partial r}\left(r\frac{\partial\Phi(r,\theta,z,t)}{\partial r}\right)+\frac{1}{r^2}\frac{\partial^2\Phi(r,\theta,z,t)}{\partial\theta^2}+\frac{\partial^2\Phi(r,\theta,z,t)}{\partial z^2}\right]=0 \tag{5.6}$$

Substituting equation (5.4) into equation (5.3), the particle velocity becomes

$$\vec{u} = \vec{a}_r\frac{\partial\Phi(r,\theta,z,t)}{\partial r} + \vec{a}_\theta\frac{\partial\Phi(r,\theta,z,t)}{r\partial\theta} + \vec{a}_z\frac{\partial\Phi(r,\theta,z,t)}{\partial z} \tag{5.7}$$

If harmonic motion is assumed, $\Phi(r, \theta, z, t)$ can then be expressed

$$\Phi(r,\theta,z,t) = \psi(r,\theta,z)\ e^{j\omega t} \tag{5.8}$$

Substituting the above equation into equation (5.6), we obtain

$$\frac{1}{r}\frac{\partial}{\partial r}\left(r\frac{\partial\psi(r,\theta,z)}{\partial r}\right)+\frac{1}{r^2}\frac{\partial^2\psi(r,\theta,z)}{\partial\theta^2}+\frac{\partial^2\psi(r,\theta,z)}{\partial z^2}+k_0^2\psi(r,\theta,z)=0 \tag{5.9}$$

with

$$\frac{\partial^2\Phi(r,\theta,z,t)}{\partial t^2}=-\omega^2\psi(r,\theta,z)e^{j\omega t} \tag{5.10}$$

where k_o is the wave number, which is expressed by the equation below

$$k_0 = \omega / c \tag{5.11}$$

Equation (5.9) is the three-dimensional Helmholtz equation in the cylindrical coordinates.

The two-dimensional Helmholtz equation in a cylindrical coordinate system can be obtained by the assumption as follows

$$\Phi(r,\theta,z,t) = \psi(r,\theta)\ e^{j(\omega t-\beta z)} \tag{5.12}$$

If only positive traveling waves are considered, where β is the propagation constant in z-direction. Substituting this equation into equation (5.6) yields

$$\frac{1}{r}\frac{\partial}{\partial r}\left(r\frac{\partial\psi(r,\theta)}{\partial r}\right)+\frac{1}{r^2}\frac{\partial^2\psi(r,\theta)}{\partial\theta^2}+(k_0^2-\beta^2)\psi(r,\theta)=0 \tag{5.13}$$

with $$\frac{\partial^2\Phi(r,\theta,z,t)}{\partial t^2}=-\omega^2\psi(r,\theta)e^{j(\omega t-\beta z)} \tag{5.14}$$

and $$\frac{\partial^2\Phi(r,\theta,z,t)}{\partial z^2} = -\beta^2\psi(r,\theta)\ e^{j(\omega t-\beta z)} \tag{5.15}$$

The cut-off frequency is reached when β equal zero. The above equation is the two-dimensional Helmholtz equation in cylindrical coordinates.

5.3 Numerical results

The application of CMoL to acoustic structures will be tested for infinitely long circular waveguide and cylindrical cavity, the results are compared to analytical solutions.

5.3.1 Circular cross-section waveguide

From Chapter Two, section 2.3, for an acoustic waveguide in circular cross-section, only J_{uk} ($k_c r$) is a physically acceptable solution in equation (2.24) since Y_{uk} ($k_c r$) becomes infinite at r = 0, and the solution to equation (2.24) becomes

$$\varphi_k = A_k J_{\mu_k}(k_c r) \tag{5.16}$$

where k=0,1,2,...,N_θ.

Since a rigid wall is located at r = b, the particle velocity in the r-direction at r = b must equal zero. From equation (5.7), we obtain

$$u_r = \frac{\partial \Phi(r,\theta,z,t)}{\partial r} \tag{5.17a}$$

or

$$\left.\frac{d\overline{\varphi}}{dr}\right|_{r=b} = 0 \tag{5.17b}$$

where $\overline{\varphi} = [\varphi_1, \varphi_2, \cdots, \varphi_k, \cdots, \varphi_{N_\theta}]$. Combining equation (5.16) and equation (5.17b), we have

$$\left.\frac{dJ_m(k_c r)}{dr}\right|_{r=b} = 0, \quad m = u_k \tag{5.18}$$

and u_k is determined by equation (2.23) in Chapter Two. If the nth root of the equation (5.18) is designated by χ_{mn}, the allowed values (eigenvalues) of k_c are

$$k_{c,mn} = \frac{\chi_{mn}}{b} \tag{5.19}$$

The values of χ_{mn} for the first seven roots for n = 0,1,2,3,4,5,6 will be given in Table 5.1 with N_θ =30, which shows a good agreement with the literature [30]. There are infinite numbers of solutions χ_{mn} (n = 0,1,2,... ...), which are satisfied for the equation (5.18).

In the following, N_θ is set to 30. Figure 5.1 shows the discretization along θ-direction. There are 30 lines in the whole circle. The size of matrix $[P]_\theta$ is 30 x 30. The elements of $[P]_\theta$ are listed in equation (2.17). An orthogonal matrix [T] is used for the orthogonal transformation of $[P]_\theta$. Based on equations (2.21) and (2.22), the elements of matrix [T] are constructed. After orthogonal transformation, the eigenvalues $\{\lambda_k\}$ are obtained. From these eigenvalues $\{\lambda_k\}$, the order of Bessel functions u_k in equation (2.23) can then be shown in Figure 5.2. We find that the values of u_k are symmetrical to k = 15. Thus, there are only 16 different values in the total 30 values. u_k is the same as u_{30-k}.

The values χ_{mn} are obtained by a root searching method based on equation (5.18). An example is used to illustrate the root searching as shown in Figure 5.3, where k equals to 1.

The x-coordinate is the $\chi_{mn} = \chi_{ukn}$ variable and the y-coordinate is the value of a function dependent on χ_{mn}, where the function is based on equation(5.18). The zero-crossing points in the curve of Figure 5.3 from left to right correspond to the solutions χ_{mn}, where $m = u_k$, n = 0, 1, 2, ...

Once χ_{mn} are known, each decoupled function φ_k can be expanded with its respective base functions φ_{mn},

$$\varphi_k(r, z)=\sum_{n=0}^{\infty} A_{mn} J_m(\chi_{mn} r/b)[B_{mn}\exp(-j(k_z)_{mn} z)+C_{mn}\exp(j(k_z)_{mn} z)] \text{ , } m = u_k \tag{5.20}$$

where B_{mn} is related to the forward wave, and C_{mn} is related to the reverse wave. Each base function corresponds to a propagation χ_{mn} mode with its respective $(k_z)_{mn}$. Based on initial conditions, the coefficients A_{mn}, B_{mn} and C_{mn} can be obtained. The base function is given by

$$\varphi_{mn} = J_m(\chi_{mn} r/b) \tag{5.21}$$

The propagation constant $(k_z)_{mn}$ for a specified χ_{mn} mode can be expressed as

$$(k_z)_{mn}^2 = k_o^2 - (\chi_{mn}/b)^2 \tag{5.23}$$

where k_0 is the wave number $k_0 = \omega/c$, $m = u_k$, k is from 1 to 30.

From equation (5.23), the cut-off frequency for each β_{mn} mode can be derived

$$(f_{mn})_{cutoff} = c\chi_{mn}/(2\pi b) \tag{5.24}$$

where c is the velocity of sound.

Four groups of base functions φ_{mn} have been shown in Figs.5.4, 5.5, 5.6 and 5.7, where k = 1, 8, 15 and 30, and n = 0, 1, 2, 3, 4, 5 and 6. Each group corresponds to its respective decoupled function φ_k. From these figures, we observe that the first order derivative of each base functions φ_{mn} is equal to zero at r = b (1m), as the boundary condition requires.

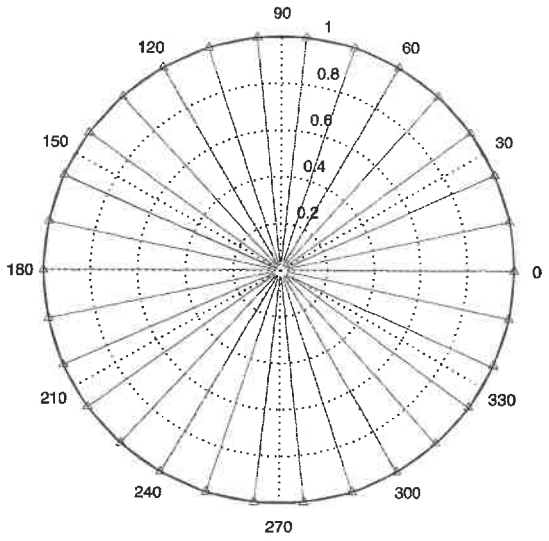

Figure 5.1 Discretization along θ-direction

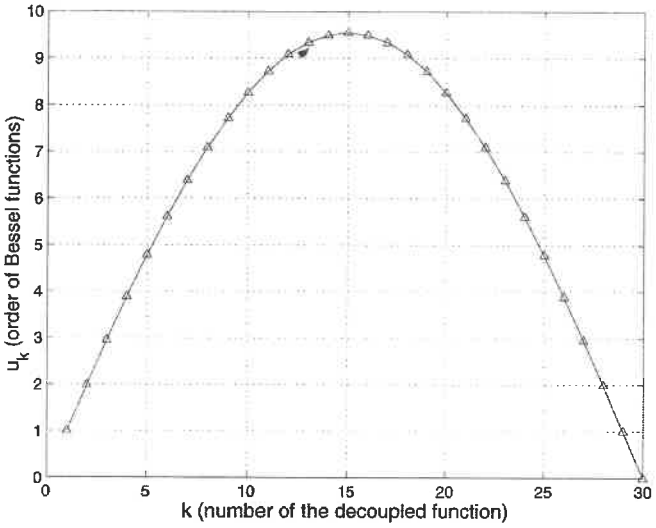

Figure 5.2 Order of Bessel functions

Table 5-1 List of χ_{mn}

k	$m=u_k$	χ_{mn}						
		0	1	2	3	4	5	6
1(29)	0.9982	1.8389	5.3289	8.5337	11.7033	14.8609	18.0128	21.1616
2(28)	1.9854	3.0372	6.6867	9.9490	13.1494	16.3262	19.4913	22.6498
3(27)	2.9509	4.1457	7.9521	11.2794	14.5173	17.7188	20.9016	24.0733
4(26)	3.8840	5.1892	9.1371	12.5287	15.8059	19.0343	22.2368	25.4234
5(25)	4.7746	6.1693	10.2431	13.6953	17.0111	20.2667	23.4895	26.6921
6(24)	5.6129	7.0823	11.2669	14.7749	18.1273	21.4093	24.6520	27.8704
7(23)	6.3897	7.9218	12.2035	15.7618	19.1480	22.4547	25.7165	28.9500
8(22)	7.0965	8.6813	13.0471	16.6502	20.0668	23.3961	26.6755	29.9231
9(21)	7.7255	9.3544	13.7920	17.4388	20.8733	24.2267	27.5219	30.7823
10(20)	8.2699	9.9351	14.4327	18.1074	21.5739	24.9406	28.2494	31.5210
11(19)	8.7237	10.4179	14.9642	18.6659	22.1512	25.5324	28.8527	32.1336
12(18)	9.0819	10.7984	15.3822	19.1048	22.6050	25.9975	29.3268	32.6152
13(17)	9.3406	11.0727	15.6833	19.4209	22.9317	26.3324	29.6682	32.9619
14(16)	9.4970	11.2385	15.8650	19.6116	23.1288	26.5344	29.8742	33.1712
15	9.4593	11.2939	15.9257	19.6753	23.1946	26.6018	29.9430	33.2411
30	0	0	3.8317	7.0156	10.1735	13.3237	16.4706	19.6159

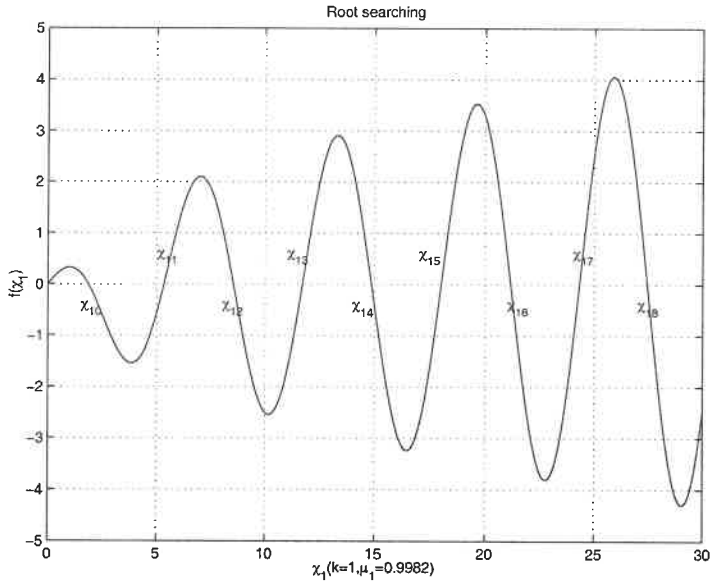

Figure 5.3 Root searching

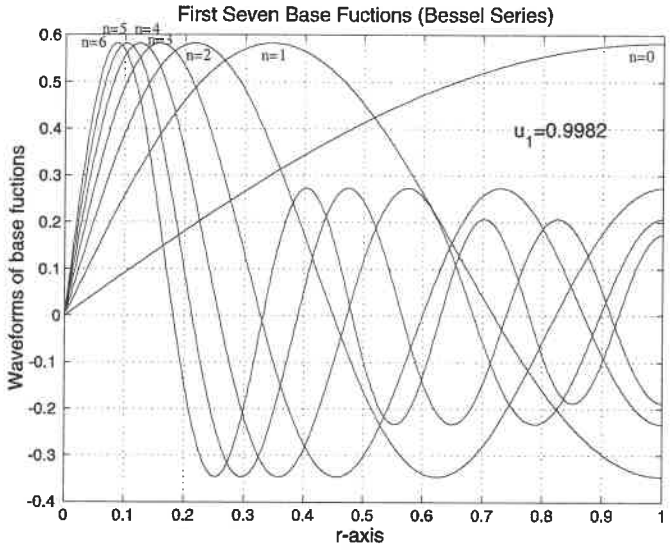

Figure 5.4 Base functions for No.1 decoupled function

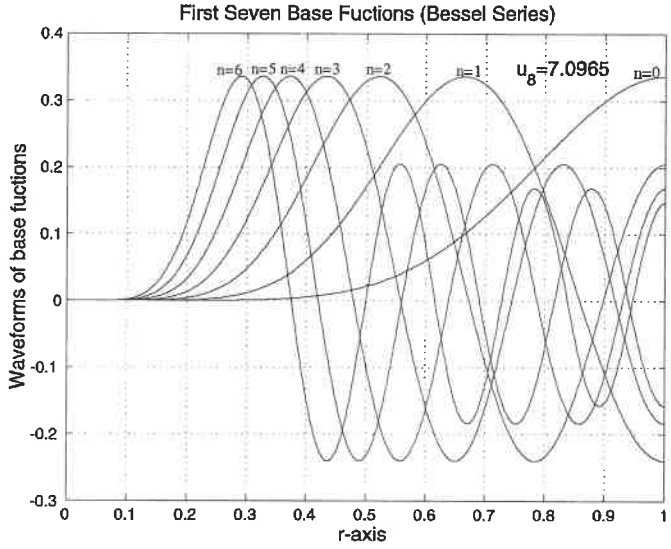

Figure 5.5 Base functions for No.8 decoupled function

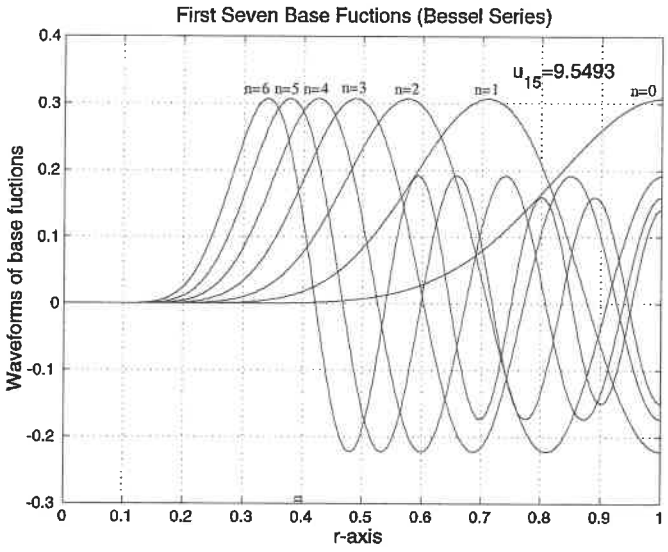

Figure 5.6 Base functions for No.15 decoupled function

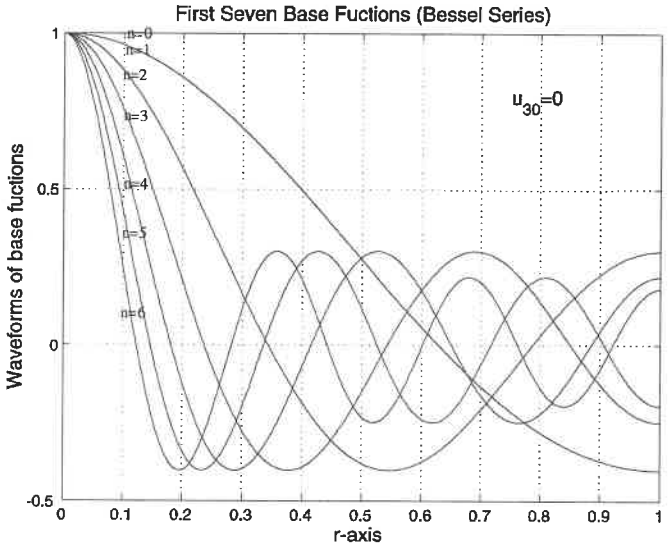

Figure 5.7 Base functions for No.30 decoupled function

5.3.1 Resonant frequencies of cylindrical cavity

For a cylindrical cavity as shown in Figure 5.8, the analysis solution begins

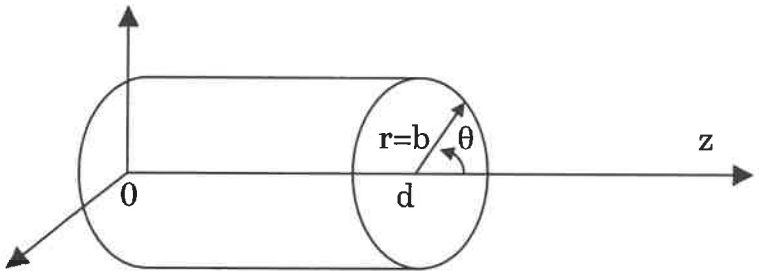

Figure5.8 Coordinate system for a cylindrical cavity

with the wave equation (5.9).

$$\frac{1}{r}\frac{\partial}{\partial r}\left(r\frac{\partial\psi(r,\theta,z)}{\partial r}\right)+\frac{1}{r^2}\frac{\partial^2\psi(r,\theta,z)}{\partial\theta^2}+\frac{\partial^2\psi(r,\theta,z)}{\partial z^2}+k_0^2\psi(r,\theta,z)=0 \qquad (5.9)$$

writing $\psi(r,\theta,z)$ in the form

$$\psi(r,\theta,z)=F(r)G(\theta)H(z) \qquad (5.25)$$

substituting this expression into equation (5.9) and separating the variables yields three ordinary differential equations of the forms

$$\frac{d^2H(z)}{dz^2}+k_z^2H(z)=0 \qquad (5.26)$$

$$\frac{d^2G(\theta)}{d\theta^2}+m^2G(\theta)=0 \qquad (5.27)$$

$$\frac{1}{r}\frac{d}{dr}\left(r\frac{dF(r)}{dr}\right)+\left(\left(k_o^2-k_z^2\right)-\frac{m^2}{r^2}\right)F(r)=0 \qquad (5.28)$$

according the boundary conditions in the z-direction

$$\left.\frac{dH(z)}{dz}\right|_{z=o,L} = 0 \tag{5.27}$$

the solution to equation (5.26) is

$$H_z = A_z \cos\left(\frac{n\pi}{L} z\right) \qquad n = 0,\ 1,\ 2,\cdots \tag{5.28}$$

$$k_z = \frac{n\pi}{L} \tag{5.29}$$

No definite boundary conditions are specified for the θ direction. However, there is a periodicity requirement such that

$$G(\theta = 0) = G(\theta = 2\pi) \tag{5.30}$$

This results in a solution for equation (5.27) of the form

$$G(\theta) = A_\theta \cos(m\theta) + B_\theta \sin(m\theta) \tag{5.31}$$

arranging equation (5.28) yields

$$r^2 \frac{d^2F(r)}{dr^2} + r\frac{dF(r)}{dr} + \left(r^2\eta^2 - m^2\right)F(r) = 0 \quad where \quad \eta^2 = k^2 - k_z^2 \tag{5.32}$$

This equation is Bessel's equation of order m. Its solution is given by

$$F(r) = A_r J_m(\eta r) + B_r Y_m(\eta r) \tag{5.33}$$

B_r must be zero since $Y_m(\eta r)$ is unbounded at r= 0. Thus equation (5.33) becomes

$$F(r) = A_r J_m(\eta r) \tag{5.34}$$

At r = b, a rigid wall located. That is to say, the particle velocity in the r direction at r = b must equal zero. From equation (5.34)

$$u_r\big|_{r=b} = \left.\frac{dF(r)}{dr}\right|_{r=b} = \frac{m}{b} J_m(\eta b) - \eta J_{m+1}(\eta b) = 0 \tag{5.35}$$

Table 5.1 gives several values of resonant frequencies of modes (m, η, n) for which the above equation (5.35) is satisfied, where m, η, n are three integers with respect to θ, r, z, respectively.

Table 5-2 Values of Resonant frequencies (Hz) when b = 5 inch d=0.5 inch

M_{110}	784
M_{210}	1301
M_{010}	1633
M_{310}	1708
M_{020}	2989
M_{030}	4335
M_{040}	5677
M_{050}	7018
M_{060}	8358

In order to get the resonant frequencies by CMoL, the discretization of the z-variable in three-dimensional Helmholtz equation(5.9) is also required. Since rigid walls are located at $z = 0, L$ (L is the length of the cavity), the lateral boundary conditions for P_z is "N-N" case, so we have

$$[P]_z = \begin{bmatrix} -1 & 1 & 0 & & & & \\ 1 & -2 & 1 & & & & \\ & \ddots & \ddots & \ddots & & & \\ & & \ddots & \ddots & \ddots & & \\ & & & 1 & -2 & 1 & \\ & & & & 1 & -1 & \end{bmatrix} \tag{5.36}$$

from Chapter Two, a transformation matrix $[T_z]$ can be found to diagonalize the matrix $[P]_Z$ as $[T_z]^t[P]_z[T_z] = diag[\delta_k] = [\delta_z]$, and $[T_z]^t = [T_z]^{-1}$, where

$$[T_z]_{mn} = \begin{cases} \sqrt{\dfrac{1}{N_z}}; & n = 1 \\ \sqrt{\dfrac{2}{N_z}} \cos \dfrac{(m-0.5)(n-1)\pi}{N_z}; & n > 1 \end{cases} \qquad (\text{m, n} = 1,2,3, \ldots, N_z) \qquad (5.37a)$$

and

$$[\delta_z]_{ii} = -4 \sin^2 \left[\frac{(i-1)\pi}{2N_z} \right]; \qquad (\text{i}=1,2,3, \ldots, N_z) \qquad (5.37b)$$

The matrices $[P]_\theta$, $[T_\theta]$ and $[\lambda]_\theta$ can be found in Chapter Two. After applying the Kronecker product, the solution of the three-dimension Helmholtz equation is obtained as shown in (2.56), B_{ki} must be zero since the region of solution contains the origin r = 0. That is

$$\varphi_{ki} = A_{ki} J_{\beta_k}(x_{ii} r) \qquad (5.38)$$

According to the acoustic boundary conditions at the circumference of r = b, where b is the radius of the cylindrical cavity, the numerical results are obtained and shown in Figure 5.9 with N_θ = 16 and N_z = 20. The values of the markers are from the analytical solution, and are shown in Table 5.1. The simulation results for the resonant frequencies by using 3D CMoL are 784, 1275, 1632, 1708 Hz for M_{110}, M_{210}, M_{010}, M_{310}, respectively. The relative difference is less than 2%.

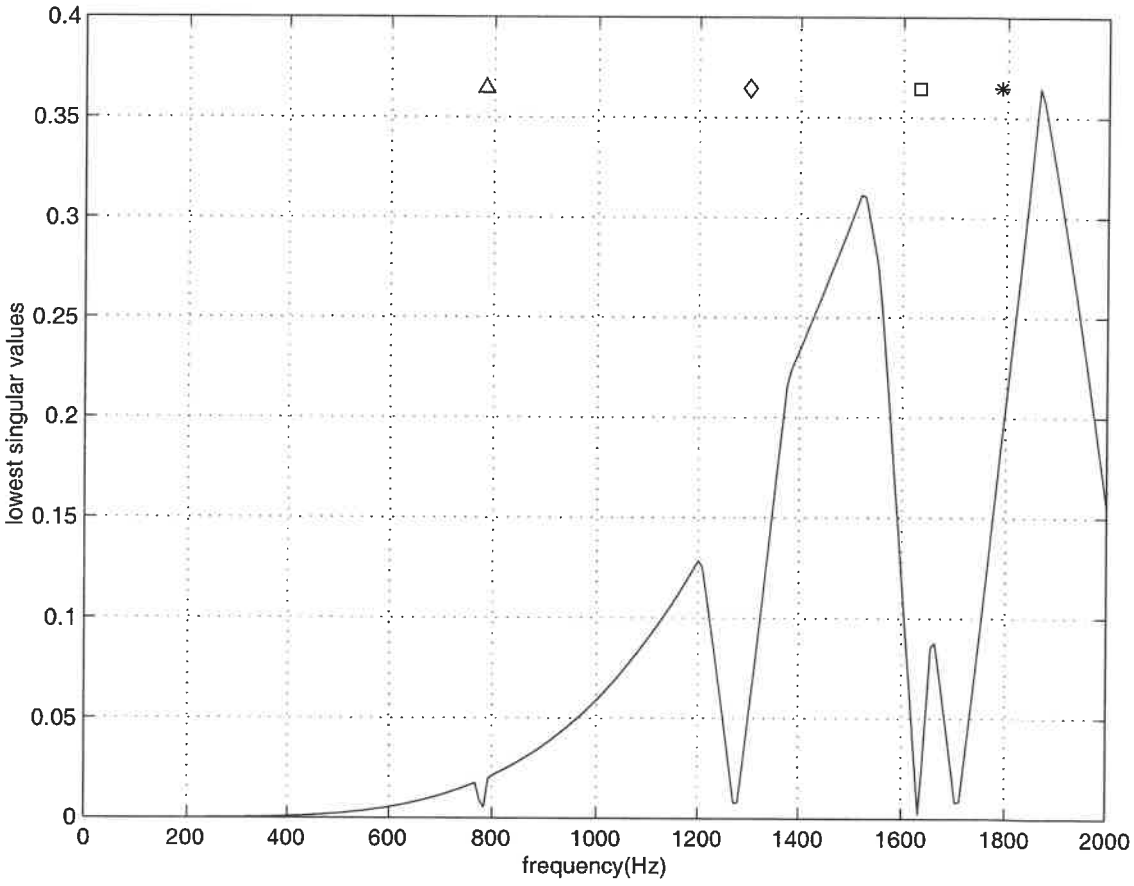

Figure 5.9 Resonant frequencies of M_{110}, M_{210}, M_{010}, M_{310} modes by 3D cylindrical MoL and by SVD technique (r = b = 5 inch, d = 0.5 inch)

If we are only interested in modes (0,n), i.e., the acoustic field is independent of the variable θ, the 2D CMoL can be used to get the resonant frequencies. Following the procedures described in Section 2.4, Chapter Two, the simulation results are obtained shown in Figure 5.10, for M_{010}, M_{020}, M_{030}, M_{040}, M_{050}, M_{060} with the frequency ascending in order. The agreements comparing with the analytical results are perfect.

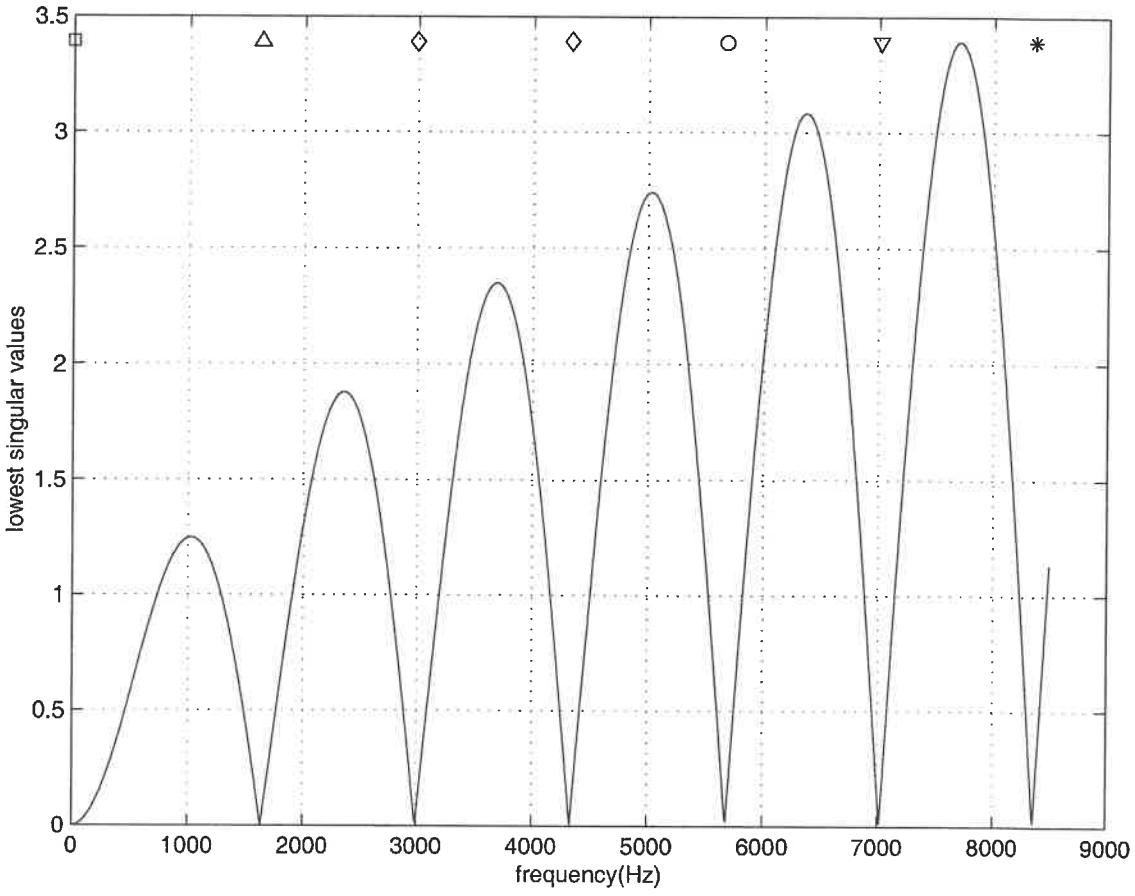

Figure 5.10 Resonant frequencies of M_{010}, M_{020}, M_{030}, M_{040}, M_{050}, M_{060} modes by 2D cylindrical MoL and by SVD technique (r = b = 5 inch, d = 0.5 inch)

5.4 Conclusion

The method of lines (MoL) has been extended to apply to acoustic waveguide structures in cylindrical coordinates. The Helmholtz equations (both 2D and 3D) are derived in details from acoustic wave equation. For an infinite long cylindrical waveguide, the cylindrical 2D method of lines (2D MoL) is used to analyze the propagation characteristics. As to an acoustic resonator, the cylindrical 2D and 3D method of lines (MoL) is utilized to obtain the resonance frequencies. In comparison with other solutions, good agreements have been found.

CHAPTER 6

DISPERSION CHARACTERISTICS OF ACOUSTIC PERIODIC DISK-LOADED WAVEGUIDE STRUCTURE

The analysis of periodic structures proceeds similarly to the analysis of resonant structures described in Chapter Five. The disk-loaded waveguide structure will be divided into two regions. After applying the boundary conditions, results expected are obtained, which will be compared with the experimental results.

6.1 Introduction

Construction of traffic noise barriers (sound walls) has been mostly used to mitigate vehicle noise for residents next to high-density highways. Effective noise barriers can reduce noise levels by 10 to 15 decibels, cutting the loudness of traffic noise in half. For a noise barrier to work, it must be high enough and long enough to block the view of a road. However, because of the structural and aesthetic reasons, they are usually limited to 25 feet in height. Therefore, the study of the acoustic model to lessen the low-frequency noise diffracting from the top of highway barriers becomes very important.

A type of acoustical waveguide low–pass filters, topping noise barriers, has first been used for many years as an effective way, both environmentally and economically, of reducing low frequency noise. This is accomplished by reducing the phase velocity of the sound transmitted through the waveguide filter, thus introducing a phase lag of 180 degree with respect to the

diffracted low frequency noise. As a result, destructive interference takes place on the receiver side behind the barrier, insuring better low frequency noise control than with a conventional barrier. However, the efficiency of these filters is limited to a narrow frequency band for normally incident plane waves. The first device, made of a series of identical rectangular cavities, has been extensively studied [31-34].

Recently, an experimental and theoretical study, conducted by Lahlou *et al.*[35], has shown that the performance of the device depends on the angle of incidence of the sound wave, dropping considerably for large incidence angles. However, it appears that this waveguide filter might still offer good performance if it is assured that the acoustic waves enter the device under normal incidence. In order to eliminate this shortcoming of the rectangular waveguide filter, this chapter presents a study of a cylindrical waveguide filter, which is a periodic disk-loaded cylindrical waveguide structure, by using CMoL. For the cylindrical structure, all direction sound waves entering the device can be assumed to be at normal incidence.

As part of this study, experimental results are compared with the theoretical predictions. The limitations of both the theoretical values and the experimental procedure are given, in order to assess the agreement between them.

6.2 Solution of Helmholtz equation

The structure is shown in Figure 6.1. Since discontinuity occurs along the z-direction, the discretization of the z-variable is required. It is subdivided into two uniform regions (Region I and Region II). We suppose only modes

(0,n) propagate in this structure. Because the initial plane mode, noted (0,0), generates superior modes (0,n) after crossing the discontinuities. Hence the Helmholtz equation is now written in the following form

$$\frac{1}{r}\frac{\partial}{\partial r}\left(r\frac{\partial\psi(r,z)}{\partial r}\right)+\frac{\partial^2\psi(r,z)}{\partial z^2}+k_0^2\psi(r,z)=0 \tag{6.1}$$

According to Floquet's theorem,

$$\psi(r,z+L)=\psi(r,z)\,e^{-j\beta L} \tag{6.2}$$

where β is the propagation constant in the z-direction and L is the period length. The discretization lines for a periodic structure are shown in Figure 6.1.

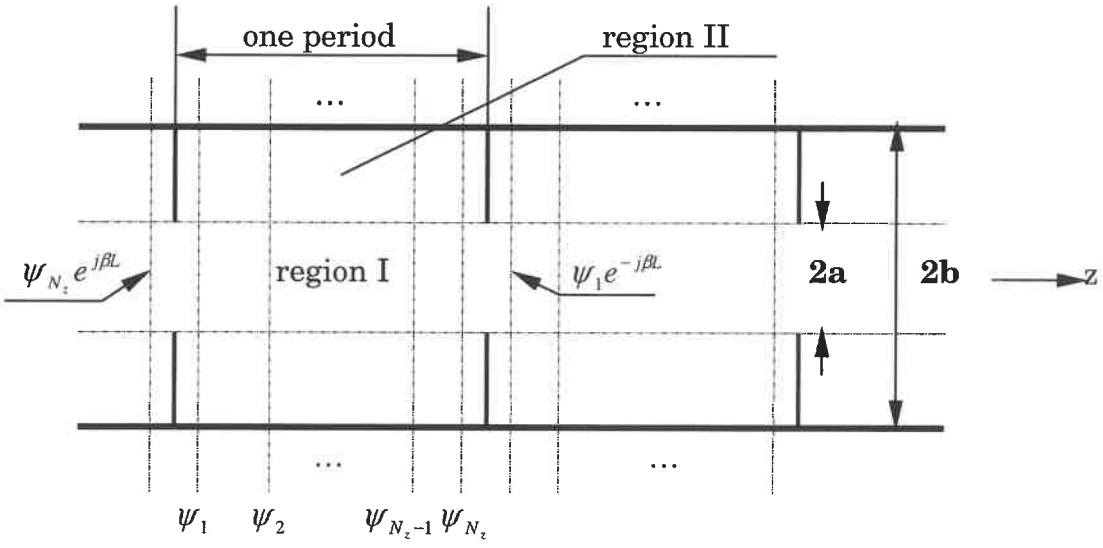

Figure 6.1 Discretization lines for a periodic cylindrical structure

For Region I, according to the periodic boundary condition, the matrix $[P]_z^l$ is given by

$$[P]_z^I = \begin{bmatrix} -2 & 1 & \cdots & \cdots & \cdots & e^{j\beta L} \\ 1 & -2 & 1 & \cdots & \cdots & \cdots \\ \cdots & \cdots & \cdots & \cdots & \cdots & \cdots \\ \cdots & \cdots & \cdots & \cdots & \cdots & \cdots \\ \cdots & \cdots & \cdots & 1 & -2 & 1 \\ e^{-j\beta L} & \cdots & \cdots & \cdots & 1 & -2 \end{bmatrix} \quad (6.3)$$

following the procedure described in Chapter Two, the solution of region I is now written as

$$\varphi_k^I = A_k J_0\left(\chi_k^I r\right) \quad (6.4)$$

and $$\overline{\psi}^I = [T]^I \overline{\varphi}^I \quad (6.5)$$

with $$[T]_{mk}^I = \sqrt{\frac{1}{N_z}}\, e^{jm\zeta_k} \quad (6.6)$$

$$\delta_k^I = -4\sin^2\left(\frac{\zeta_k}{2}\right) \quad (6.7)$$

$$\zeta_k = \frac{2\pi(k-1)-\beta L}{N_z} \quad (6.8)$$

$$\left(\chi_k^I\right)^2 = k_0^2 + \frac{\delta_k^I}{h_z^2} \quad (6.9)$$

where $m, k = 1, 2, \cdots, N_z$.

For region II, since rigid walls are located at two lateral sides, the particle velocities in the z-direction must equal zero. The lateral boundary conditions belong to N-N case. So the finite difference operator $[P]_z^{II}$ is expressed as

$$[P]_z^{II} = \begin{bmatrix} -1 & 1 & \cdots & \cdots & \cdots & \cdots \\ 1 & -2 & 1 & \cdots & \cdots & \cdots \\ \cdots & \cdots & \cdots & \cdots & \cdots & \cdots \\ \cdots & \cdots & \cdots & \cdots & \cdots & \cdots \\ \cdots & \cdots & \cdots & 1 & -2 & 1 \\ \cdots & \cdots & \cdots & \cdots & 1 & -1 \end{bmatrix} \quad (6.10)$$

an orthogonal matrix $[T]^{II}$ can be found in Chapter two to diagonalize the matrix $[P]_z^{II}$. The solution in this uniform region is as follows,

$$\varphi_k^{II} = B_k J_0\left(\chi_k^{II} r\right) + C_k Y_0\left(\chi_k^{II} r\right) \quad (6.11)$$

and $$\overline{\psi}^{II} = [T]^{II}\,\overline{\varphi}^{II} \quad (6.12)$$

with $$[T]_{mn}^{II} = \begin{cases} \sqrt{\dfrac{2}{N_z}} \cos\dfrac{(m-0.5)(n-1)\pi}{N_z} & ; n > 1 \\ \sqrt{\dfrac{1}{N_z}} & ; \quad n = 1 \end{cases} \quad (6.13)$$

$$\delta_k^{II} = -4\sin^2\left(\frac{(k-1)\pi}{2N_z}\right) \quad (6.14)$$

$$\left(\chi_k^{II}\right)^2 = k_0^2 + \frac{\delta_k^{II}}{h_z^2} \quad (6.15)$$

where $m, n, k = 1, 2, \cdots, N_z$.

6.3 Eigenvalue equation of inhomogeneous waveguide

After the Helmholtz equations are solved in each uniform region, we need to match the fields at the interfaces between the uniform regions in order to solve the whole structure. The acoustic pressure and particle velocity at interface are obtained from ψ. For the continuity condition $r = a$, we have

$$\begin{aligned} &\overline{\psi}^{I} = \overline{\psi}^{II} \\ &\Rightarrow \quad [T]^{I}\left[J_0\left(\chi_k^{I}a\right)\right][A_k] = [T]^{II}\left[J_0\left(\chi_k^{II}a\right)\right][B_k] + [T]^{II}\left[Y_0\left(\chi_k^{II}a\right)\right][C_k] \end{aligned} \tag{6.16}$$

$$\begin{aligned} &\left.\frac{\partial \overline{\psi}^{I}}{\partial r}\right|_{r=a} = \left.\frac{\partial \overline{\psi}^{II}}{\partial r}\right|_{r=a} \\ &\Rightarrow [T]^{I}\left[-\chi_k^{I}J_1\left(\chi_k^{I}a\right)\right][A_k] = [T]^{II}\left[-\chi_k^{II}J_1\left(\chi_k^{II}a\right)\right][B_k] + [T]^{II}\left[-\chi_k^{II}Y_1\left(\chi_k^{II}a\right)\right][C_k] \end{aligned} \tag{6.17}$$

From the boundary condition at r = b, we get

$$\begin{aligned} &\left.\frac{\partial \overline{\psi}^{II}}{\partial r}\right|_{r=b} = 0 \\ &\Rightarrow [T]^{II}\left[-\chi_k^{II}J_1\left(\chi_k^{II}b\right)\right][B_k] + [T]^{II}\left[-\chi_k^{II}Y_1\left(\chi_k^{II}b\right)\right][C_k] = 0 \end{aligned} \tag{6.18}$$

In equations (6.16), (6.17), and (6.18), $[T]^{I}$ and $[T]^{II}$ are N_z by N_z matrices, $[A_k]$, $[B_k]$ and $[C_k]$ are $N_z \times 1$ matrices. $\left[J_0\left(\chi_k^{I}a\right)\right]$, $\left[J_0\left(\chi_k^{II}a\right)\right]$ and $\left[Y_0\left(\chi_k^{II}a\right)\right]$; $\left[-\chi_k^{I}J_1\left(\chi_k^{I}a\right)\right]$, $\left[-\chi_k^{II}J_1\left(\chi_k^{II}a\right)\right]$ and $\left[-\chi_k^{II}Y_1\left(\chi_k^{II}a\right)\right]$ are N_z by N_z diagonal matrices.

We can re-write equations (6.16), (6.17), and (6.18) as a matrix form in the following,

$$\begin{bmatrix} [T]^{I}\left[J_0\left(\chi_k^{I}a\right)\right] & -[T]^{II}\left[J_0\left(\chi_k^{II}a\right)\right] & -[T]^{II}\left[Y_0\left(\chi_k^{II}a\right)\right] \\ [T]^{I}\left[-\chi_k^{I}J_1\left(\chi_k^{I}a\right)\right] & [T]^{II}\left[\chi_k^{II}J_1\left(\chi_k^{II}a\right)\right] & [T]^{II}\left[\chi_k^{II}Y_1\left(\chi_k^{II}a\right)\right] \\ [0] & \left[\chi_k^{II}J_1\left(\chi_k^{II}b\right)\right] & \left[\chi_k^{II}Y_1\left(\chi_k^{II}b\right)\right] \end{bmatrix}_{(3N_z \times 3N_z)} \begin{bmatrix} A_k \\ B_k \\ C_k \end{bmatrix}_{(3N_z \times 1)} = [0] \tag{6.19}$$

If

$$[Z]=\begin{bmatrix} [T]^{I}\left[J_0(\chi_k^{I}a)\right] & -[T]^{II}\left[J_0(\chi_k^{II}a)\right] & -[T]^{II}\left[Y_0(\chi_k^{II}a)\right] \\ [T]^{I}\left[-\chi_k^{I}J_1(\chi_k^{I}a)\right] & [T]^{II}\left[\chi_k^{II}J_1(\chi_k^{II}a)\right] & [T]^{II}\left[\chi_k^{II}Y_1(\chi_k^{II}a)\right] \\ [0] & \left[\chi_k^{II}J_1(\chi_k^{II}b)\right] & \left[\chi_k^{II}Y_1(\chi_k^{II}b)\right] \end{bmatrix}_{(3N_z\times 3N_z)} \tag{6.20}$$

the nontrivial solution of equation (6.19) requires that the determinant of the matrix [Z] is zero,

$$\det\{[Z]\}=0 \tag{6.21}$$

The propagation constant β in the z-direction can be obtained by solving the above equation. Due to the presence of poles, SVD technique is again used. Thus, the determinant calculation is equivalent to finding all the local minimum points of the lowest singular values of [Z] along the frequency axis.

Once the propagation constant β is obtained, we can obtain the phase delay of the sound signal through the periodic structures or waveguides. For comparison, we can also get the phase delay of the sound signal through free space for the same geometrical length as that of the periodic structures. Here, we define the phase lag as the difference of phase delays between the sound wave propagating in free air and one traveling through the periodic waveguide. The phase lag is expressed as below

$$-\Delta\Phi=\frac{2\pi L_g}{\lambda_{air}}-\beta L_g=\frac{2\pi f}{c_{air}}L_g-\beta L_g \tag{6.22}$$

where f and c_{air} are the sound frequency and the sound speed in free space, and L_g is the length of the periodic waveguide.

6.4 Experimental arrangement diagram

In order to validate our method, a periodic structure as shown in Figure 6.2 has been machined. There are four periods in total, where the diameter of the cylindrical waveguide is 10 inches and the length of one period is 0.5 inch. The outer diameter of inserted disk is 10 inches as that of the cylindrical waveguide and the inner diameter of the open part of the disk is 1 inch.

Experimental measurement of the periodic structure has been performed on a 1/8 scale model in an anechoic chamber. The test configuration is shown in Figure 6.2. Here, a loudspeaker, which is about 2 meters away from the periodic structure, is used as a source of white noise. As illustrated in Figure 6.2, two microphones as loads of sound are placed in the front of the loudspeaker with an identical distance. Sound can propagate through the periodic cylindrical waveguide to reach one microphone, or it can directly reach the other microphone in free space. These two microphones were chosen with a diameter small enough not to disturb either the field radiating out of the slit (exit of the periodic waveguide) or the field diffracted by the wedge above the periodic waveguide. Acoustic wave propagates through the periodic structure with a much lower speed than it travels in free space. Thus, there is a phase lag between the two microphones. Moreover, there are passbands and stopbands created by the periodic structure. Related processing instruments are also shown in Figure 6.2. Data are sampled from two microphones and are then processed by FFT. Finally phase delays of the two microphones and phase lag between them are obtained.

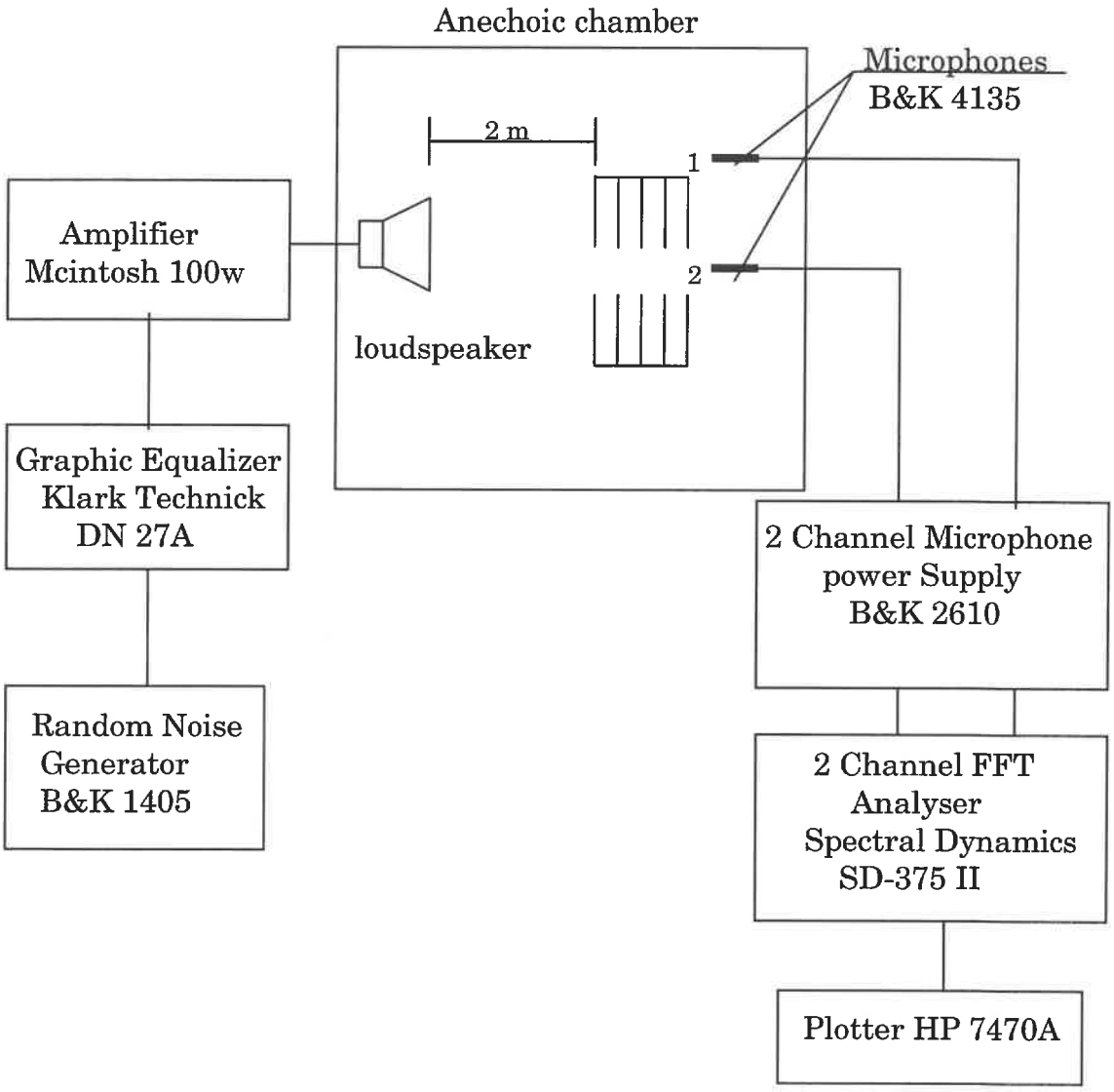

Figure 6.2 Block diagram of the measurement system

6.5 Experimental and theoretical Results

By using 2D CMoL method, the propagation characteristics of the periodic structure described in Section 6.4 are obtained and then compared with the above experimental data. Parametric analysis is also performed to illustrate the variation of phase delay with the change of geometrical parameters of the periodic structure.

6.5.1 Comparison between numerical and experiment results

Based on the method described above, the theoretical values of phase lags between the two microphones in Figure 6.2 have been obtained. As listed in Table 6-1, there are total six passbands alternatively separated by stopbands for the frequencies below 8kHz.

Table 6-1 Frequency range for passbands below 8kHz

Number of passband	Frequency range (Hz)
PB-I	0 – 430
PB-II	1630-2040
PB-III	2990-3515
PB-IV	4340-4970
PB-V	5680-6420
PB-VI	7018-7858

Figure 6.3 shows the theoretical values of the phase lag for the whole frequency band below 8kHz. Note that the phase lag in the frequency range out of the passbands listed in Table 6-1, for the periodic structure, linearly increases with the increase of frequency as illustrated in Figure 6.3, because in the frequency range of the stopbands, the wave does not propagate, power is reflected back to the input of the structure, the phase delay βd equals zero or π as mentioned in Chapter 4.

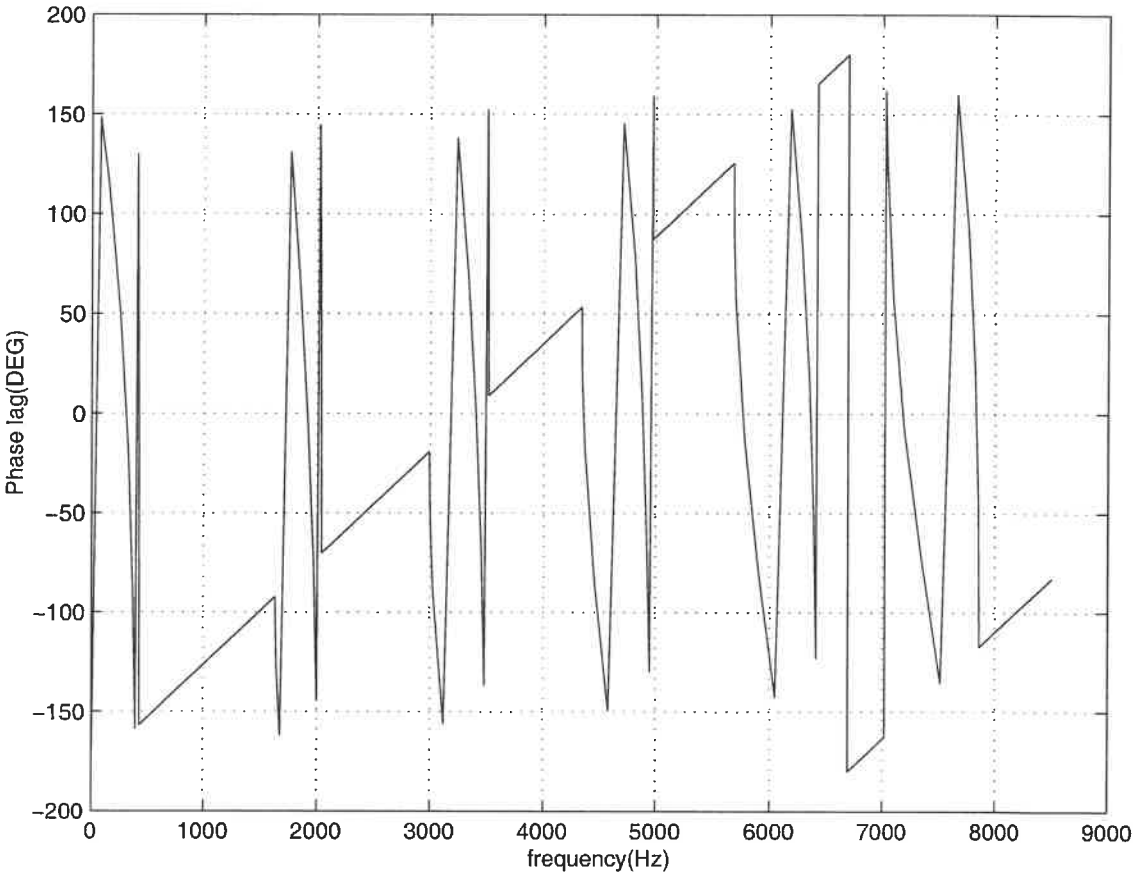

Figure 6.3 Phase lag for a periodic structure with four periods by using 2D CMoL

Figures 6.4a, 6.4b, 6.4c, 6.4d and 6.4e show the phase lags in the frequency ranges of five passbands PB-I, PB-II, PB-III, PB-IV and PB-V, respectively. The phase lag of passband PB-VI is not analyzed here, because the signal to noise (S/N) ratio is low for the experiment data.

The first passband is called PB-I listed in Table 6-1, where the frequency of interest varies from DC to 430 Hz. The phase lag of the corresponding frequency points in PB-I is shown in Figure 6.4a, where the solid curve represents the numerical results from 2D CMoL, while the dash-dotted curve with the symbol "◊" stands for the measurement results. As expected, there is one passband occurring in the frequency range from DC to 430 Hz. However, the theoretical results deviate from the experimental ones. Such deviation may due to diffraction and refraction of the sound wave, which lead to small difference of phase delay between the sound wave propagating in free air and one traveling through the periodic waveguide.

Figure 6.4b shows the phase lag of the frequency points in the second passband PB-II. As listed in Table 6.1, the covered frequency is from 1630 to 2040 Hz. The solid curve represents the numerical results form 2D CMoL and the dash-dotted curve with the symbol of "Δ" stands for the measurement results. As expected, there is one passband occurring in passband PB-II. An excellent agreement is achieved between theoretical and experimental results in the middle of passband PB-II. The theoretical results in the left transitional range between stopband and passband differ a lot from the experimental ones.

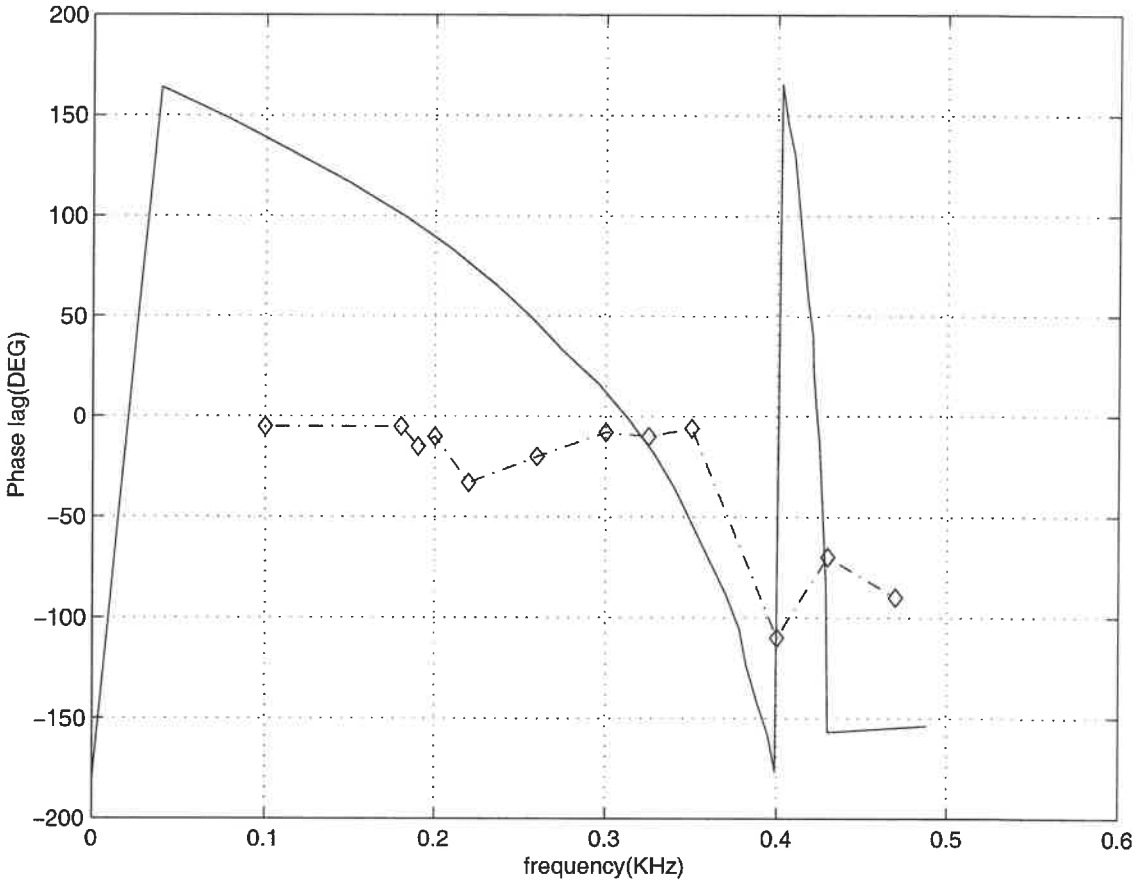

Figure 6.4a Theoretical and experimental phase lag from 0 to 430 Hz

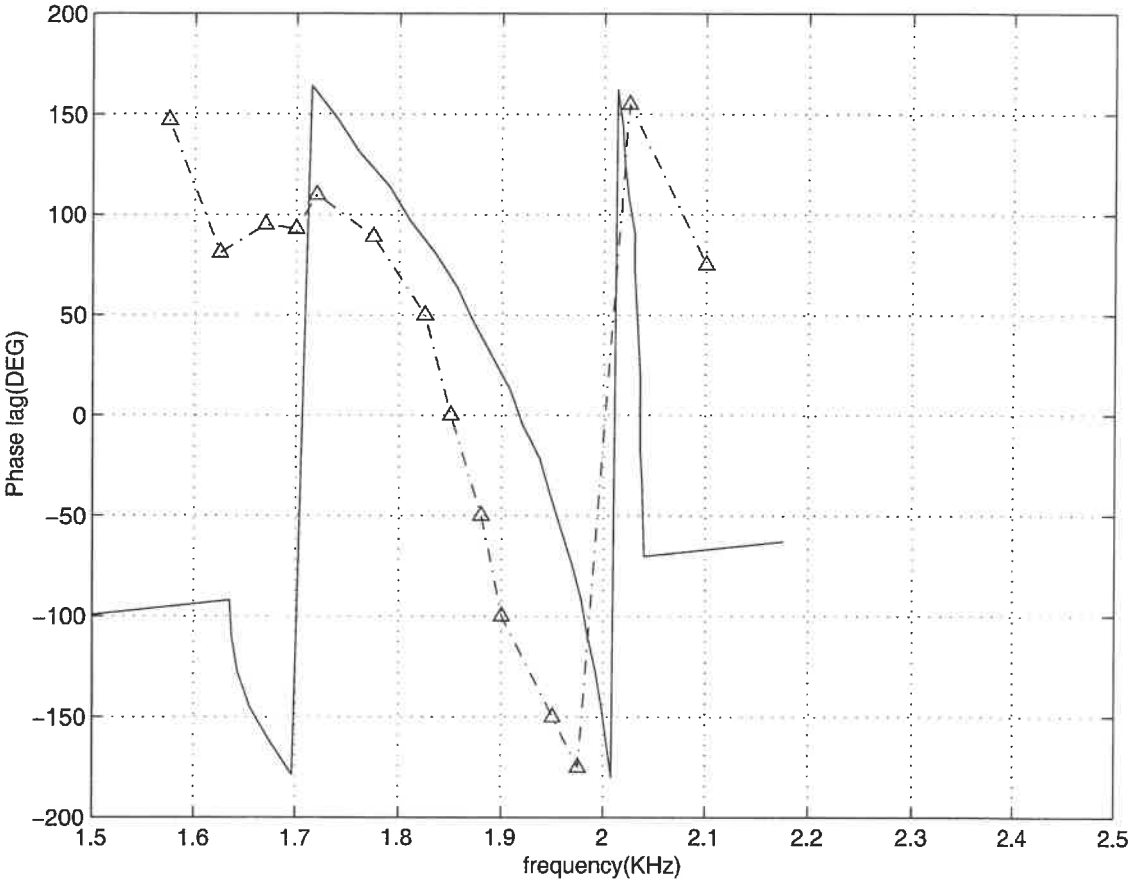

Figure 6.4b Theoretical and experimental phase lag from 1630 to 2040 Hz

The covered frequency of third passband PB-III as listed in Table 6-1 is from 2990 to 3515 Hz. The phase lag of the frequency points is shown in Figure 6.4c. The solid curve represents the numerical results form 2D CMoL. The dash-dotted curve with the symbol of "□" stands for the measurement results. As expected, there is one passband occurring in passband PB-III. An excellent agreement is achieved between theoretical and experimental results in the middle of passband PB-III. The theoretical results in the right transitional range between stopband and passband differ a lot from the experimental ones.

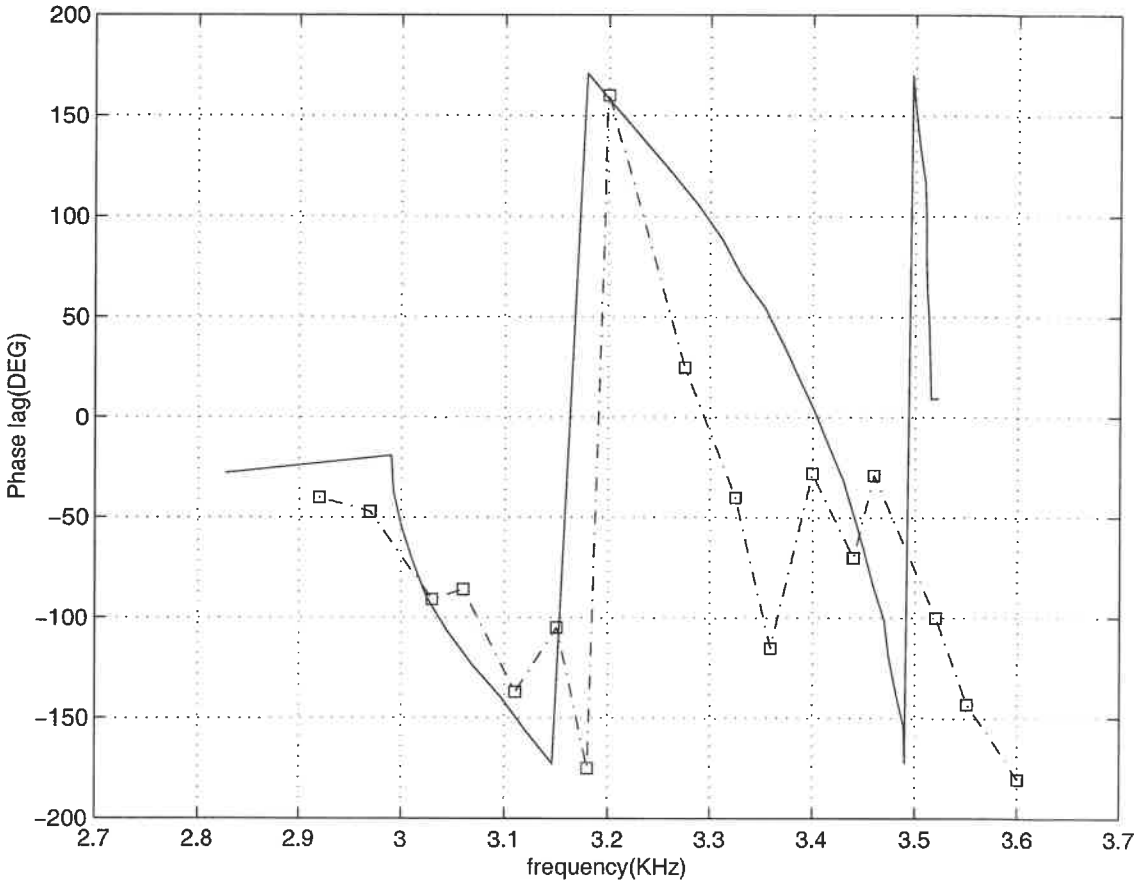

Figure 6.4c Theoretical and experimental phase lag from 2990 to 3515 Hz

Figure 6.4d shows the phase lag of the frequency points in passband PB-IV. The frequency is from 4340 to 4970 Hz. The solid curve represents the numerical results form 2D CMoL. The dash-dotted curve with the symbol of "∇" stands for the measurement results. As expected, there is one passband occurred in passband PB-IV. However, there is big difference between theoretical and experimental results in this passband. Comparing to theoretical data, it seems that the experimental results enlarged the width of the passband and shifted the centre of such a passband.

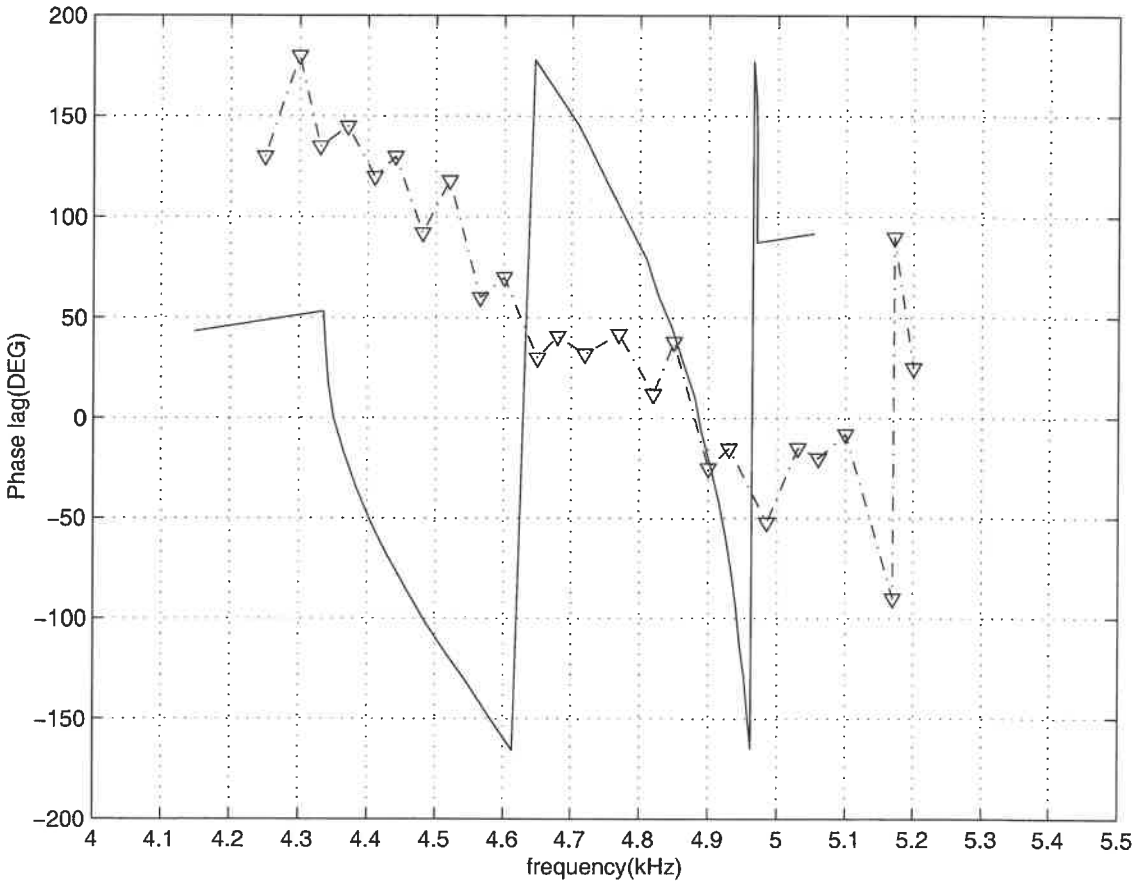

Figure 6.4d Theoretical and experimental phase lag from 4340 to 4970 Hz

The phase lag versus frequency in passband PB-V is displayed in Figure 6.4e. The covered frequency is from 5680 to 6420 Hz. The solid curve represents the numerical results form 2D CmoL, while the dash-dotted curve with the symbol of "◊" stands for the measurement results. As expected, there is one passband occurred in passband PB-V. An good agreement is achieved between theoretical and experimental results in the middle of passband PB-V.

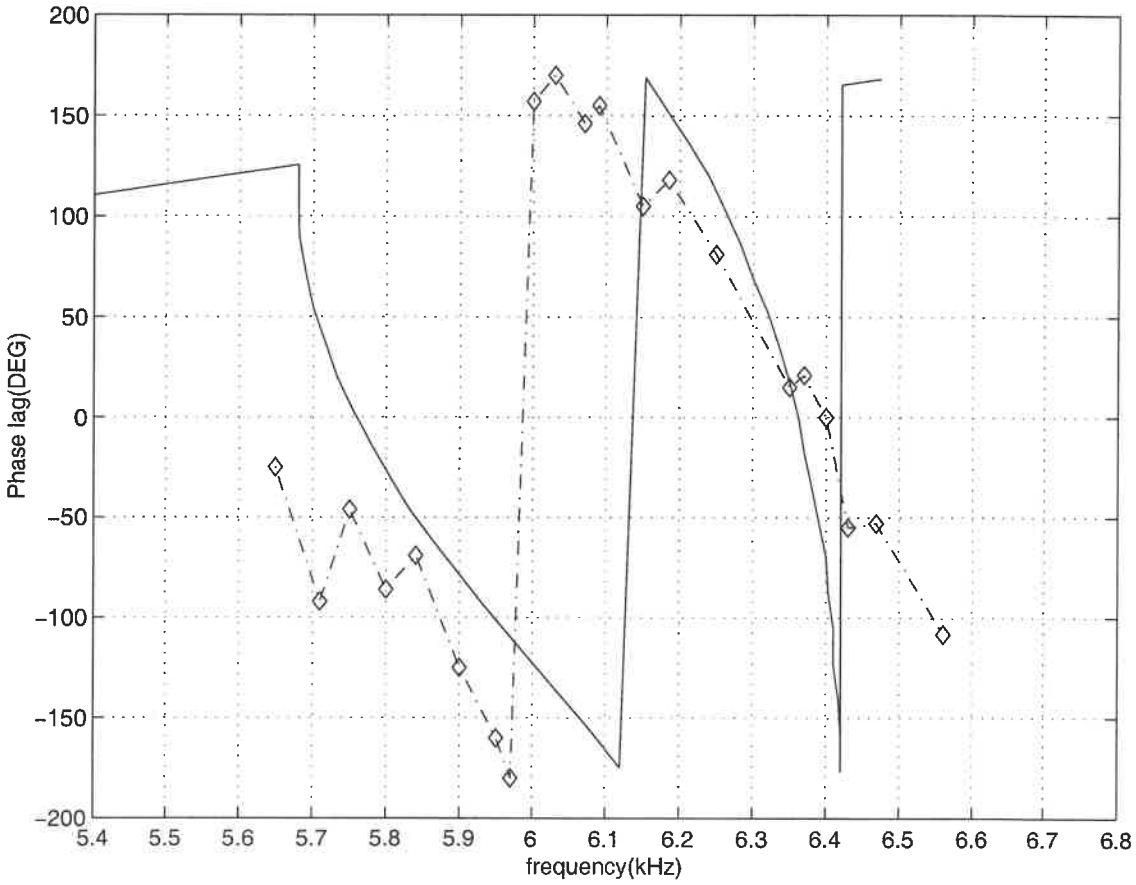

Figure 6.4e Theoretical and experimental phase lag from 5680 to 6420 Hz

6.5.2 Parametric analysis

In order to investigate the dependence of phase delay βd on the geometrical parameters, two special groups of numerical simulations have been performed. Only one parameter varies in each group. In group one, the inner diameter of inserted disks changes from 0.5, 1 to 2 inches, while in group two, the distance of one period varies from 1, 2 to 4 inches.

Figure 6.5 shows the phase delay βd of the frequency points with variation of the inner diameter of the inserted disks. The solid, dash-dotted and dashed curves represent the periodic structures with the values of inner diameter of inserted disks 0.5, 1 and 2 inches, respectively. As shown in Figure 6.5, the phase delay decreases with the increase of the inner diameter of the inserted disks for such special cases.

The phase delay βd versus to the frequency points with the variation of the length of one period for the periodic structure is shown in Figure 6.6. The solid, dash-dotted and dashed curves represent the situations with the length of one period 1, 2 and 4 inches, respectively. As shown in Figure 6.6, the phase delay increases with the increase of the length of one period for such special case.

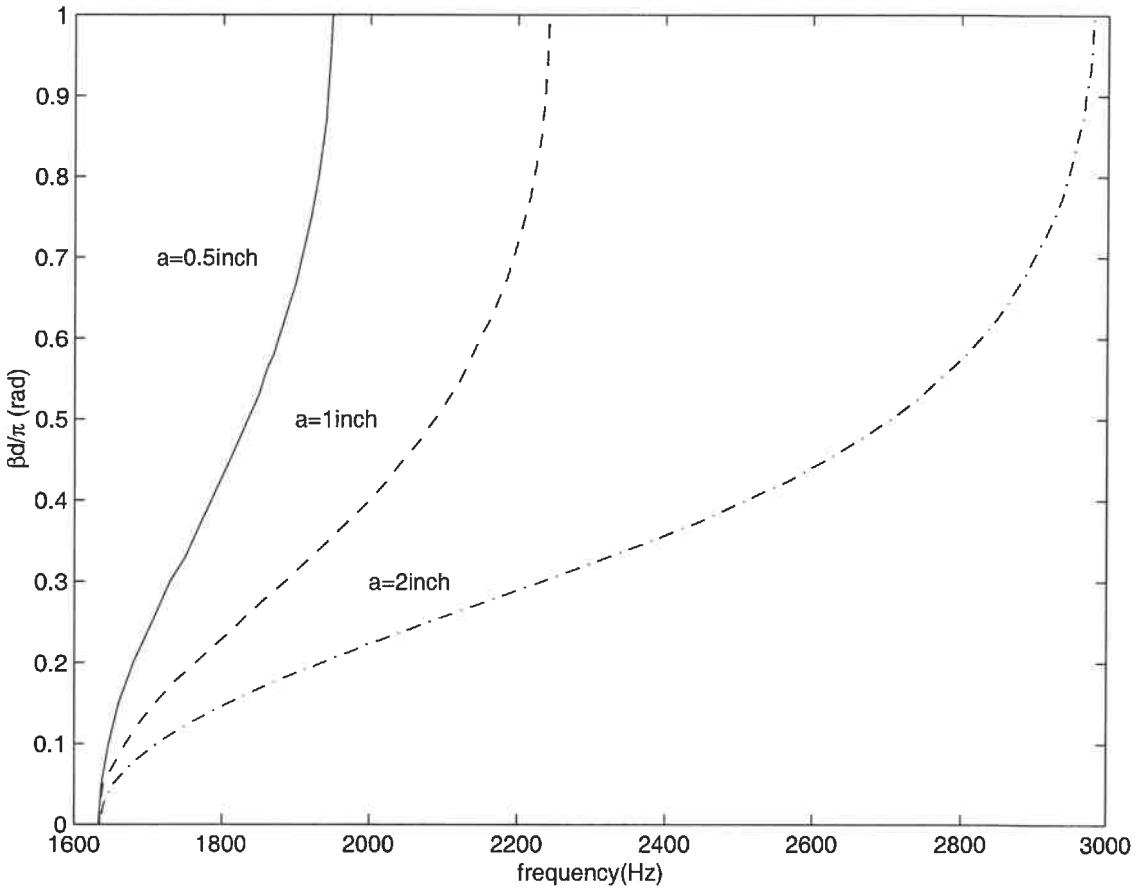

Figure 6.5 Variation of phase delay
with the change of inner diameter of the inserted disks

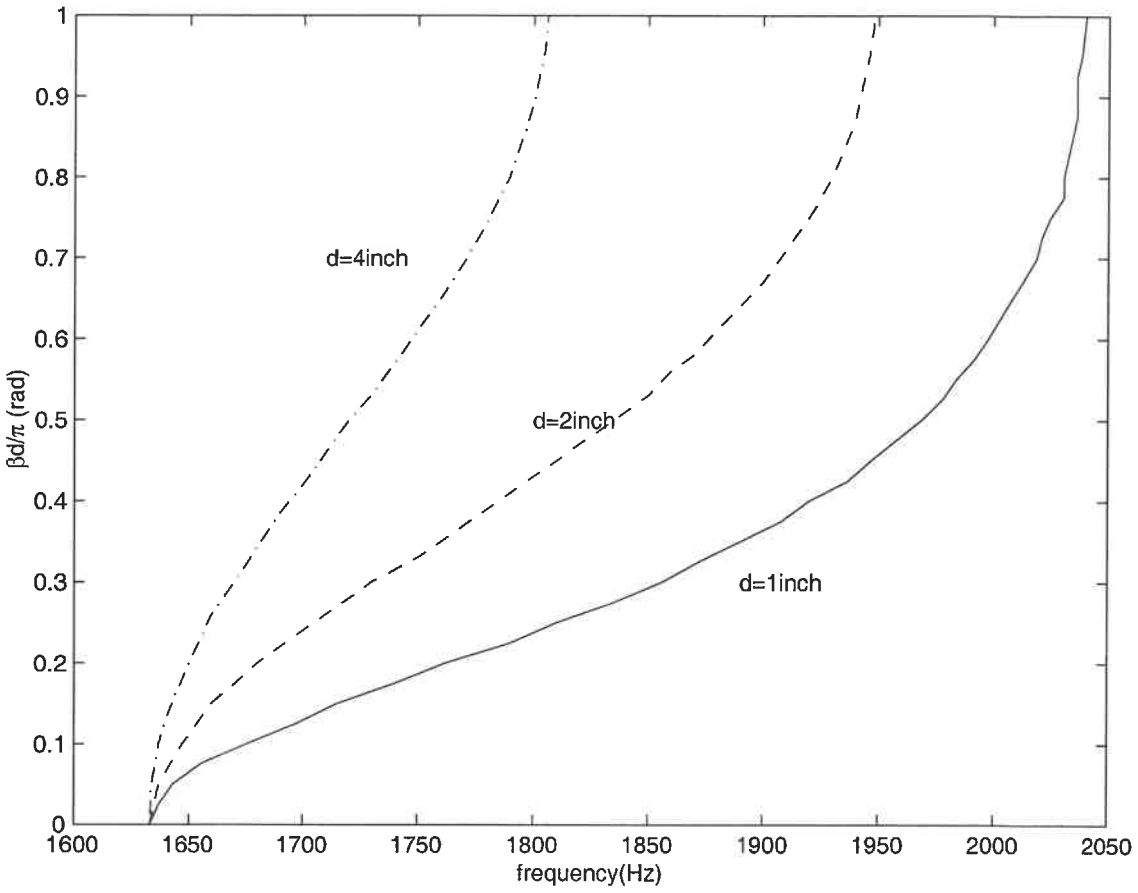

Figure 6.6 Variation of phase delay
with the change of the length of one period

6.7 Conclusion and discussion

In this chapter, by using 2D CMoL, dispersion characteristics have been analyzed for a periodic acoustic waveguide. Good agreements have been achieved between theoretical and experimental results in passbands PB-II, PB-III and PB-V. For passbands in PB-I and PB-IV, there is difference between the simulation results from 2D CMoL and the measurement results. Deviation appears in the transitional range from passband to stopband between the phase lag from 2D CMoL and those from experimental measurements. Such deviation is near the frequency of the resonance where instability occurs. It may come from the input and output places of the periodic cylindrical waveguides. Different input and output structures influence the width of the expected passband. Another reason is that there are only four periods in the measurement structure; but we assume sufficient number of periods in our theoretical analysis. Moreover, our method is focused on passband, thus discrepancy may easily occur between the theoretical and the experimental results in the transitional range between the stopband and the passband.

In order to illustrate the variation of phase lag with the change of geometrical parameters of the periodic structure, parametric analysis is also performed. For such special case, we find that the phase delay decreases with the increase of the inner diameter of the opening part of the disks, and that the phase delay increases with the increase of the length of one period.

It should be noted that the thickness of disk has not been included in our analysis. Accurate analysis need include the impact of the thickness of disk.

Moreover, the theoretical data are valid on the assumption that there are lot of periods. In experimental measurement, only four periods have been used, due to the limitation of our resource. Furthermore, the phase lag obtained by measurement including the discontinuity effect at the input and output positions of the periodic acoustic structure while the theoretical method only calculates the phase delay of four periods.

CHAPTER 7
CONCLUSIONS

7.1 Conclusions

In this thesis, a comprehensive numerical study of cylindrical cavities and periodic disk-loaded cylindrical waveguide for both microwave and acoustic applications have been presented by using 2D and 3D Method of Lines (MoL).

Procedures of the Method of Lines in cylindrical coordinates have been described in detail. Microwave and acoustic cylindrical resonators have been analyzed by using both 2D and 3D CMoL. Excellent agreements have been achieved between theoretical results from CMoL and those from analytical expressions.

As to periodic cylindrical structures, due to axial symmetry of the periodic structure, and due to the axial symmetry of wave propagating, only 2D CMoL has been used to analyze the dispersion characteristics of the periodic disk-loaded waveguides. Here, the acoustic source is a plane wave coming from a loudspeaker, and the electromagnetic source is TEM wave travelling from a coaxial connector. The passbands for both microwave and acoustic cases occur as expected. There is a slight difference between theoretical and experimental phase lags. Such deviation partly arises from the numerical error as implementing 2D CMOL to analyze the periodic structure. Another comes from the impact of input and output discontinuity. Finally, nonaxial modes may exist if the structures do not have strictly axial symmetry or if

the source propagating causes the component of wave field depends on the angular variable.

7.2 Recommendations for future work

To continue the work in this thesis, firstly, the analysis of periodic disk-loaded cylindrical waveguide structures in microwave engineering can be extended to hybrid mode analysis by using 3D CMoL.

Secondly, in acoustic engineering, the cross-section of the structure may not have axial symmetry. Under this circumstance, the discretization of the θ-variable is required. It is needed to implement 3D CMoL to analyze such kind of periodic structures. More research is required in the optimization of the disk position and the ratio of open versus closed part of the disk in order to introduce a phase lag close to "π" without creating a large impedance mismatch. The latter may reduce acoustic energy associated with low frequency noise propagating through the waveguides.

Finally, the semi-analytical MoL can be utilized to analyze acoustic mode existing in some piezoelectric substrates with a periodic grating.

These three topics are the recommended as the future work.

BIBLIOGRAPHY

[1] R. Pregla and W. Pascher, "The method of lines," in *Numerical Techniques for Microwave and Millimeter Wave Passive Structures*, T. Itoh, Ed. New York, Wiley, 1989, pp. 381-446.

[2] C. C. Johnson, *Field and Wave Electrodynamics*. McGraw-Hill, NewYork,1965. pp. 254, 268-272.

[3] R.E.Collin, *Field Theory of Guided Waves*, in series of Electromagnetic Waves, 2nd ed. New York: IEEE Press, 1991, chapters. 6.2 and 9.1

[4] R.E.Collin, *Foundations for Microwave Engineering*, 2nd ed. McGraw-Hill pp.555-556

[5] E.L.Chu, and W.W.Hansen, "The theory of disk-loaded wave guides," *Journal of Applied Physics*, pp.996-1008, vol.18, Nov. 1947

[6] Thomas M. Wallet, and A. Haq Qureshi, "Charateristics of a cylindrical disk-loaded slow-wave structure found by theoretical, experimental, and computational techniques," *International Journal of Microwave and Millimeter-Wave Computer-Aided Engineering*, vol.4, no.2, pp.125-129, 1994

[7] J.P.Pruiksma, R.W.de Leeuw, J.I.M. Botman, H.L. Hagedoorn, and A.G.Tijhuis, "Electromagnetic fields in periodic linear travelling-wave structures," *Proceedings of the XVIII International linear Accelerator Conference*, vol.1, pp. 89-91.

[8] U.Schulz and R.Pregla, "A new technique for the analysis of the dispersion characteristics of planar waveguides," *Arch. Elek. Ubertragung.*, vol.34, pp.169-173, Apr.1980

[9] S. B. Worm and R. Pregla, "Hybrid-Mode Analysis of Arbitrarily Shaped Planar Microwave Structures by the Method of Lines," *IEEE Trans. Microwave Theory Tech.*, vol. MTT-32, no.2, pp. 191-196, Feb. 1984

[10] H. Diestel and S. B. Worm, "Analysis of hybrid field problems by method of lines with nonequidistant discretization," *IEEE Trans. Microwave Theory Tech.*, vol. MTT-32, no.6, pp. 633-638, June 1984

[11] W. Pascher and Reinhold Pregla, "Full wave analysis of complex planar microwave structures," Radio Sci., vol.22, no.6, pp.999-1002, Nov.1987.

[12] K.Wu, Y. Xu, and R.G. Bosisio, " A technique for Efficient Analysis of Planar Integrated microwave Circuits including Segmented Layers and Miniature Topologies," *IEEE Trans. Microwave Theory Tech.*, vol.42, pp. 826-833, may 1994.

[13] K.Wu, Y. Xu, and R.G. Bosisio, " A Recusive Algorithm for Analysis of planar Multiple lines on Composite Substrates for M(H)MIC's and High-Speed Interconnects," *IEEE Trans. Microwave Theory Tech.*, vol. 43, no.4, pp. 904-907, april, 1995.

[14] M.Thorburn, A. Agostron, and V. K. Tripathi, "Application of method of lines to cylindrical inhomogeneous propagation structures," *Electronics letters*, vol. 26, no.3, pp. 170-171,1990.

[15] S. Xiao and R.Vahldieck, "Full-wave characteristic of cylindrical layered multiconductor transmission lines using the MoL," *1994 IEEE MTT-S International Microwave Sym. Dig.*, San Diego, CA, May 23-27, 1994.

[16] V.A.Labay and J.Bornemann, "Matrix singular value decomposition for pole-free solutions of homogeneous matrix equations as applied to numerical modeling methods," *IEEE Microwave and Guided Wave Letters*, vol.2, no.2, Feb.1992.

[17] Y.Xu, "Application of method of lines to solve problems in the cylindrical coordinates," *Microwave and optical Technology letters*, vol.1, no.5, pp. 173-175, July 1998.

[18] G. Matthaei, L. Young, and E.M.T.Jones, *Microwave filters, impedance-matching networks, and coupling structures*, Artech House, 1980, pp.247.

[19] C.G.Montgomery, *Technique of Microwave Measurements*, Secs.5.4 and 5.5, McGraw-Hill, New York, N.Y., 1947.

[20] A.F.Harvey, " Periodic and guiding structures at microwave frequencies," *IRE Trans. On Microwave Theory and Techniques*, pp. 30-60.

[21] P. J. B. Clarricoats and K.R. Slinn, " Computer solution of waveguide discontinuity problems," pp.23-27

[22] N.A. Mcdonald, "Electric and magnetic coupling through small apertures in shield walls of any thickness," *IEEE Trans. on Microwave Theory and Techniques*, vol.20. no.10, pp. 689-695,Oct.1972.

[23] N.A. Mcdonald, "Polynomial Approximations for the Electric Polarizabilities of Some Small Apertures," *IEEE Trans. on Microwave Theory and Techniques*, vol.33, no.11, pp. 1146-1149, Nov.1985.

[24] M.F. Iskander, and M.A.K. Hamid, "Iterative solutions of waveguide discontinuity problems," *IEEE Trans. on Microwave Theory and Techniques*, vol.25, no.9, pp. 763-768, Sept.1977.

[25] G.B. Eastham and K. Chang, " Analysis and closed-form solutions of circular and rectangular apertures in the transverse plane of a circular waveguide," *IEEE Trans. on Microwave Theory and Techniques*, vol.39, no.4, pp.718-723, April, 1991.

[26] P. M. Morse, *Vibration and Sound*, McGraw-Hill, New York, 1948, pp. 305-311.

[27] P. M. Morse and K. U. Ingard, *Theoretical Acoustics*, McGraw-Hill, New York, 1968, p.509.

[28] E. Skudrzyk, *The Foundations of Acoustics*, Sprinder-Verlag, New York, 1971, pp. 430.

[29] L. J. Erikson, " Higher order mode effects in circular ducts and expansion chambers," *J. Acoust. Soc. Am.*, Vol. 68, No. 2, August 1980, pp.545-550.

[30] Douglas D. Reynolds, *Engineering Principles of Acoustics, Noise and Vibration Control*, Allyn and Bacon, Boston, 1981,pp.359-362

[31] M. Amram and R. Stern, "Refractive and other acoustic effects produced by a prism-shaped network of rigid strips," *Journal of the Acoustical Society of America* 70, pp.1463-1472, 1981

[32] M. Amram and V.J. Chvojka, "A slow-waveguide filter as anacoustic interference controlling device," *Journal of the Acoustical Society of America* 77, pp.394-401, 1985

[33] L. Mongeau, M. Amram and J. Rousselet, "Scattering of sound waves by aperiodic array of slotted waveguides," *Journal of the Acoustical Society of America* 80, pp.665-671, 1986

[34] M. Amram, L.P.Simard, V.J.Chvojka and G. Ostiguy, "Experimental study of forward scattering for a periodic arrangement of slotted waveguides," *Journal of the Acoustical Society of America* 81, pp.215-221, 1987

[35] R.Lahlou, M. Amram, and G. Ostiguy, "Oblique acoustic wave propagation through a slotted waveguide," *Journal of the Acoustical Society of America* 85, pp.1449-1455, 1989.

APPENDIX A

MEASUREMENT RESULTS OF THE PERIODIC ACOUSTIC STRUCTURE

The measurement results obtained from the FFT analyser SD-375 II in Figure 6.2 are displayed in Figures A.1 to A.7.

Figures A.1 and A.2 show the existing phase lag (unit in degree) and the relative sound level difference (expressed in decibels) between the noise at microphones 1 and 2 in free-field condition, where the periodic disk-loaded structure is not inserted.

The relative sound level and the phase difference between the microphones with the periodic disk-loaded structure are illustrated in Figures A.3, A.4 and A.5, corresponding to the frequency from 0 to 3.2 kHz, from 3.2 to 6.4 kHz and from 6.4 to 9.6 kHz, respectively.

Experimental measurement for the whole frequency range from 0 to 12.8 kHz has also been performed. The relative phase difference and the sound level with the periodic disk-loaded structure of the whole frequency range are displayed in Figure A.6 and A.7, respectively.

These measurement results are compared with the numerical prediction by using 2D CMoL in Chapter Six.

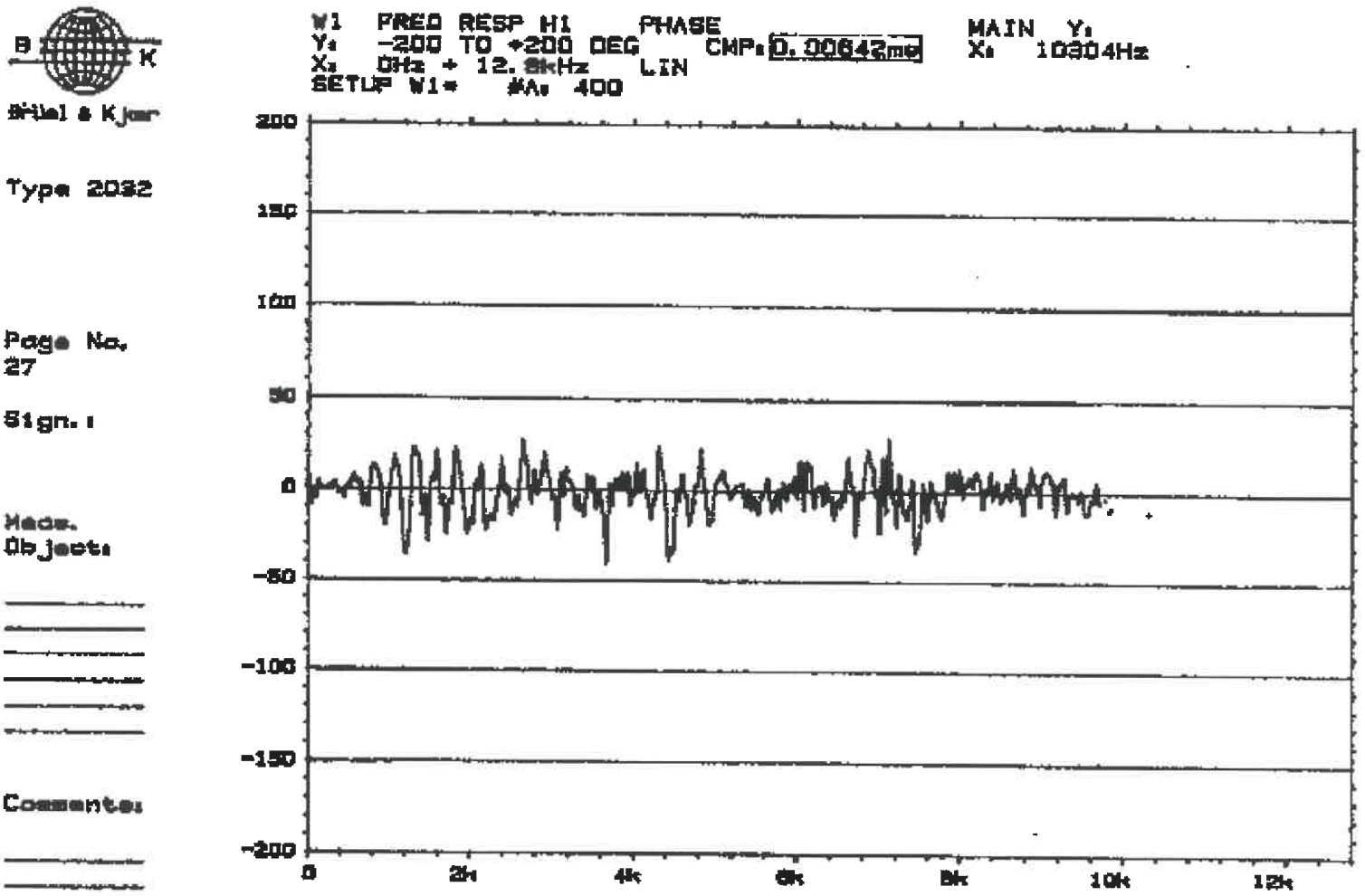

Figure A.1 Phase lag existing between the noise at microphones 1 and 2 in free-field condition.

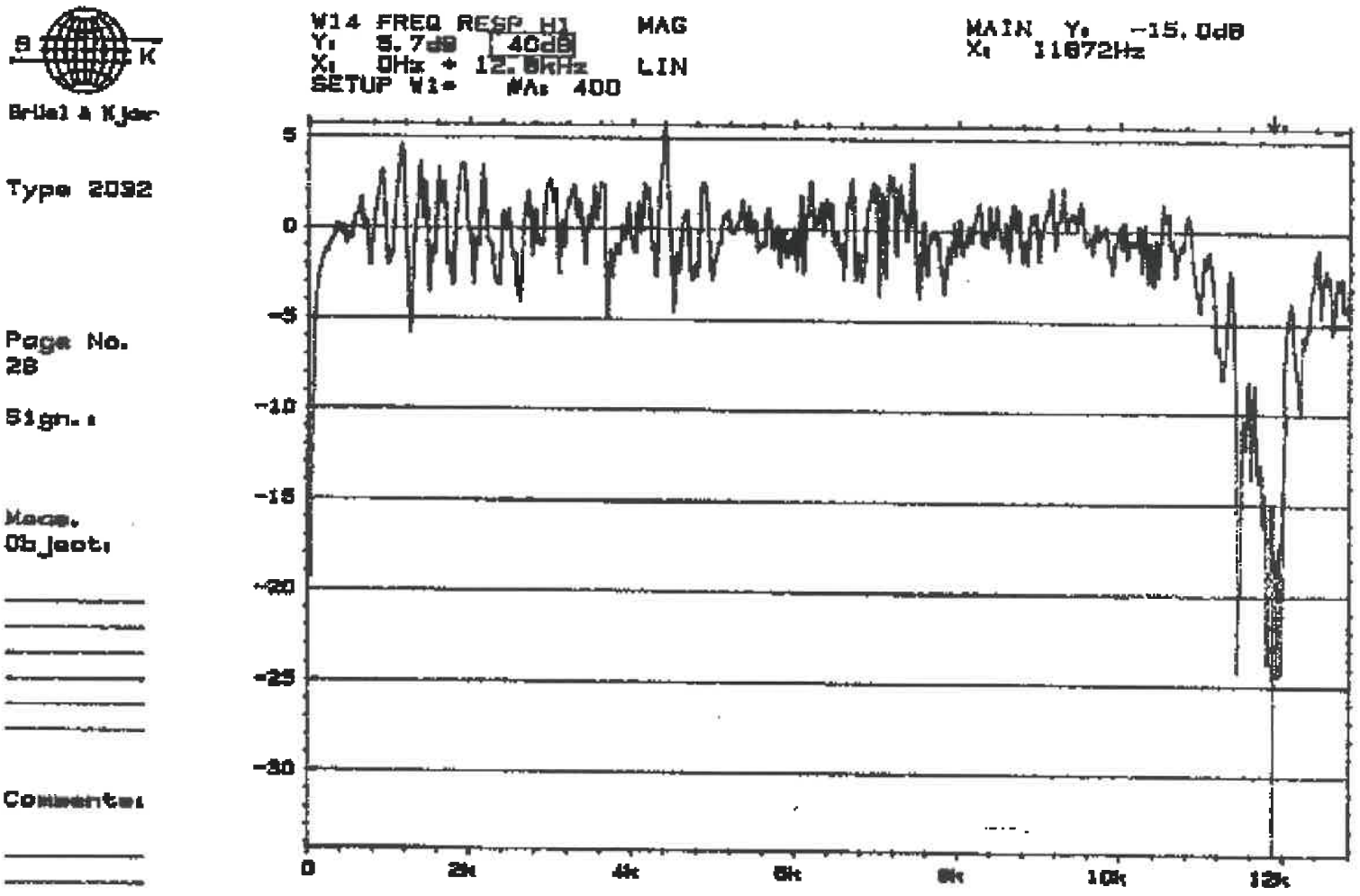

Figure A.2 The relative sound level difference between the noise at microphones 1 and 2 in free-field condition.

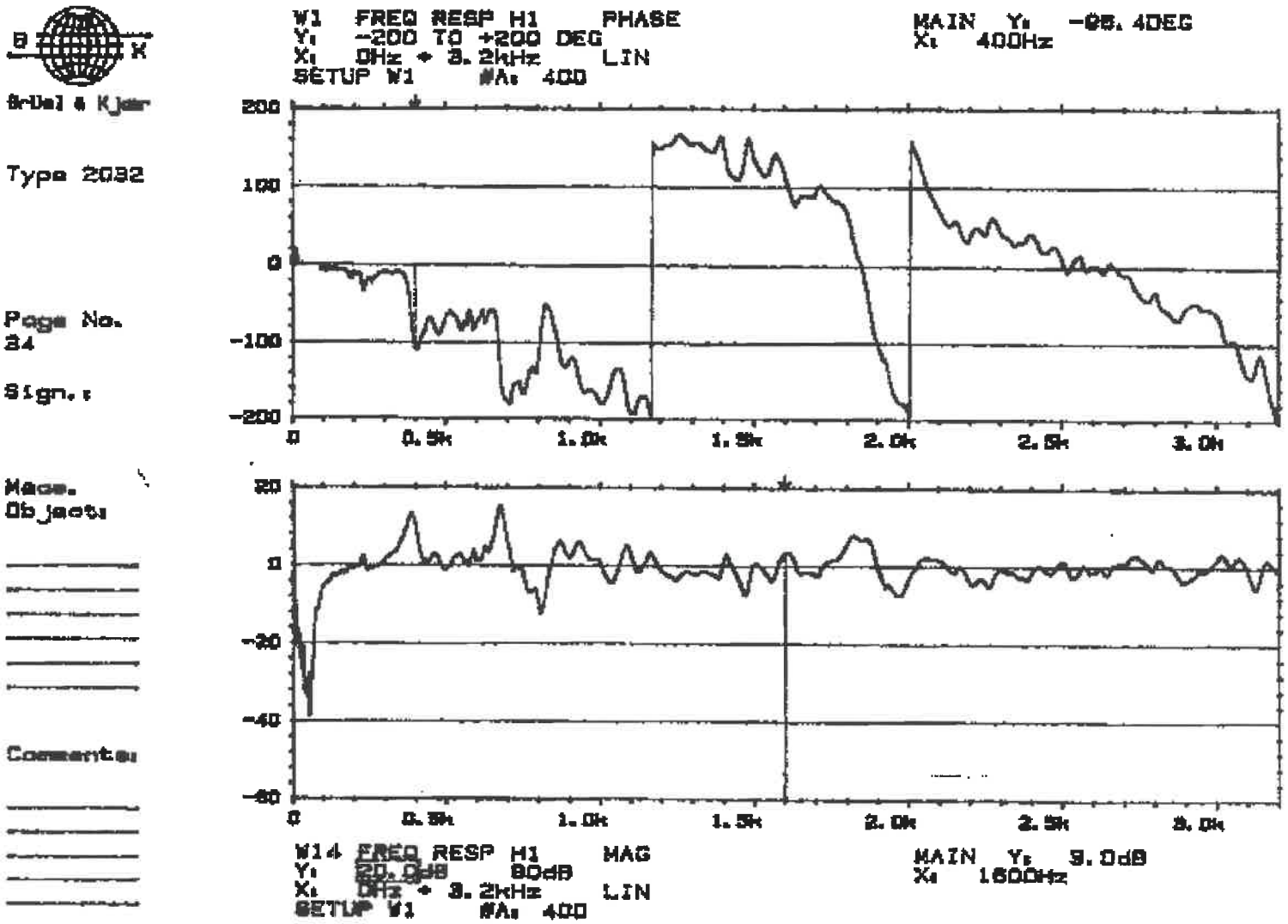

Figure A.3 The relative sound level and phase difference between the microphones at frequency from 0 to 3.2 kHz

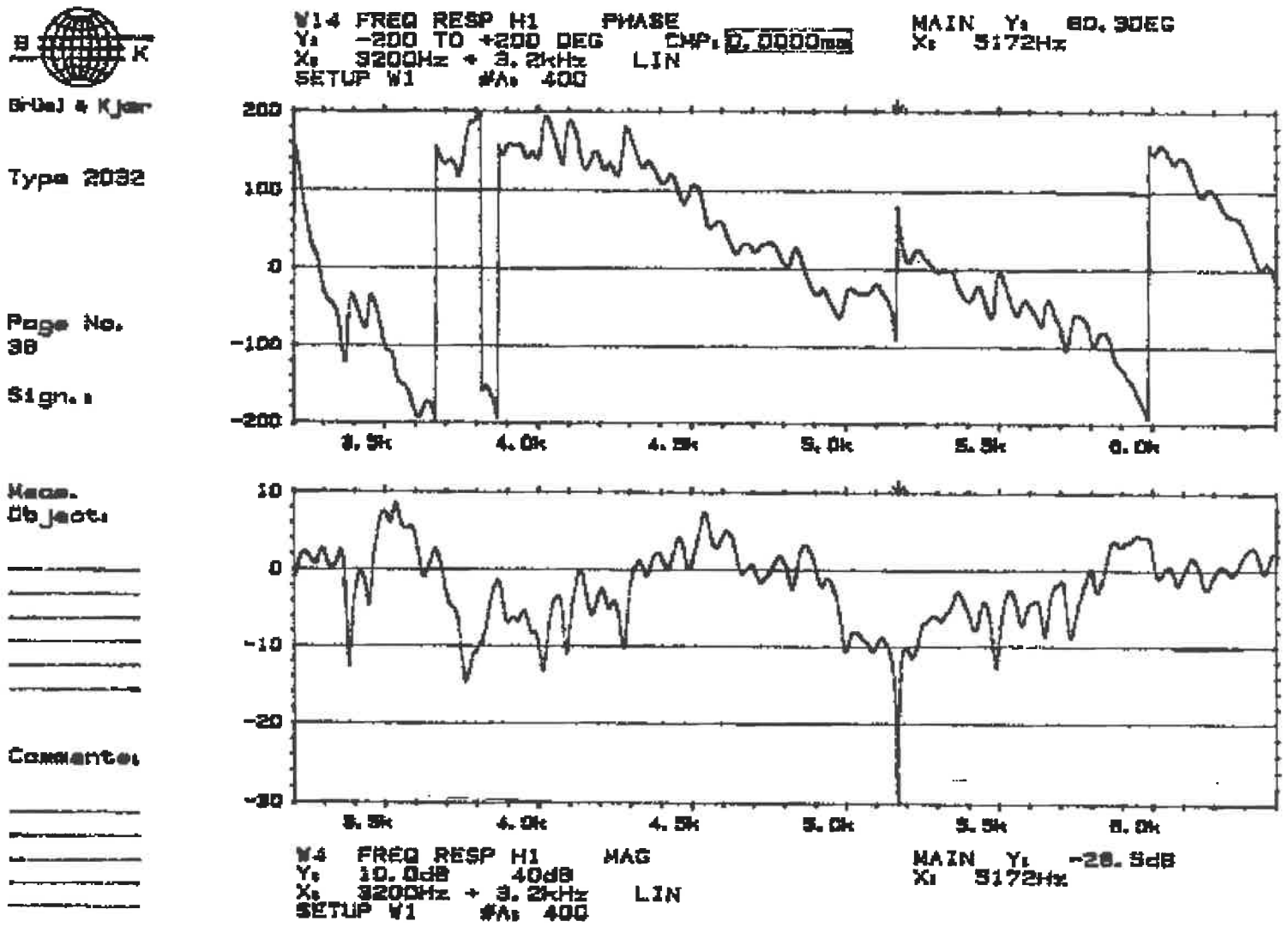

Figure A.4 The relative sound level and phase difference between the microphones at frequency from 3.2 to 6.4 kHz

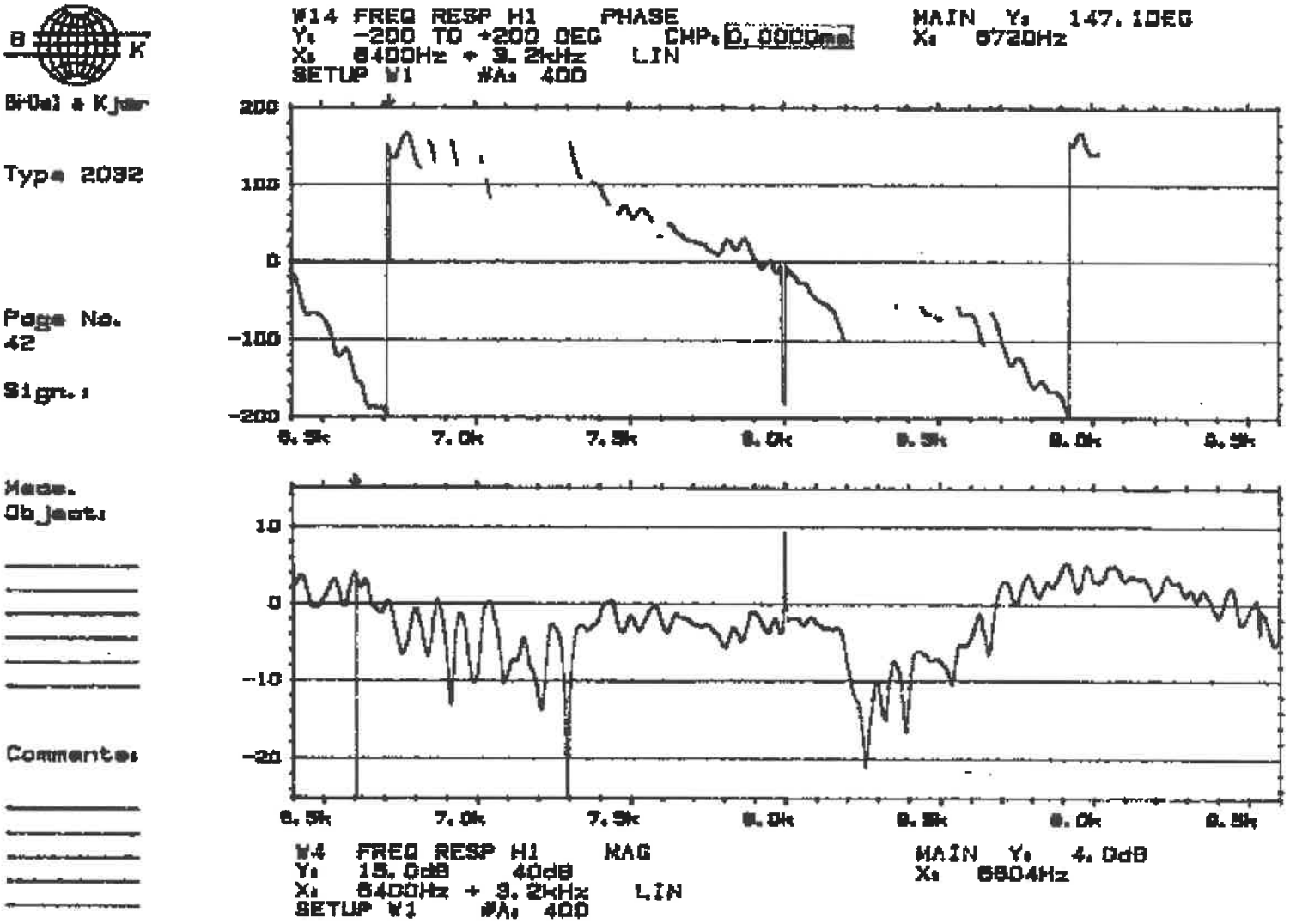

Figure A.5 The relative sound level and phase difference between the microphones at frequency from 6.4 to 9.6 kHz

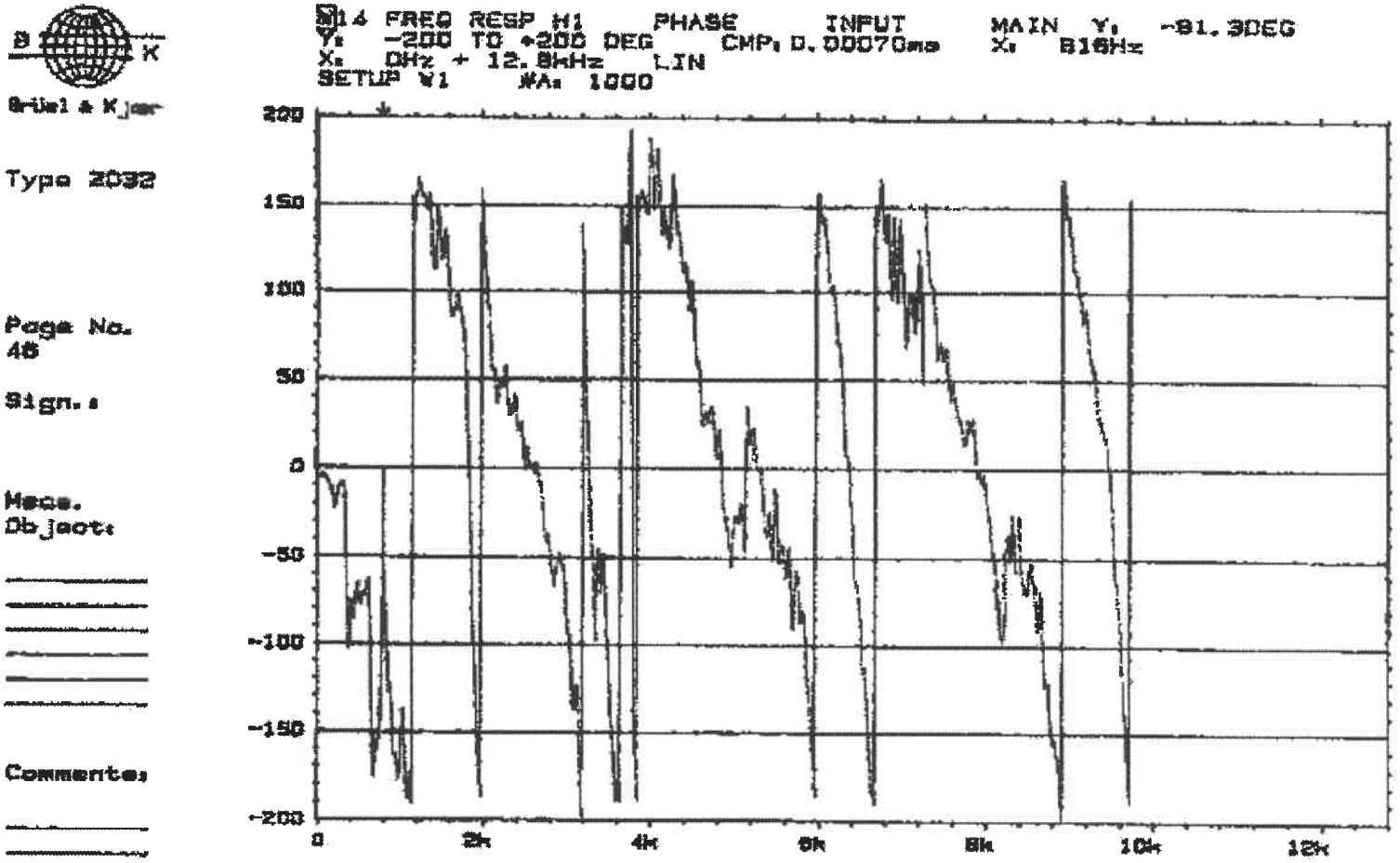

Figure A.6 The relative phase difference between the microphones at frequency from 0 to 12.8 kHz

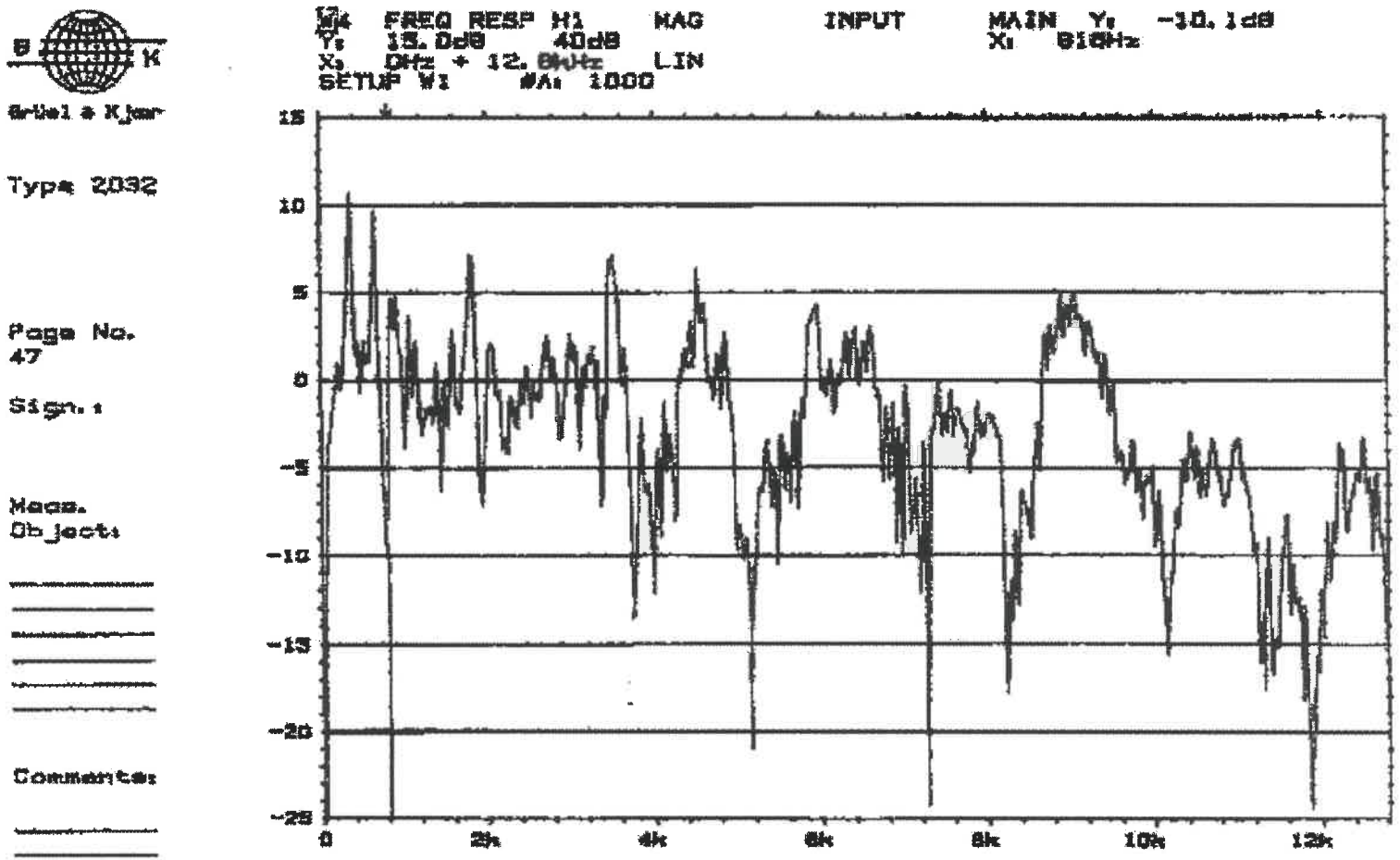

Figure A.7 The relative sound level difference between the microphones at frequency from 0 to 12.8 kHz

APPENDIX B
EXPERIMENTAL ARRANGEMENT OF THE PERIODIC ACOUSTIC STRUCTURE

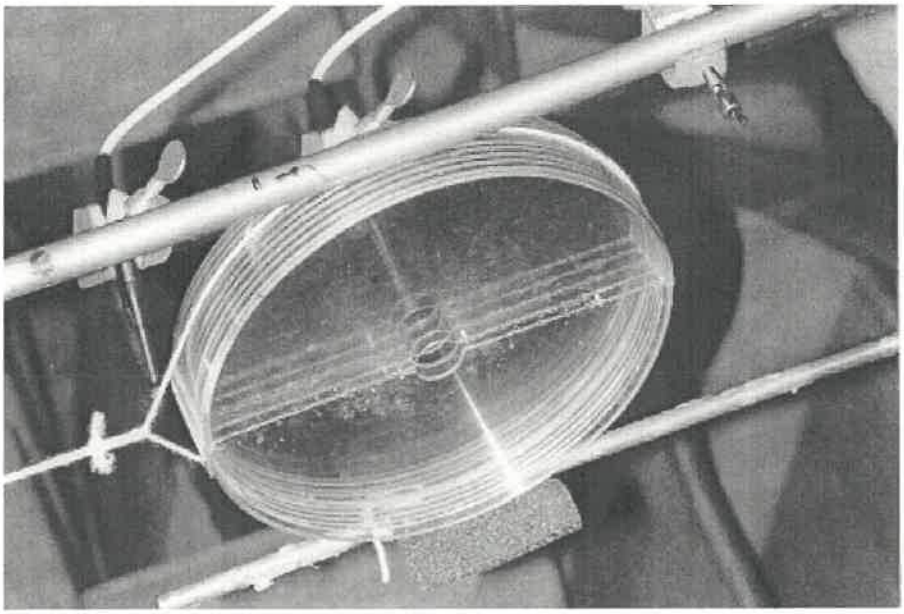

Figure B.2 The position of two microphones

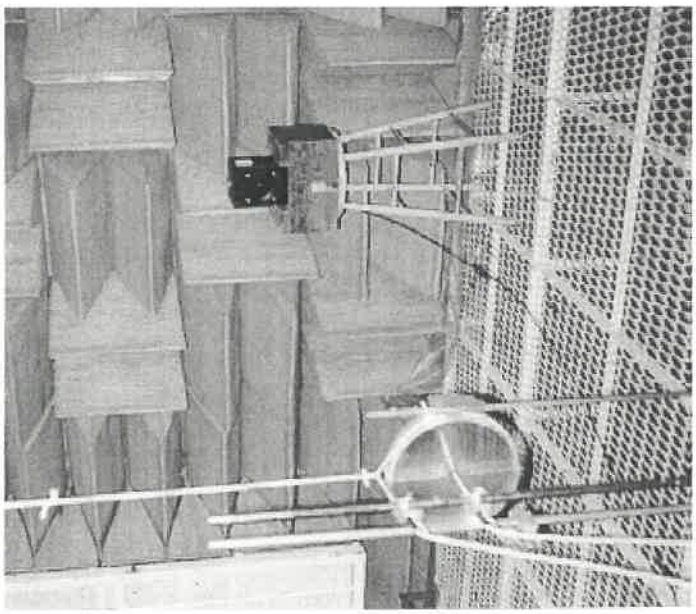

Figure B.1 The arrangement from source to receiver.

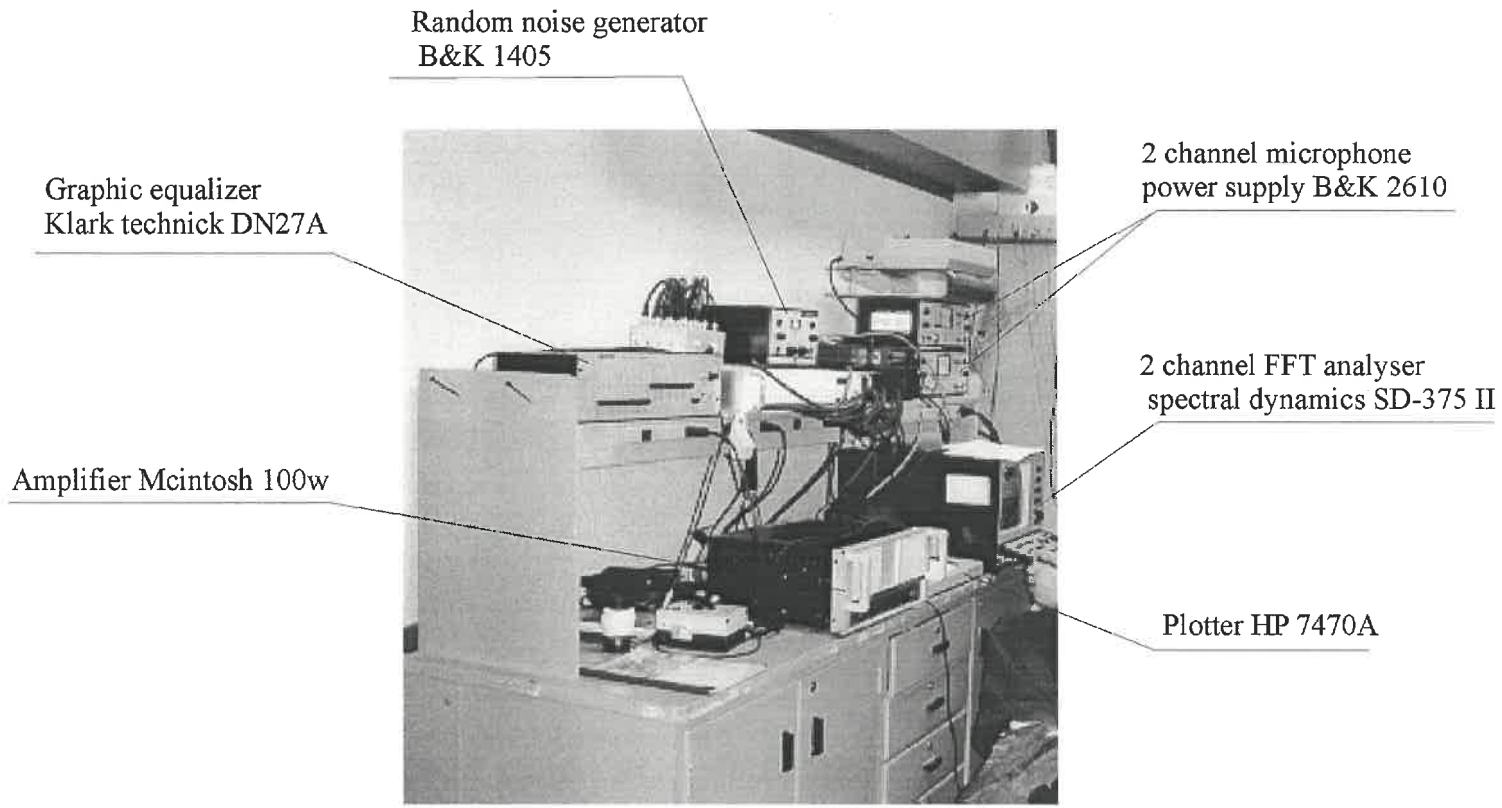

Figure B.3 The laboratory instruments used for experiments